Synthesis of New Hydrocarbon Biodiesel (HiBD) from Waste Cooking Oil over MgO-Based Catalyst

A dissertation submitted to

The University of Kitakyushu

By

Paweesuda Natewong

In Partial Fulfillment of the Requirement

for the Doctoral Degree in

Chemical and Environmental Engineering

The University of Kitakyushu

September, 2016

Contents

CHAPTER 2

EFFECT OF SUPPORT MATERIALS ON MgO-BASED CATALYST FOR PRODUCTION OF NEW HYDROCARBON BIO-DIESEL

CHAPTER 3

DEVELOPMENT OF HETEROGENEOUS BASIC CATALYSTS SUPPORTED ON SILICA FOR THE SYNTHESIS OF HIGH QUALITY BIO-DIESEL FROM WASTE COOKING OIL

CHAPTER 4

EFFECT OF ADDITION OF CaO AND ZrO_2 ON THE PERFORMANCE OF MgO/AC CATALYST FOR THE SYNTHESIS OF NEW BIODIESEL (HiBD) FROM WASTE COOKING OIL

List of Tables

List of Figures

List Abbreviations

Catalysts: a general form of presenting the catalysts, in which

Precursor/Silica

10M/SiO_2	silica impregnated with 10 wt% of magnesium nitrate
10C/SiO_2	silica impregnated with 10 wt% of calcium nitrate
10Z/SiO_2	silica impregnated with 10 wt% of zirconyl nitrate
5M5C/SiO_2	silica impregnated with 5 wt% of magnesium nitrate and 5 wt% calcium nitrate
5M5Z/SiO_2	silica impregnated with 5 wt% of magnesium nitrate and 5 wt% zirconyl nitrate
5M5C5Z/SiO_2	silica impregnated with 5 wt% of magnesium nitrate, 5 wt% calcium nitrate and 5 wt% zirconyl nitrate

Precursor/Activate carbon

10M/AC	activate carbon impregnated with 10 wt% of magnesium nitrate
10C/AC	activate carbon impregnated with 10 wt% of calcium nitrate
10Z/AC	activate carbon impregnated with 10 wt% of zirconyl nitrate
5M5C/AC	activate carbon impregnated with 5 wt% of magnesium nitrate and 5 wt% calcium nitrate
5M5Z/AC	activate carbon impregnated with 5 wt% of

	magnesium nitrate and 5 wt% zirconyl nitrate
5M5C5Z/AC	activate carbon impregnated with 5 wt% of magnesium nitrate, 5 wt% calcium nitrate and 5 wt% zirconyl nitrate
Precursor/γ-Alumina	
10M/Al_2O_3	γ-Alumina impregnated with 10 wt% of magnesium nitrate
Precursor/Zirconium oxide	
10M/ZrO_2	zirconium oxide impregnated with 10 wt% of magnesium nitrate

Methods:

CO_2-TPD	Temperature programmed desorption of CO_2
NH_3-TPD	Temperature programmed desorption of NH_3
XRD	X-ray Diffraction
TGA	Thermogravimetric analysis
Fe-SEM	Field Emission Scanning Electron
BET	Brunauer, Emmett and Teller
BJH	Barret-Joyer-Halenda
FID	Flame-Ionization Detector
HDO	Hydrodeoxygenation
MS	Mass Spectroscopy
TCD	Thermal Conductivity Detector
WHSV	Weight Hourly Space Velocity
HiBD	High Quality Bio-Diesel
CO_2	Carbon dioxide

CO	Carbon monoxide
FFAs	Free fatty acids
FAME	Fatty acid methyl ester
H_2	Hydrogen
NO_x	Nitrogen Oxide
LPG	Liquefied petroleum gas
CNG	Compressed natural gas

ABSTRACT

The purpose of this thesis is to develop an MgO-based catalyst with high activity and stability for the production of new hydrocarbon biodiesel by catalytic decarboxylation of triglycerides and their derivatives in waste cooking oil. This thesis is composed of 5 chapters as below.

Chapter 1, general introduction and literature review related in this field are described. Decarboxylation is usually conducted over noble metal-based catalysts (Pd and Pt). However, considering the high cost of above noble metals, it is more practical in industrial standpoint to develop cheaper catalysts showing similar performance and stability. It has been reported that MgO displayed catalytic performance comparable with that of a metal catalyst. Nevertheless, MgO exhibits a poor CO_2 adsorption capacity due to its low surface area and pore volume.

In chapter 2, effect of support material of MgO is examined. The MgO-based catalysts supported on γ-Al_2O_3, SiO_2, ZrO_2 and active carbon were prepared by incipient wetness impregnation method and tested in an agitated reactor at 430 °C under helium at a flow rate 50 mL/min. All catalysts can convert triglycerides into hydrocarbons in diesel specification range (C_{10}-C_{20}) via two parallel pathway: decarboxylation or subsequent cracking reaction. The 10M/SiO_2 catalyst was selective toward cracking reaction, whereas 10M/AC catalyst showed highest selectivity to decarboxylation. The addition of 10wt% ZrO_2 to MgO/AC catalyst increased the yield of hydrocarbon in diesel range and also resistant to coke formation on the surface catalyst.

In chapter 3, the development of MgO catalysts supported on silica with the best

CO_2 capture capacities (CaO and ZrO_2) is reported. The addition of CaO and/or ZrO_2 exhibited a good catalytic activities, which gave higher CO_2 yields and lower total acid values than MgO/SiO_2 catalyst, due to they had higher surface area and pore volume in comparison to the monometallic $10M/SiO_2$ catalyst.

In chapter 4, the effect of the addition of CaO and ZrO_2 on the performance and stability of MgO supported on active carbon is studied. The addition of CaO and ZrO_2 significantly improved the catalyst activity and stability. The addition of CaO lead to the formation of increased lighter hydrocarbons (C_1-C_9), whereas the addition of ZrO_2 was found to increase the yield in diesel fraction for the catalytic decarboxylation of waste cooking oil.

Finally, conclusions of this work and prospects for the future of HiBD and the design of its production catalysts are described in Chapter 5.

CHAPTER I

Introduction

1.1 World energy demand

Global energy demand has been drastically increased during the 20th century with the rapidly growing population. **Figure 1.1** shows the relationship between world fuel consumption and population, and implies that increased energy consumption has supported the increase in population. Currently, most of global energy demands of the countries are usually supplied by the conventional sources such as oil, natural gas, coal, nuclear and renewable energy. As known as fossil fuels are limited sources, and the world is confronted with the twin crisis of the fossil fuel depletion and the serious environmental impacts as global warming, deforestation, ozone depletion, photochemical smog and acid rain related with NO_x and SO_x emissions [1]. The increasing demand for energy has led

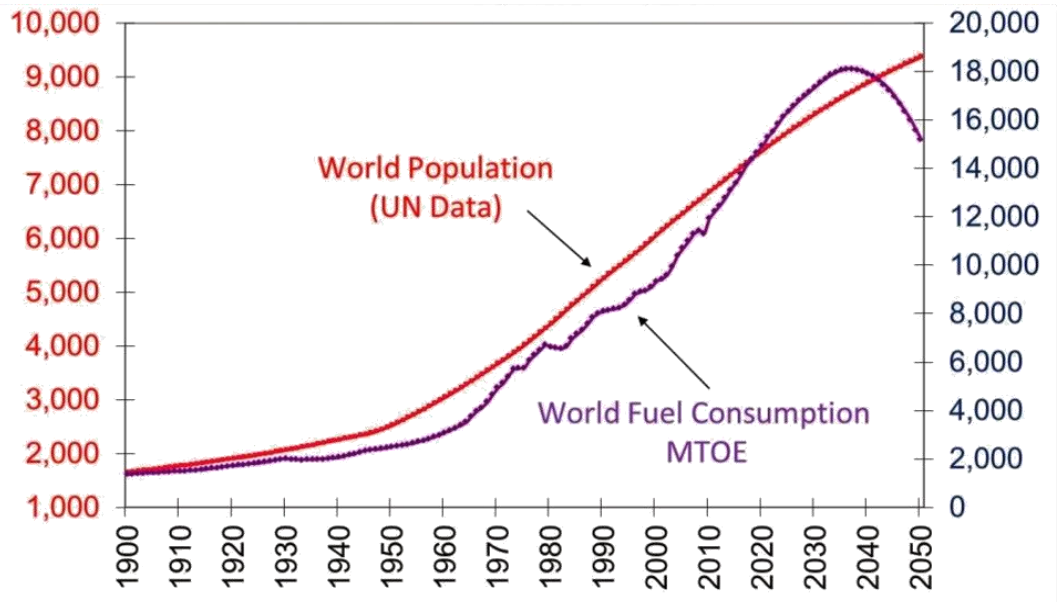

Figure 1.1 World fuel consumption and population 1900-2050. [2]

to a search for alternative and renewable sources of energy that would be economically efficient and environmentally sound. Wind, solar, nuclear and hydrogen are a promising alternative energy sources, but all of these resource currently have minimal application to the realm of transportation fuel. The transport sector is the largest energy consumers of petroleum fuels such as gasoline, diesel, liquefied petroleum gas (LPG) and compressed natural gas (CNG).

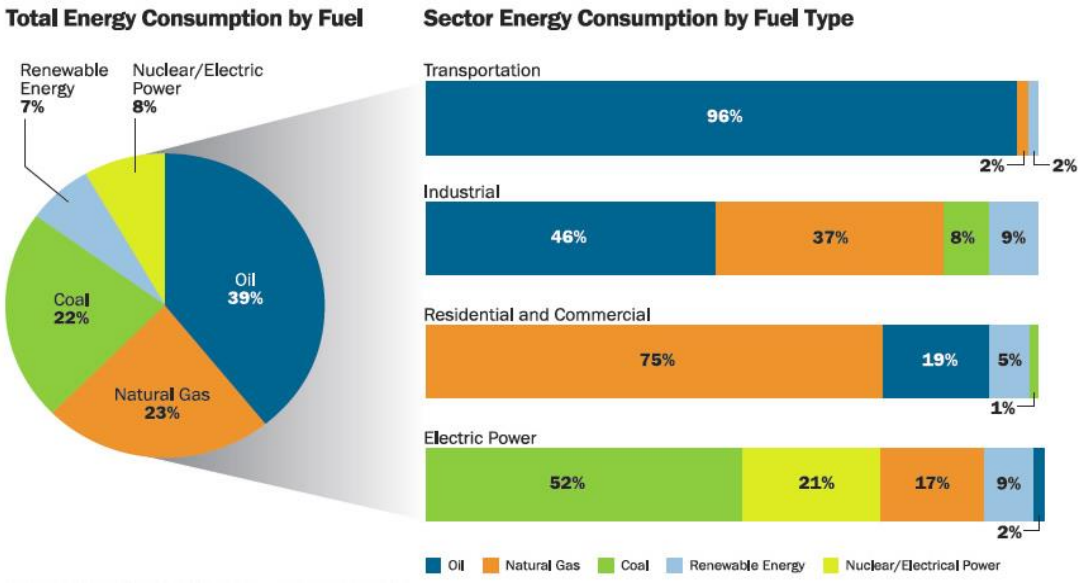

Figure 1.2 Total energy consumption by sector. [3]

According to the Annual Energy Outlook 2009 (AEO 2009) as shown in **Figure 1.2,** oil, natural gas and coal continue to be the most important primary energy sources and demand will continue to grow rapidly. Petroleum based oil was the dominant fuel source accounting for 39% share of the total global energy consumption followed by natural gas (23%) and coal (22%). Transport sector is the major consumer of oil products (96% of oil consumption) over 90% directed to fuels used in transportation is petroleum based, which includes gasoline and diesel. However, resource of these fossil fuels are

running out, prices of fuels are expected to rise. Moreover, the burning of fossil fuels is also a major producer of greenhouse gases (26% of greenhouse gas emissions from transportation). The emissions of CO_2 grew by 26% (1990) to 34% (2012) [4]. This contributes to rise in average temperature of the Earth's near-surface air and oceans. The environmental repercussions of fossil fuels and concerns about petroleum supplies have spurred interest in active search for renewable fuel sources.

1.2 Biofuels

Biofuel is a promising alternative clean fuels, which can replace for transportation fuels due to their ability to lower greenhouse gas emission, provide sustainable supplies of energy and create cleaner environments. In recent years biofuel production exhibits an increasing trend from about 60 billion liters during 2007 to 127.7 billion liters in 2014, with further dramatic increases in future [5]. The most widely used liquid biofuels for transport are bioethanol and biodiesel.

1.2.1 Bioethanol

Bioethanol is probably the most common alternative liquid fuel in the world. It can be produced by using biological production technology, which is fermentation and distillation of sugar or starch crops such as corn, sugarcane, or wheat crops. Bioethanol is mainly used in petrol engines as a replacement for gasoline; it can be blended with gasoline at concentration of 5 to 15 percent to allow more oxygen into the fuel mixture, resulting in more complete combustion and less polluting emissions. The world’s largest ethanol producers are the United States and Brazil. The USA, which produces ethanol primary from corn, and Brazil was ethanol from sugar cane, both countries are responsible for 89% of the world’s ethanol fuel production in 2009 [6].

1.2.2 Biodiesel

Biodiesel is a renewable fuel and clean-burning diesel replacement that physical properties are similar to those of petroleum diesel, as it has several advantages including high cetane number, high flash point, excellent lubricity, and extremely low sulfur emission comparing with the petroleum diesel [7,8]. Biodiesel is defined as mono-alkyl esters of long chain fatty acids derived from many feedstocks such as vegetable oils, palm oil, soybean, rapeseed, jatropha, sunflower, algae, animal fats, or waste cooking oils, Typically, biodiesel is produced by transesterification of the parent oil with an alcohol (typically methanol) and usually in presence of a catalyst (acids, alkalis, or lipase enzymes). In order to achieve as high yield of fatty acid methyl ester (FAME) product as 99.7% and generate glycerol as a by-product under mind reaction conditions. The overall reaction is shown in **Figure** 1.**3** [9,10].

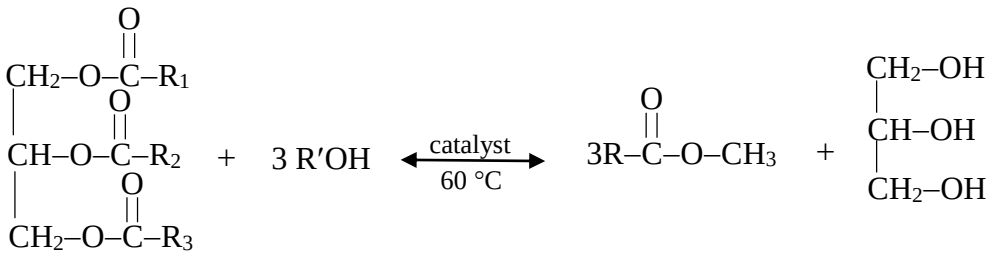

Figure 1.3 Transesterification of triglyceride to biodiesel

Biodiesel is produced, mainly in the European Union, which can be blended with petroleum diesel fuel in any proportion (The most common biodiesel blend is 20% biodiesel) or be used in its pure form is designated B100 (100% biodiesel) with minimal engine modification. However, many car manufactures are now designing cars so that they can run on B100 without any engine modification and the CO_2 emissions were reduced up to 60% for B100 compared to diesel [11]. According to biodiesel have oxygen present in their functional group, meaning it contains a reduced amount of carbon and higher hydrogen and oxygen content than regular diesel fuel, which contributes for its better combustion characteristics and reduces the particulate emissions from unburnt hydrocarbon [12]. However, there are some disadvantages associated with biodiesel including its lower energy density, higher viscosity, and poor oxidation stability. Moreover, biodiesel in particular, has higher freeze point and is unsuitable to use in the cold weather due to issues of crystalline of fuel particles at lower temperatures. Therefore, to improve the biodiesel properties, biodiesel need to be upgraded by remove oxygen in the biodiesel molecule.

Table 1.1 Diesel properties [13,14]

Properties	Petroleum diesel	Biodiesel	Renewable diesel
Cetane	40-55	50-65	75-90
Sulfur	<10 ppm	<5 ppm	<10 ppm
NO_x emission	Baseline	+10	-10 to 0
Energy density, MJ/kg	43	38	44
Density, g/ml	0.83-0.85	0.88	0.78
Cloud point, °C	-5	20	-10
Oxidative stability	Baseline	Poor	Excellent
Cold flow properties	Baseline	Poor	Excellent
Lubricity	Baseline	Excellent	Similar

1.2.3 Renewable diesel

As mentioned previously, the direct use of biodiesel as diesel fuel is not desirable due to engine compatibility problems. Therefore, several upgrading processes have been developed over the years to produce renewable diesel which is compliant with modern infrastructure. Renewable diesel, often called "green diesel" or "second generation diesel". It is not a fossil fuel. But it is made of nonpetroleum renewable resources such as natural fats, vegetable oils and greases. Renewable diesel, much like biodiesel, is a mixture of diesel-like hydrocarbons produced from various agricultural feedstocks by a catalytic reaction involving hydrodeoxygenation and decarboxylation/decarbonylation of triglycerides [15,16]. Although both biodiesel and renewable diesel are lipid-derived liquid transportation biofuels, but there are significant differences between them. Biodiesel is contained of alkyl ester molecules, while renewable diesel's main components are hydrocarbons. Therefore, renewable diesel does not contain oxygen

molecules, resulting in high energy density and heating value. Moreover, it has a similar properties like petroleum diesel (**Table 1.1**), such as higher cetane number, lower NO_x emission, and cloud point than biodiesel. Therefore, renewable diesel can be used to displace petroleum diesel in engines that are designed to run on conventional diesel fuel, with no blending required.

1.3 Technology for production of renewable diesel

1.3.1 Hydrodeoxygenation (HDO)

Hydrodeoxygenation reduces oxygen species by reacting triglycerides or fatty acids with high pressure of hydrogen to break all C-O bonds to form water and straight chained n-paraffins (**Figure 1.4**). HDO process is operated at moderate temperatures, between 250-400 °C, and under high hydrogen pressure, typically between 3.5 MPa to 15 MPa. The reaction rate of HDO is mainly determined by the activity of catalyst involved, different catalysts are essential for HDO reactions and have also led to significantly different product distributions. NiMo and CoMo sulfides catalysts supported on Al_2O_3 have been widely used for the HDO reactions [17,18]. This catalyst has a high activity and mild acidity which are also appropriate for the hydroconversion of triglycerides into diesel hydrocarbons [19]. It was found that the $NiMo/Al_2O_3$ catalyst has better HDO activity, having high selectivity toward diesel range products than $CoMo/Al_2O_3$ catalyst. In the literature, NiMo catalysts have often been used for the HDO of unsaturated acids such as fatty acids and resin acids. However, the catalyst has to be sulfide to maintain catalytic activity at relatively low temperatures because non–sulfided $NiMo/Al_2O_3$ exhibits a low activity and selectivity towards hydrocarbons [20,21].

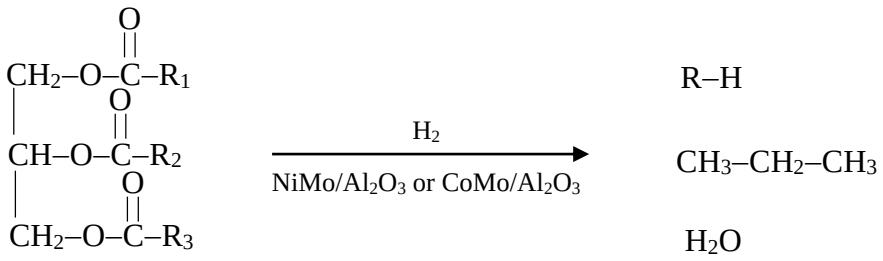

Figure 1.4 Hydrodeoxygenation of triglyceride

Recently, Liu et al. [22] studied the hydrotreatment process of vegetable oils by using Ni-Mo and solid catalysts in a fixed bed flow reactor system at 350 °C under hydrogen pressure of 4 MPa. Ni-Mo/SiO_2 catalyst favored the production of n-$C_{18}H_{38}$, n-$C_{17}H_{36}$, n-$C_{16}H_{34}$ and n-$C_{15}H_{32}$ hydrocarbons. These long normal hydrocarbons have a high melting point and thus the liquid hydrocarbon product has poor cold properties. While Ni-Mo supported on zeolites (H-Y or H-ZSM5), resulted in the production of a large amount of gasoline hydrocarbons due to strong acid sites of zeolites. When SiO_2-Al_2O_3 was used as a support, vegetable oil was converted from some n-paraffins (C_{15}-C_{18}) to iso-paraffins and the pour point of the liquid hydrocarbon was similar to those of a normal diesel. Sotelo-Boyás et al. [17] produced diesel hydrocarbons from rapeseed oil by hydrotreating on three different types of bifunctional catalysts: Pt/H-Y, Pt/H-ZSM5, and sulfided NiMo/γ-Al_2O_3 in a batch reactor at reaction temperature range of 300 to 400 °C and initial hydrogen pressures from 5 to 11 MPa. Among the three different types of catalysts, the Ni-Mo/γ-Al_2O_3 catalyst gave the highest yield of liquid hydrocarbons containing mainly n-paraffins from C_{15} to C_{18}, and therefore with poor cold flow properties. While, both Pt-zeolites-supported catalysts had a strong cracking activity because of their strong acid sites, lead to favor producing *iso*-paraffins than *n*-paraffins in the boiling range of C_5 to C_{22} (green gasoline and green diesel), which are desirable for

the diesel to have a low pour point. Therefore, it is necessary to moderate the acidity of the zeolite catalysts to increase the isomerization activity while keeping a moderate cracking.

However, for sulfur-free feedstocks such as bio-oils, the sulfided catalysts are unstable, and the feed needs to be added sulfur to compensate for the sulfur loss. Addition of sulfur is undesired because the product can be contaminated by sulfur-containing species. There has therefore been research of using noble metals and other sulfur-free metals as HDO catalysts.

Liu et al. [23] have been tested ruthenium catalyst supported on different of supporting: Ru/Al_{13}-Mont (Al-polyoxocation-pillared montmorillonite), Ru/SiO_2, and Ru/H-Y by hydrotreatment of waste cooking oil at 350 °C and 2 MPa. Ru-H-Y gave a large amount of gasoline-ranged paraffins. While, Ru-SiO_2 catalyst had a long chain of normal hydrocarbon, but had a high pour point of 20 °C. When Al_{13}-Mont was used as a support, the pour point of the liquid hydrocarbon decreased to -15 °C with the conversion of C_{15}-C_{18} *n*-paraffins to *iso*-paraffins and light paraffins, which the physical properties are similar to those of commercial petro-diesel. Kikhtyanin et al. [24] studied the single-stage hydroconversion of sunflower oil over a bifunctional catalyst: Pd supported on Silico-alumino-phosphates (Pd/SAPO-31) to produce hydrocarbons in the diesel fuel range. Transformation of sunflower oil was performed at temperatures range of 310 to 360 °C under a pressure of 2.0 MPa with WHSV of 0.9 to 1.6 h^{-1}. The concentration of hydrocarbons at temperatures between 320- 350 °C, the liquid phase product contained of C_{17} and C_{18} *n*-alkanes and *i*-alkanes. The Pd/SAPO-31 catalyst demonstrated a high initial activity for the one-stage hydrocarbon conversion and good isomerization activity, but its deactivation occurred after several hours of operation. Murata et al. [25] produced renewable green diesel-type alkanes by hydrotreating of jatropha oil with Pt/H-ZSM5 and

rhenium-modified Pt/H-ZSM5 catalysts at standard conditions (i.e. 270-300 °C, 2 MPa). The non-modified Pt/H-ZSM5 catalyst was not effective to produce a high conversion of C_{15}-C_{18} alkanes at high oil/catalyst ratios. Rhenium-modified Pt/H-ZSM5 catalysts were found to be much more effective for hydrotreating of jatropha oil even at a high oil/cat ratio of 10, and 80% conversion and 70% selectivity to C_{18} were achieved.

However, expensive operating conditions such as a high hydrogen pressures is often required for complete conversion.

1.3.2 Decarboxylation-Decarbonylation (DCO)

In contrast with HDO, decarboxylation and decarbonylation can take place even in the absence of H_2 gas under mild heating. Decarboxylation is a chemical reaction in which removes a carboxyl group (-COOH) by the carbon–carbon bond cleavage, releasing CO_2 and producing n-alkanes, whereas, decarbonylation refers to a reaction of carboxylic acids, removing oxygen in the form of CO, water and producing n-alkene. The general equation for a decarboxylation/decarbonylation reactions as presented in **Figure 1.5**. [26].

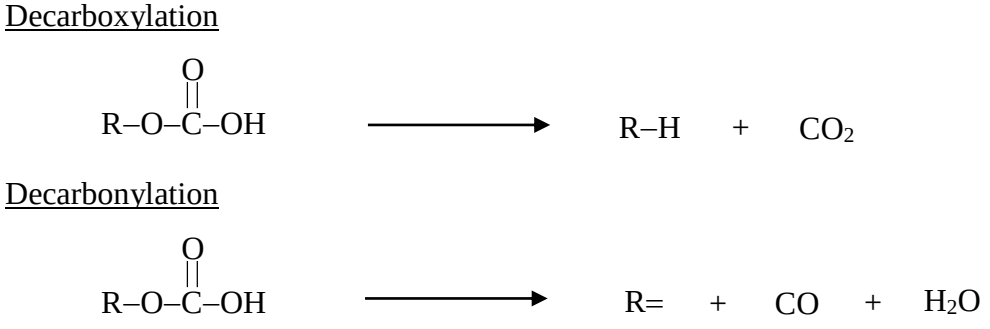

Figure 1.5 Decarboxylation and decarbonylation of fatty acids

1.4 Catalysts for decarboxylation

1.4.1 Noble metal catalysts

Recent studies of catalytic decarboxylation of fatty acids were published by the Murzin et al. [27-37]. Various metals Ni, Ru, Ir, Pd, Pt, Rh and Os on supports like Raney-Ni, Al_2O_3, SiO_2, Cr_2O_3, MgO and activated carbons were screened in the decarboxylation of stearic acid under He atmosphere at 300 °C and 6 bars pressure. The results revealed that palladium supported over active carbon showed superior activity and selectivity to towards n-heptadecane (C_{17}) by decarboxylation and yielding of CO_2 in comparison to platinum on active carbon which was more selective towards decarbonylation yielding high amounts of CO. The initial reaction rate was the highest for 5wt% of Pd/C, which showed the best performance. With Ru/C and Rh/C catalysts, it was observed that their selectivity toward unsaturated products was higher, which resulted in their deactivation [36]. Subsequent studies by Murzin's group investigated liquid phase deoxygenation of different free fatty acids (C12:0, C16:0, C17:0-C20:0 and C22:0) varying in chain length under inert atmosphere (He) and mixture of H_2 and He over Pd/C catalyst. It was noted that, under inert atmosphere (He) the catalyst deactivated quickly after initially showing a high activity selective towards decarboxylation. The deactivation was attributed to coke formation on the surface of catalyst. Use of a mixture of H_2 and He as the carrier gas instead of only He, extended the catalyst activity and maintained a high deoxygenation rate, suggesting that H_2 helps to prevent coking of the catalyst [28, 38]. However, presence of high partial pressure of H_2 or CO in the system inhibits the decarboxylation pathway and favors decarbonylation reaction which consumes H_2 [26].

1.4.2 Basic metal oxides

Zhang et al. [39] investigated the decarboxylation of aromatic acids using naphthoic acid over series of alkaline-earth metal oxides such as CaO, MgO, SrO, and BaO. All of these oxides showed high catalytic activity in naphthoic acid conversion by 55 to 95%. CO_2 formation was observed only in magnesium oxide, yielding 18%. Tani et al [40] studied the catalytic cracking of palm oil and other triglyceride to overcome middle-distillate range hydrocarbons over MgO–supported catalyst. The results revealed that MgO–supported catalyst promoted decraboxylation, which was the mixture of straight chain and branched chain structure of olefins and paraffins, which were assumed to be derived from the dehydration of glycerol and the decarboxylation of ester or the free acid which is followed by the C–C bond dissociation. The supported MgO promoted the formation of CO_2 and the suppression of free acid formation. Khromova et al. [41] studied the effect of dopants on the activity and stability of magnesium-containing catalysts in decarboxylation of bio-oil. The MgO containing 10 wt% ZrO_2, SiO_2 and Al_2O_3 were prepared by introducing an oxide (zirconium nitrate) into the aqueous suspension of magnesium oxide. The mixed suspension was dried at room temperature for 24 h and calcined at 1200 °C for 2 h. The process has been carried out in a fixed-bed flow reactor at a temperature of 350 °C in an inert (argon) atmosphere at pressures of 0.32-0.50 MPa and a reactant hourly space velocity of 1.5-2.5 h^{-1}. Results showed that the major products of the reaction are dibutyl ketone, CO_2 and water for all the catalysts. The MgO-SiO_2 affords the highest reactant conversion and CO_2 yield. In this process magnesium oxide containing a stabilizer are mainly deactivated through the formation of carbonates rather than the formation of soluble magnesium salts. Watanabe et al. [42] have studied the catalytic decarboxylation of stearic acid with alkaline hydroxide (KOH and NaOH) and metal oxides (CeO_2, Y_2O_3 and ZrO_2) in supercritical water. The major products of this

reaction were n-heptadecane, n-hexadecane and CO_2. As a consequence, ZrO_2 showed the highest activity with approximately 68% and 9% for conversion of stearic acid and yield of CO_2, respectively.

1.5 Catalyst supports

Generally, chemical manufacturing processes employ catalysts in order to increase the reaction rate and control the selectivity to the desired products. The activity of a catalyst depends not only on its chemical composition, but other factors can also be important, such as surface area, porosity, pore size and suitable physical properties. Therefore, the supported catalyst has been successfully used in the chemical industries for some time. The purpose of the support is to keep the active phase of the catalyst material in a highly dispersed state maximize reaction rates and to provide a stable platform for reactions in a chemical process. Additional benefits of a support include: dissipation of reaction heat and improved poisoning resistance.

The catalyst- support surface interaction is significantly important because it has an effect on the catalytic activity. For example, sulfide metal catalysts supported on alumina (γ-Al_2O_3), which is employed in HDS processes, can effectively disperse large amounts of metal sulfides. However, the HDS activity is reduced because of the strong interactions between the transition metal oxides and the γ-Al_2O_3 support. Therefore, a much more inert support could be more suitable for sulfide catalysts. There are several parameters that must be considered in choosing a suitable support: surface area, porosity, inertness, stability, physical form and mechanical properties. The support should also help inhibit undesirable reactions. The high surface area of a support may also enhance the catalytic activity or affect diffusion rates of reactants and products. However, high surface area is not always desirable. For instance, porous structures and the pore size of the

catalyst are very essential in terms of accessibility. While large pores favor gas-liquid heterogeneous catalysis which has a slow diffusion in the liquid phase, small pore and particle size increase the number of possible active sites. This is the main reason why the porous structure and the pore size distribution should be modified.

Because of these factors, there are four catalyst support materials that are typically considered as an optimum support for catalytic decarboxylation applications utilized in new hydrocarbon biodiesel production: alumina, silica, zirconium oxide and activated carbon.

Alumina (Al_2O_3) is one of the most material widely used as a support for transition metal catalysts because of its excellent thermal and mechanical stability. Alumina can exist in several structures, and the most common structure of alumina is widely used as a support catalyst: α-Al_2O_3 and the porous amorphous γ-Al_2O_3. α-Al_2O_3 is used in high temperature processes, such as steam reforming, and where low surface areas are desired. γ-Al_2O_3 can be used as a catalyst without metal particles in the Claus process (production of elemental sulfur from H_2S), alkylation of phenol and dehydration of formic acid [43]. It has high surface areas, 50−300 m^2g^{-1}, mesopores between 5 and 15 nm and pore volumes of 0.6 cm^3g^{-1}. γ-Al_2O_3 can also be shaped into mechanically stable extrudates and pellets.

Silica (SiO_2) is mainly used in processes below 300°C, such as hydrogenations, polymerizations and oxidations. SiO_2 has a relatively low thermal stability, and at higher temperatures, silica can form volatile hydroxides. It is easy to adjust the properties of SiO_2, such as pore size, particle size and surface area. SiO_2 supports are amorphous, but can still exhibit some local order similar to the mineral β-crystoballite. The surface area can range up to 300 m^2g^{-1}, the pore diameter 7 nm and above and does not contain micropores.

Zirconia (ZrO_2) is an oxide with a high thermal stability with both acid and base properties. It is also stable under reduced pressure and reducing atmosphere. There are three stable crystalline modifications of zirconia, the monoclinic, tetragonal and cubic phases. A monoclinic structure is stable up to 1200 °C. In this temperature, monoclinic was transformed into the tetragonal phase, tetragonal structure is stable up to 1800 °C. Above 1800 °C, this transformed into cubic phase and had stability until end of solid state at melting point 2700 °C. Due to the martensitic nature of the transformations, neither the high temperature tetragonal nor cubic phase could be instantaneously quenched to room temperature but still could observe tetragonal phase zirconia as metastable phase or thermodynamical phase. This was not the expected behavior according to the phase diagram of zirconia. Many parameters were offered that played a role for this metastable phase such as chemical effects, structural similarities between the tetragonal phase and the precursor amorphous phase as well as particle size effects based on the lower surface energy in the tetragonal phase compared to monoclinic phase. A metastable phase still could completely transform into monoclinic phase when annealed at temperature about 650-700 °C, is frequently used as catalyst supports.

Activated carbon is defines a materials with a high degree of internal surface area and porosity and hence a large capacity for adsorbing chemicals from gases and liquids. Carbon supports have several benefits in catalytic reactions such as its resistance to acidic/basic atmospheres, its flexibility of being more / less hydrophilic based on the preparation method and the precursor, and the ease of recycling the used expensive metal catalysts by burning away the carbon support [44]. The adsorption on the surface is essentially due to Van der Waals or London dispersion forces. This force is strong over short distances, equal between all carbon atoms and not dependent on external parameters such as pressure or temperature. Thus, adsorbed molecules will be held most strongly

where they are surrounded by the most carbon atoms. The area presenting a high density of graphitic basal structural units will favor a high adsorption. High temperature treatment (>1200 °C) of AC can favor the adsorption sites by increasing the density of "π-sites" present on partly graphitized structure. The most commonly used raw materials always are biological in nature. For example, carbon derived from coconut shells, wood (both soft and hard), peat, coal, and petroleum based residues or agricultural residues [44]. While activated carbon usually has a BET surface area around 1000 m^2 g^{-1}, some highly activated carbon can be as high as 3000 m^2 g^{-1}. Active carbon is manufactured from suitable precursors in two ways: chemical activation and physical activation. In the same way, the manufacture of AC involves two main stages, the carbonization of the starting material and the activation of the resulting char. The choice of the activation method is dependent upon the starting material and whether a low or high density, powdered or granular carbon is desired [45]. Activated carbon can be classified into three groups depending on their pore sizes: micro-porous (less than 2 nm), mesa-porous (2 - 50 nm), and macro-porous (more than 50 nm) [46]

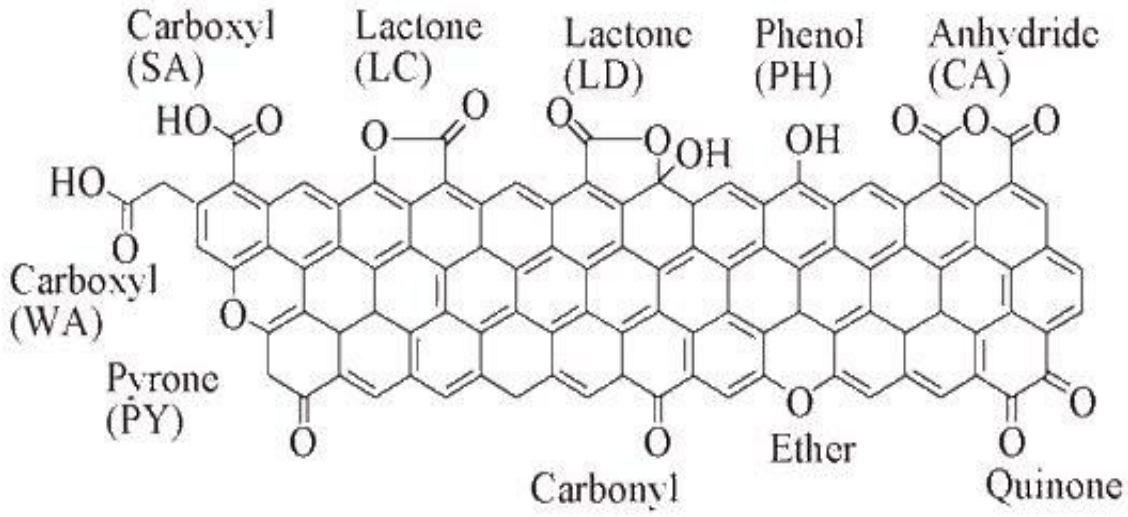

Figure 1.6 Functional groups in active carbon [47]

1.6 Purpose of this study

Most of the research work on decarboxylation of fatty acids has been done with noble metal-based catalysts (Pd/C, Pt/C or Rh/C) to produce renewable diesel. However, considering the high cost of above noble metals, it is more practical in industrial standpoint to develop the cheaper catalysts which showing similar performance and stability. It has been reported that MgO displayed near performance comparable with precious metal catalyst. Nevertheless, MgO exhibits a poor CO_2 adsorption capacity due to its low surface area and pore volume. Therefore, the purpose of this thesis is to develop an MgO-based catalyst with high activity and stability for the production of new hydrocarbon biodiesel by catalytic decarboxylation of triglycerides and their derivatives in waste cooking oil.

Moreover, in Japan, more than 90% of cooking oil was imported from other countries because the amount of flat land available for cultivation is limited. The 59% of total Japanese vegetable and seed oil were canola (40%) and soy (19%). Nine percent of oils from rice bran (3%), corn (3%), sesame (2%) and safflower (1%). The consumption of cooking oil from food industry and ordinary households was about 2.3 million tons, which generated 20% (about 460,000 tons) waste cooking oil. The Government of Japan (GOI) maintains its plan to recycle waste cooking oil into biodiesel which is an effective way to reduce the raw material cost and solve the problem of waste oil disposal. So waste cooking oil is a promising resource as a raw material for produced hydrocarbon biodiesel.

Generally, catalysts are a combination of an inert support to increase the active surface sites and improved poisoning resistance. Moreover, the high surface area of a support may also improve the catalytic activity or affect diffusion rates of the reactants and products. Therefore, the decarboxylation activity of MgO-based catalysts supported on different supports (γ-Al_2O_3, SiO_2, ZrO_2 and active carbon) for the production of new

hydrocarbon biodiesel from waste cooking oil was investigated. The physical properties, decarboxylation activity, selectivity toward to diesel range product and stability were considered in selecting a suitable support for MgO-based catalyst. In addition, the coke deposition on the surface of all catalysts was also investigated.

In many instances, addition of metal oxide results in the modification of the catalytic properties of the single-component metal oxides. In this study, the effect of the addition of metal oxide to magnesium oxide supported on silica and active carbon was investigated. The high CO_2 capture capacities of CaO and high oxygen vacancies of ZrO_2 were selected as the metal oxide to improve CO_2 adsorption properties of MgO-based catalyst by investigated the CO_2 formation, durability and selectivity toward to hydrocarbon in diesel fraction.

References

[1] J. Van Gerpen, Fuel Process. Technol. 86 (2005) 1097.

[2] The Cultural Economist, Peak Energy (2014), http://tceconomist.blogspot.fi/2014/05/peak-energy.html

[3] Annual Energy Outlook (AEO), 2009. Available from http://blog.fuelclinic.com/2009/06/22/breakdown-oils-monopoly-in-transportatio/

[4] Ontario's Climate Change Report, 2014. Available from https://dr6j45jk9xcmk.cloudfront.net/documents/3618/climate-change-report-2014.pdf

[5] Renewables Global Status Report, 2015. Available from http://www.ren21.net/wp-content/uploads/2015/07/REN12-GSR2015_Onlinebook_low1.pdf

[6] European Biomass Industry Association. http://www.eubia.org/index.php/about-biomass/biofuels-for-transport/bioethanol

[7] B. Smith, H.C. Greenwell, and A. Whiting, Energy & Environmental Science, vol. 2, pp. 262, 2009.

[8] C. C. Akoh, S.W. Chang, G.C. Lee, and J.F. Shaw, Journal of Agricultural and Food Chemistry, vol.55 (22), pp. 8995-9005, 2007.

[9] H. Fukuda, A. Kondo, and H.J. Noda, Journal of Bioscience and Bioengineering, vol.92, pp. 405-416, 2001.

[10] A.A. Mohamed, E.A. Gordon and H. Li, American Journal of Engineering Research, vol. 3 (11), pp. 290-298, 2014.

[11] D.A. Guerrieri, P. J. Caffrey, and V. Rao, Society of Automotive Engineers, 400 Commonwealth Drive Warrendale, PA, 15096, USA: 1995.

[12] A.B. Taylor, D.P. Moran, A.J. Bell, N.G. Hodgson, I.S. Myburgh, and J.J. Botha, Special Publications – SAE International, vol. 1208, pp. 135-152, 1996.

[13] T. Kalnes, T. Marker, D.D. Shonnard, and K. Koers, 1st Alternative Fuels

Technology Conference 18 Feb. 2008. Web-page.

http://www.uop.com/renewables/Presentations/Green_Diesel_AFTC_Kalnes%20rev2.pdf

[14] “Properties of Fuel”

http://www.afdc.energy.gov/afdc/pdfs/fueltable.pdf

[15] S.K. Hoekman, Renewable Energy, vol. 34, pp. 14-22, 2009.

[16] I. Simakova, O. Simakova, P. Maki-Arvela, and D.Y. Murzin, Catalysis Today, vol. 146, pp. 16-171, 2009.

[17] J. Ancheyta, F. Trejo, and M.S. Rana, CRC Press, Taylor & Francis, 2009.

[18] T. Makoto, A. Yohko, K. Hidetoshi, O. Masahiro, T. Mochizuki, and Y. Yoshimura, Catalysis Today, vol. 164, pp. 533-537, 2011.

[19] R. Sotelo-Boyás, Y. Liu, and T.Minowa, Industrial & Engineering Chemistry Research, vol. 50 (5), pp. 2791-2799, 2010.

[20] E.M. Ryymin, M.L. Honkela, T.R. Viljava, and O.I. Krause, Applied Catalysis A: General, vol. 358, pp. 42-48, 2009.

[21] O. Şenol, T.R. Viljava, and O. I. Krause, Applied Catalysis A: General, vol. 326, pp. 236-244, 2007.

[22] Y. Liu, R. Sotelo-Boyás, K. Murata, T. Minowa, and K. Sakanishi, Energy & Fuels, vol. 25, pp. 4675-4685, 2011.

[23] Y. Liu, R. Sotelo-Boyás, K. Murata, T. Minowa, and K. Sakanishi, Catalysts, vol. 2 (1), pp. 171-190, 2012.

[24] O.V. Kikhtyanin, A.E. Rubanov, A.B. Ayupov, and G. Echevsky, Fuel, vol. 89 (10), pp. 3085-3092, 2010.

[25] K. Murata, Y. Liu, M. Inaba, and I. Takahara, Energy Fuels, vol. 24 (4), pp. 2404-2409, 2010.

[26] J. Immer, M.J. Kelly, and H.H. Lamb, Applied Catalysis A: General, vol. 375, pp. 134-139, 2010.

[27] M. Snare, P. Maki-Arvela, I.L. Simakova, J. Myllyoja, and D.Y. Murzin, Russian Journal of Physical Chemistry B, vol. 3, pp. 1035-1043, 2009.

[28] I. Simakova, O. Simakova, P. Maki-Arvela, A. Simakov, M. Estrada, and D.Y. Murzin, Applied Catalysis a-General, vol. 355, pp. 100-108, 2009.

[29] S. Lestari, P. Maki-Arvela, I. Simakova, J. Beltramini, G.Q.M. Lu, and D.Y. Murzin, Catalysis Letters, vol. 130, pp. 48-51, 2009.

[30] S. Lestari, P. Maki-Arvela, H. Bernas, O. Simakova, R. Sjoholm, J. Beltramini, G.Q.M. Lu, J. Myllyoja, I. Simakova, and D.Y. Murzin, Energy & Fuels, vol. 23, pp. 3842-3845, 2009.

[31] M. Snare, I. Kubickova, P. Maki-Arvela, D. Chichova, K. Eranen, and D.Y. Murzin, Fuel, vol. 87, pp. 933-945, 2008.

[32] P. Maki-Arvela, M. Snare, K. Eranen, J. Myllyoja, and D.Y. Murzin, Fuel, vol. 87, pp. 3543-3549, 2008.

[33] S. Lestari, I. Simakova, A. Tokarev, P. Maki-Arvela, K. Eranen, and D.Y. Murzin, Catalysis Letters, vol. 122, pp. 247-251, 2008.

[34] M. Snare, I. Kubickova, P. Maki-Arvela, K. Eranen, J. Warna, and D.Y. Murzin, Chemical Engineering Journal, vol. 134, pp. 29-34, 2007.

[35] P. Maki-Arvela, I. Kubickova, M. Snare, K. Eranen, and D.Y. Murzin, Energy & Fuels, vol. 21, pp. 30-41, 2007.

[36] M. Snare, I. Kubickova, P. Maki-Arvela, K. Eranen, and D.Y. Murzin, Industrial & Engineering Chemistry Research, vol. 45, pp. 5708-5715, 2006.

[37] I. Kubickova, M. Snare, K. Eranen, P. Maki-Arvela, and D.Y. Murzin, Catalysis Today, vol. 106, pp. 197-200, 2005.

[38] J.G. Immer, and H.H. Lamb, Energy & Fuels, vol. 24 (10), pp. 5291-5299, 2010.

[39] A. Zhang, Q. Ma, K. Wang, X. Liu, P. Shuler, and Y. Tang, Applied Catalysis A: General, vol. 303, pp. 103-109, 2006.

[40] H. Tani, M. Hasegawa, K. Asami, and K. Fujimoto, Catalysis Today, vol. 164, pp. 410-414, 2011.

[41] S.A. Khromova, A.A. Smirnov, S.A. Selishcheva, R.G. Kukushkin, V.O. Dundich, L.I. Trusov, and V.A. Yakovlev, Biocatalysis, vol. 5, pp. 260-268, 2013.

[42] M. Watanabe, T. Iida, and H. Inomata, Energy Conversion and Management, vol. 47, pp. 3344-3350, 2006.

[43] I. Chorkendorff, and J. Niemantsverdriet, Concepts of Modern Catalysis and Kinetics; WILEY-VCH GmbH & Co. KGaA Weinheim, 2007.

[44] E. Arnold, Porosity in Carbons; Hodder Headline Group, London, 1995.

[45] S. Philippe, and M. Bruno, Royal Society of Chemistry Catalysis, vol. 23, 2015.

[46] K.S.W. Sing, D.H. Everett, R.A.W. Haul, L. Moscou, R.A. Pierotti, J. Rouquerol, and T. Siemieniewska, Pure and Applied Chemistry, vol. 57, pp. 603-619, 1985.

[47] N. Li, J, Zhu, and Q.F. Zha, Chemical Journal of Chinese University, vol. 33, pp. 548-554, 2012.

CHAPTER 2

Effect of Support Materials on MgO-Based Catalyst for Production of New Hydrocarbon Bio-Diesel

Abstract: The catalytic-decarboxylation of waste cooking oil was carried out over 10 wt% MgO catalysts supported on different supports, γ-Al_2O_3, ZrO_2, SiO_2, and active carbon. The prepared catalysts were characterized by BET, XRD, FE-SEM and TGA. The results of XRD and BET indicated that the obtained catalysts were highly dispersion on the support with large specific surface area. The catalytic-decarboxylation performance of catalysts was investigated by the CO_2 yield and carried out in an agitated reactor under inert gas for 7 h at 430 °C. The triglycerides in waste cooking oil were converted into a mixture of hydrocarbons, CO, CO_2 and water by breaking C-C and C-O bonds by direct decarboxylation and subsequent cracking. The supported MgO-based catalysts showed high catalytic activity and could convert triglycerides to long chain hydrocarbons in diesel specification range (C_{10}-C_{20}). In the case of 10M/AC catalyst, the addition of ZrO_2 exhibited an inhibitor the coke formation on the catalyst surface, due to surface oxygen vacancies, which help gasify the carbon that deposit on the surface of the catalyst.

2.1 Introduction

Biodiesel is renewable and clean-burning fuel that is made through a chemical process which converts vegetable oils or animal fats into fatty acid methyl esters (FAME)[1]. However, the high oxygen content in the ester component limits their application for vehicle fuels due to their unfavorable cold flow properties (CFPP-cold filter plugging point: >25°C) and poor storage (oxidation and heat stability) of fatty acid esters[2,3]. Therefore, increasing attentions have moved towards catalytic deoxygenation processes in which oxygen is eliminated mostly as H_2O or CO_x. Of these deoxygenation methods, hydrodeoxygenation (HDO) via hydrotreating catalysts such as NiMo and CoMo-based sulfide catalysts are normally used to convert vegetable oils to liquid hydrocarbon as the following equation (2.1). On the other hand, the requirement of hydrogen is the main drawback of this method as well as sulfide catalysts which can contaminate the products and become deactivated in the presence of water [4-6].

Hydrodeoxygenation

$$R\text{–}COOH + 3H_2 \longrightarrow R\text{–}CH + 2H_2O \qquad (2.1)$$

In view of this, alternative method in which deoxygenation is achieved by decarboxylation of fatty acids or derivatives have been reported[7-19]. In decarboxylation, the hydrocarbon chain in fatty acid is inert towards catalyst surface, whereas the carboxylic group is adsorbed on the catalyst surface resulting in the removal of the carboxylic group through C-C cleavages to release CO_2 (and possibly carbonyl group through C-C and C-O cleavages to release CO) as the following equations (2.2) and (2.3), thereby the formation of hydrocarbon production exhibited one carbon less than the

original fatty acid chain.

Decarbonylation

$$R–COOH + H_2 \longrightarrow R–H + CO + H_2O \quad (2.2)$$

Decarboxylation

$$R–COOH \longrightarrow R–H + CO_2 \quad (2.3)$$

The most active catalysts such as Pd, Pt and Rh were found to be effective in catalyzing the deoxygenation reaction [20,21]. However, the high cost of these noble metals represents an important drawback from an economic standpoint, which leads to search for a cheaper catalyst. In previous work we have demonstrated that a typical basic metallic oxide, MgO displayed near performance comparable with precious metal catalyst in the upgrading of triglycerides and fatty acids to hydrocarbons[22-24]. Zhang et al. [25] investigated the decarboxylation of aromatic acids using naphthoic acid over series of alkaline-earth metal oxides such as CaO, MgO, SrO, and BaO. All of these oxides showed high catalytic activity in naphthoic acid conversion by 55 to 95%. CO_2 formation was observed only in magnesium oxide, yielding 18%. In spite these promising results, MgO exhibits a poor CO_2 adsorption capacity due to its low surface area and pore volume. As a result, many studies were conducted to improve the activity of MgO. It is well known that the supports could be improved the performance of the catalysts since the major roles of them are to prepare and preserve the capability to stabilize metal particles against thermal sintering as well as well-dispersed catalytic phases during the reaction. In literature, the high surface area supports are widely often used to enhance the activity for various catalysts such as γ-alumina, silica, active carbon, cerium oxide and zirconia. CeO_2

and ZrO_2 have proved to be catalyst supports with high oxygen storage capability which would improve catalytic performance and solve sintering problem of MgO catalysts.

Therefore, the aim of this work is to investigate the influence of the nature of support, namely γ-Al_2O_3, SiO_2, ZrO_2 and AC and the effect of the addition of zirconia to MgO supported on active carbon on catalytic performance in the catalytic cracking-decarboxylation of waste cooking oil.

2.2 Experimental

2.2.1 Catalyst preparation

MgO supported on different support materials

The magnesium oxide catalysts supported on different supports were prepared by the incipient wetness impregnation method, with aqueous solution of magnesium nitrate hexahydrate ($Mg(NO_3)_2.6H_2O$, 99.0% purity, Wako, Japan). A commercial γ-alumina (S_{BET} = 225 m^2/g and PV = 0.494 cm^3/g), silica (S_{BET} = 259 m^2/g and PV = 1.02 cm^3/g), zirconium oxide (S_{BET} = 15 m^2/g and PV = 0.01 cm^3/g) and active carbon (S_{BET} = 813 m^2/g and PV = 0.638 cm^3/g) were used as the supports in this study. The supports were initially dried at 110 °C overnight to remove adsorbed moisture. Magnesium nitrate hexahydrate was dissolved in the deionized water and then added dropwise into the supports. After the impregnation, the impregnated samples were evaporated at 40 °C and then dried in an oven at 110 °C overnight followed by calcined at 500 °C for 3 h. The total MgO loading was 10wt% for all of the supports. The catalysts were denoted as $10M/Al_2O_3$, $10M/SiO_2$, $10M/ZrO_2$ and 10M/AC.

The addition of ZrO_2 to MgO/AC

The magnesium oxide supported on active carbon catalysts with the addition of ZrO_2 (10 wt% and 20wt%) were prepared by the incipient wetness impregnation method, with aqueous solution of magnesium nitrate hexahydrate ($Mg(NO_3)_2.6H_2O$, 99.0% purity, Wako, Japan) and zirconyl nitrate dihydrate ($ZrO(NO_3)_2.2H_2O$, 97.0% purity, Wako, Japan). A commercial active carbon (S_{BET} = 813 m^2/g and PV = 0.638 cm^3/g) was used as the support. The active carbon was initially dried at 110 °C overnight to remove

adsorbed moisture. Magnesium nitrate hexahydrate and zirconyl nitrate dihydrate were mixed in the deionized water and then added dropwise into the active carbon. After the impregnation, the impregnated samples were evaporated at 40 °C and then dried in an oven at 110 °C overnight followed by calcined in N_2 flow at 500 °C for 3 h. The total MgO loading was 5wt% for all of the catalysts and ZrO_2 loading was 10 and 20wt%. The catalysts were denoted as 5M10Z/AC and 5M20Z/AC.

2.2.2 Catalyst characterization

The specific surface area, pore volume and pore diameter of the fresh and spent catalysts were determined by N_2 adsorption-desorption measurements using a BELSORP-mini II instrument (Japan Bel Inc.). The spent catalysts were heated at 250 °C for 3 h to remove any trace oils that may have accumulated on the catalyst pores. Before analyzing, the catalysts were degassed at 200 °C for 2 h in order to remove the moisture adsorbed on the surface. Catalyst surface area was calculated using the Brunauer, Emmett and Teller (BET) method, total pore volume was determined by measuring the volume of adsorbed gas at a P/P_0 of 0.99, and pore size distribution were obtained using the Barrett-Joyner-Halenda (BJH) method. The powder X-ray diffraction (XRD) patterns of the fresh and spent catalysts were obtained using a RIGAKU, XRD-DSC-XII diffractometer via CuKα as the radiation source (λ = 1.54 Å) at running conditions for the X-ray tube 40 kV and 20 mA at room temperature. Diffraction patterns were collected from 10° to 80°. Surface morphologies of both fresh and spent catalysts were performed using a Hitachi S5200 field emission scanning electron microscope (FE-SEM) operated at 20.0 kV. The amount of coke on the spent catalysts was measured using the simultaneous thermogravimetric (TG) and differential thermal analysis (DTA) . Around 5 mg of spent catalyst was placed

in a platinum crucible that was introduced in a RIGAKU TG-DTA 8210. The spent sample was heated under air flow (50 mL/min) from room temperature up to 900 °C at heating rate of 10 °C/min.

2.2.3 Catalyst testing

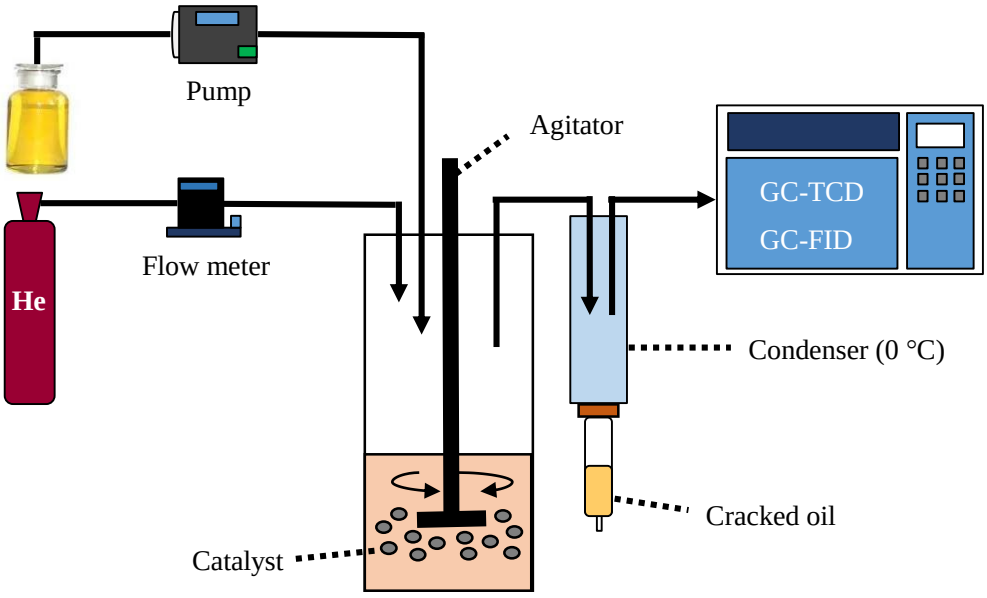

Figure 2.1 Reaction apparatus for catalytic decarboxylation

Reaction experiments for evaluating catalytic performance were performed in an agitated reactor system at 430 °C under atmospheric pressure as shown in **Figure 2.1**. Catalyst was charged into the reactor and was heated up to 430 °C at the same time of a carrier gas He at a flow rate 50 mL/min. The waste cooking oil was supplied from the university restaurant was fed continuously at a rate 0.25 mL/min. The gaseous products exiting the reactor were cooled and condensed at 0 °C. The uncondensed gaseous products were analyzed every 30 min by a GC-TCD and a GC-FID on line (Shimadzu GC-14A). The liquid trap product was analyzed carbon number distribution by GC-MS (*Agilent GC-*

7980A). Total acid value of the product oil was measured by potentiometric titration methods according to JIS 2501-2003. The product selectivity could be calculated by using the calculation equation listed below:

$$\text{Selectivity (C\%)} = \frac{C\ atoms\ in\ each\ product}{Sum\ of\ C\ atom\ in\ all\ the\ product} \times 100\% \qquad (2.4)$$

2.3 Results and Discussion

2.3.1 Catalyst characterization

Table 2.1 Textural properties of the catalysts

Catalysts	Fresh			Spent		
	S_{BET} (m^2g^{-1})	V_{Total} (cm^{3g-1})	D_{Pore} (nm)	S_{BET} (m^2g^{-1})	V_{Total} (cm^3g^{-1})	D_{Pore} (nm)
10M/ZrO_2	6	0.04	23.77	23	0.03	4.95
10M/Al_2O_3	175	0.39	8.96	158	0.20	5.12
10M/SiO_2	186	0.14	2.94	185	0.67	14.57
10M/AC	549	0.44	3.21	45	0.05	7.01

The textural properties of the fresh and spent catalysts with different supports evaluated by nitrogen adsorption-desorption are summarized in **Table 2.1**. It can be observed that the high surface area of 10M/Al_2O_3, 10M/SiO_2 and 10M/AC exhibited higher surface area and pore volume than 10M/ZrO_2, due to those of support having high surface area. As for spent catalysts, the surface area and pore volume of the active carbon (AC) which were the highest among the four supports, were decreased dramatically after decarboxy-cracking reaction due to the partial blockage of pores of support by carbon formation over the catalyst and active metal sintering, which was in agreements with FE-SEM and XRD results. While the surface areas of the alumina and silica supports were preserved. On the other hand, the surface area of zirconium oxide support increased significantly from 6 to 23 m^2/g while their pore volume and pore diameter decrease, may be coke deposit unevenly in catalyst pore wall layer by layer, but to form micropore in

macropores or large mesopores via pore-making as shown in **Figure 2.2** [26]. Resulting in surface area increased and pore diameter decreased.

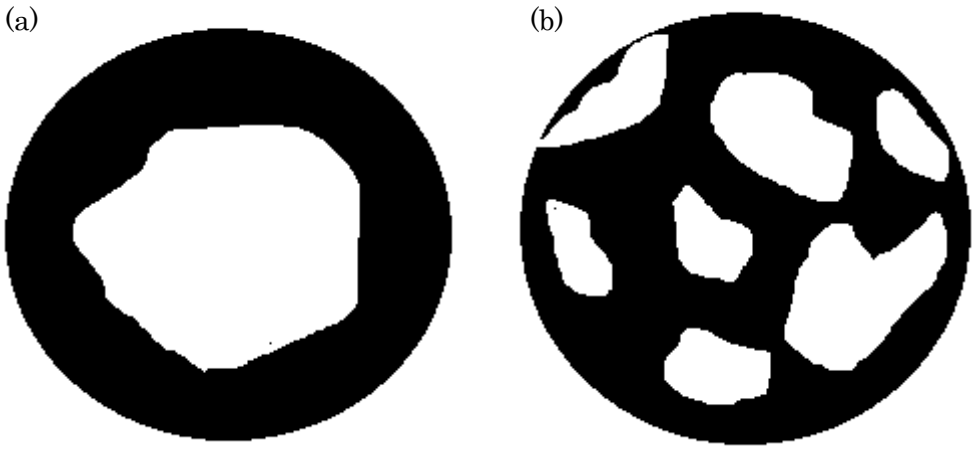

Figure 2.2 Different pore structure of catalyst (a) pore of normal deposition and (b) pore-making in catalyst pore.

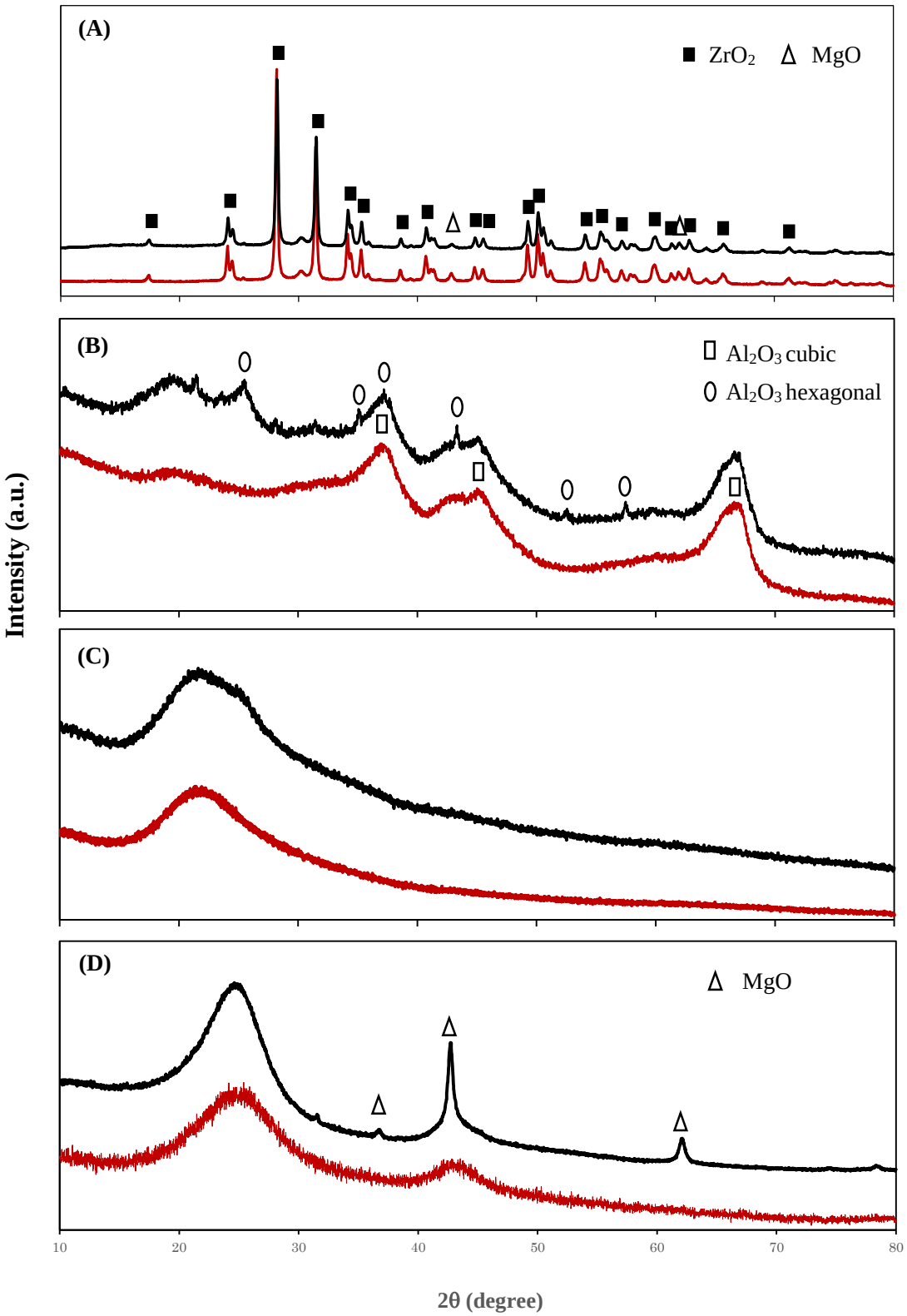

Figure 2.3 XRD patterns for fresh (Red line) and spent (Black line) catalysts with different supporting (A) 10M/ZrO_2, (B) 10M/Al_2O_3, (C) 10M/SiO_2 and (D) 10M/AC.

In **Figure 2.3** displays the XRD patterns of the fresh and spent MgO-based catalysts with different supports. The XRD patterns of MgO species were only detectable in 10M/ZrO_2 catalyst with low intensity diffraction peaks at $2\theta = 42°$ and 62°. While the XRD patterns of γ-alumina, silica and active carbon supports showed a similar profile with broad diffraction peaks of amorphous phase. The absence of diffraction peaks of MgO in 10M/Al_2O_3, 10M/SiO_2 and 10M/AC ascribed to its very high dispersion throughout the support, with a particle size under the detection limit of XRD technique. This is indicated that the high surface area of γ-alumina, silica and active carbon promote the dispersion of MgO. The XRD patterns of spent catalysts are also shown in **Figure 2.3**. The XRD patterns of the spent 10M/SiO_2 catalyst showed only amorphous peak, suggesting that catalytic structure had no change during the catalytic reaction. Although no bulk peak of MgO specie was detected in case of fresh 10MgO/AC catalyst, the detection of MgO peaks in spent catalyst as the following diffraction peaks detected at $2\theta = 36°$, 42° and 62° was confirmed the presence of MgO species in fresh catalyst. The detected diffraction peaks of MgO in spent 10MgO/AC catalyst could be related to a strong sintering occurred over MgO after reaction. The low intensity diffraction peaks observed at $2\theta = 38°$, 46° and 67° in the case of 10M/Al_2O_3 catalyst were assigned to the Al_2O_3 cubic phase which had transformed into a Al_2O_3 with hexagonal type of corundum structure, which was consistent with SEM results.

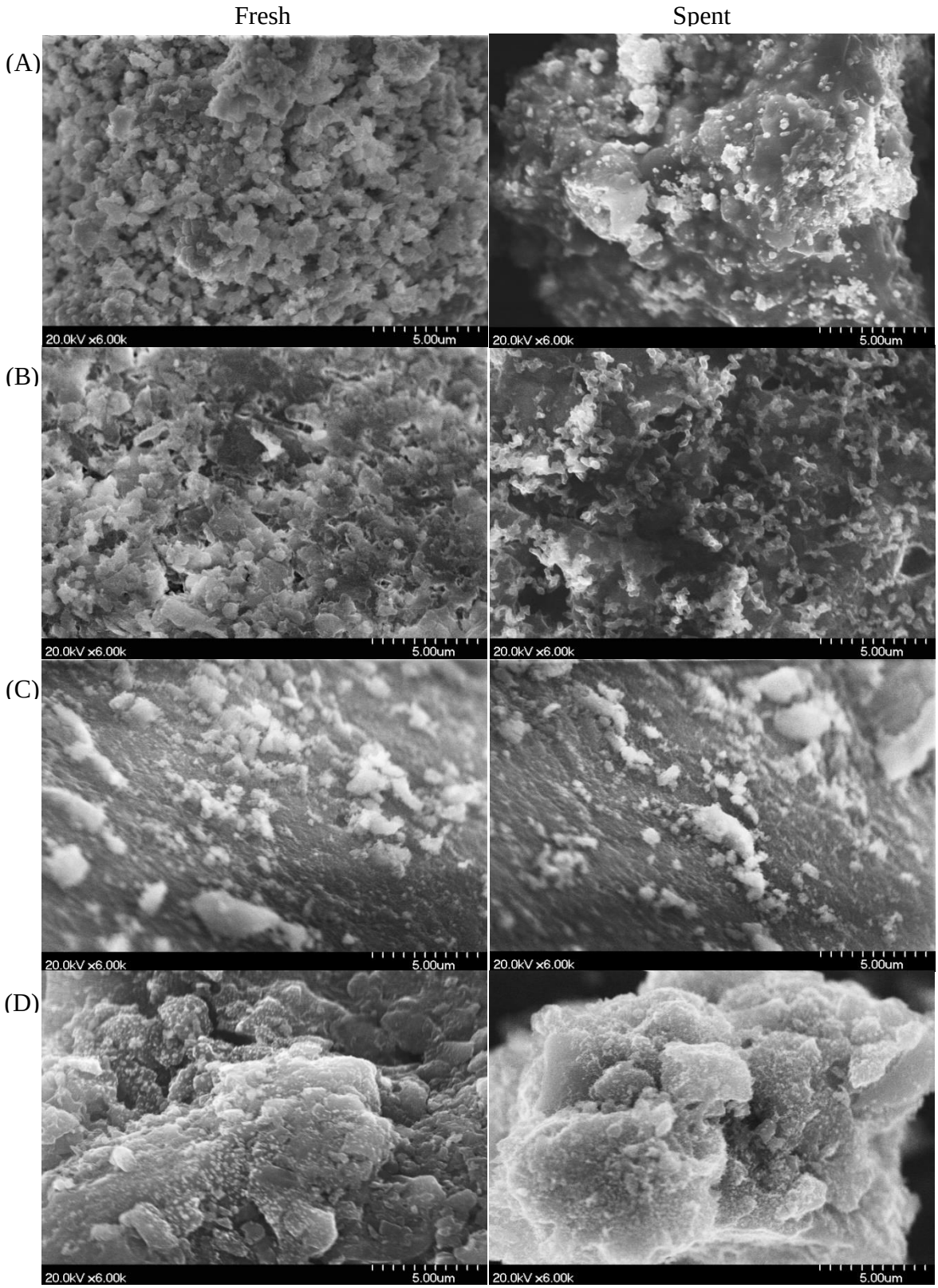

Figure 2.4 FE-SEM images of fresh and spent catalysts (A) 10M/ZrO_2, (B) 10M/Al_2O_3, (C) 10M/SiO_2 and (D) 10M/AC

Figure 2.4 shows the morphology of the fresh and spent catalyst surfaces applying FE-SEM analysis. As for the fresh catalysts, a large crystallite of 10M/ZrO_2 is evident in **Figure 2.4 (A)** due to low surface area. In **Figure 2.4 (B)** shows a kind of a non-uniformity of γ-Al_2O_3. On the other hand, the small dispersion of MgO on the supports was observed in **Figure 2.4 (C-D)**. The 10M/SiO_2 catalyst exhibited undefined shape of magnesium oxide, while uniform distribution of MgO particles was observed 10M/AC catalyst. As for the reacted catalysts, it can be clearly seen that the morphology of 10M/Al_2O_3, 10M/AC and10M/ZrO_2 catalysts changed significantly after the decarboxylation reaction. For 10M/ZrO_2 catalyst, large deposits of amorphous were observed. This heavy carbon formation on the10M/ZrO_2 catalyst can be attributed to its structure which was low surface area and large MgO particles. In addition, some hexagonal phase and agglomeration had been found for 10M/Al_2O_3. On the contrary, there were no significant differences in the morphology changes between the fresh and spent catalysts observed for the 10M/SiO_2 catalyst. Spent 10M/AC catalyst was seriously covered by deposited the whisker carbon formed on the surface of the catalyst. This is in line with BET results since surface area of 10M/AC decreased dramatically after reaction.

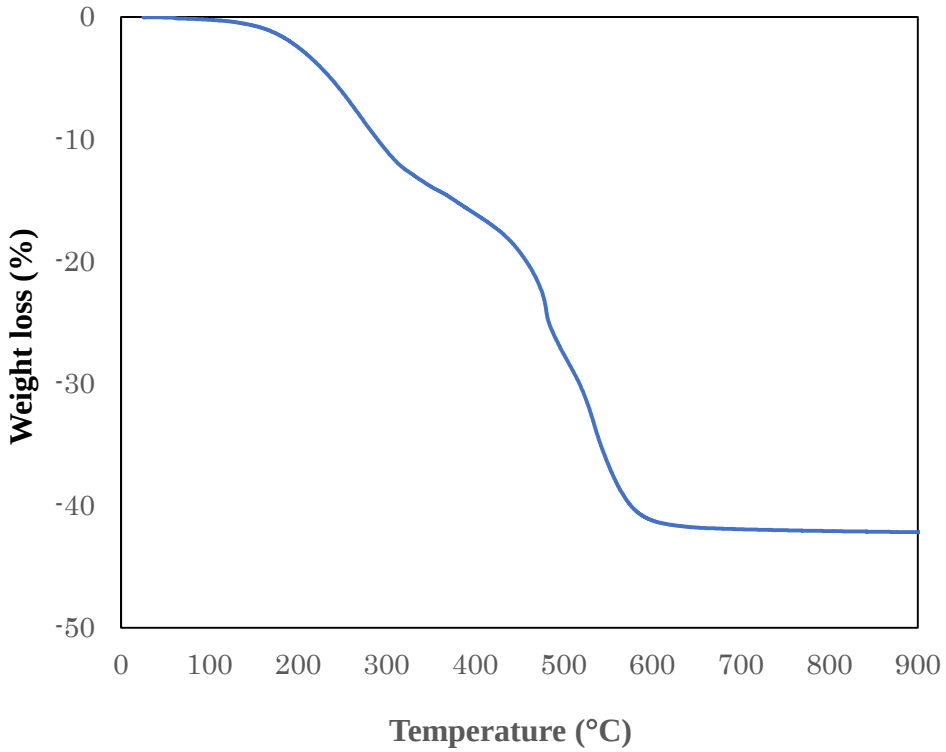

Figure 2.5 Weight losses determined by TGA analysis of the spent catalyst after catalytic decarboxylation of waste cooking oil

Table 2.2 Amount of coke deposit on the spent catalysts

Catalysts	Coke deposit (%)
10M/ZrO_2	8.87
10M/Al_2O_3	16.4
10M/SiO_2	8.76
10M/AC	38.1
5M10Z/AC	15.8
5M20Z/AC	13.9

Figure 2.5 shows the TGA profile of the spent 10M/Al_2O_3 catalyst (after 7 h catalytic decarboxylation reaction). The weight loss started at 320-480 °C. The weight loss in this temperature range could be attributed to the combustion of the high molecular weight derived from waste cooking oil. The peak of coke deposit on all of the spent

catalysts was observed at temperature above 480 °C, indicating the strongly coke deposit. The amount of coke deposit on the spent catalysts is illustrated in **Table 2.2**. It was found that the coke amount significantly depended on the type of support. This result suggested that two catalysts supported on SiO_2 and ZrO_2 produced less coke compared with the catalysts supported on Al_2O_3 and AC. The highest level of coke was formed on active carbon support, approximately 38.1%. Since the problem of coking was greatest on active carbon to find ways of reducing coking on this material. It was found that ZrO_2 inhibited the coking due to its mobile oxygen species, which help gasify the carbon that deposit on the surface of the catalyst.

2.3.2 Catalytic performance

2.3.2.1 Effect of support materials

Table 2.3 Material balance of waste cooking oil by decarboxy-cracking

Catalyst	Product yield (%wt)					
	Cracked oil	Dry gas	CO	CO_2	H_2O	Residue
10M/ZrO_2	69.8	4.8	1.4	5.5	3.0	8.8
10M/Al_2O_3	62.0	6.1	0.7	5.3	3.9	9.9
10M/SiO_2	63.3	9.3	0.6	3.7	6.4	8.4
10M/AC	64.8	4.1	1.0	5.9	4.4	13.4

Reaction conditions: He = 50 ml/min, oil feed flow rate = 0.25 ml/min, reaction temperature 430 °C.

Catalytic activity of the MgO-based catalysts with different supports and %ZrO_2 loading in the catalytic cracking decarboxylation reaction was carried out using an agitated reactor. The finding results are included in **Table 2.3**. The major products from this reaction were a mixture of liquid hydrocarbons, dry gas (C_1-C_4 hydrocarbons), CO, CO_2, water and residue. According to the results, **Scheme 2.1** displays the probable pathway for the catalytic cracking-decarboxylation of triglycerides as follows: triglyceride molecules in waste cooking oil have been primarily hydrolyzed to produce 1 mol of glycerine and 3 moles of free fatty acids. The glycerol can be converted to gaseous hydrocarbons and water by dehydration. While, fatty acid would be cracked into hydrocarbons by breaking of the C-C and C-O bonds follows two competitive routes: (1) direct decarboxylation (-CO_2) reaction followed by C-C bond cleavage of the resulting hydrocarbon radicals or (2): C-C and C-O cleavages within the hydrocarbon section of

the oxygenated hydrocarbon molecule followed by decarboxylation and decarbonylation of the resulting short chain molecule. These reactions finally yield CO, CO_2 and water as main oxygenated compounds and a mixture of hydrocarbons produced by different reactions such as β-scission, hydrogen transfer or isomerization.

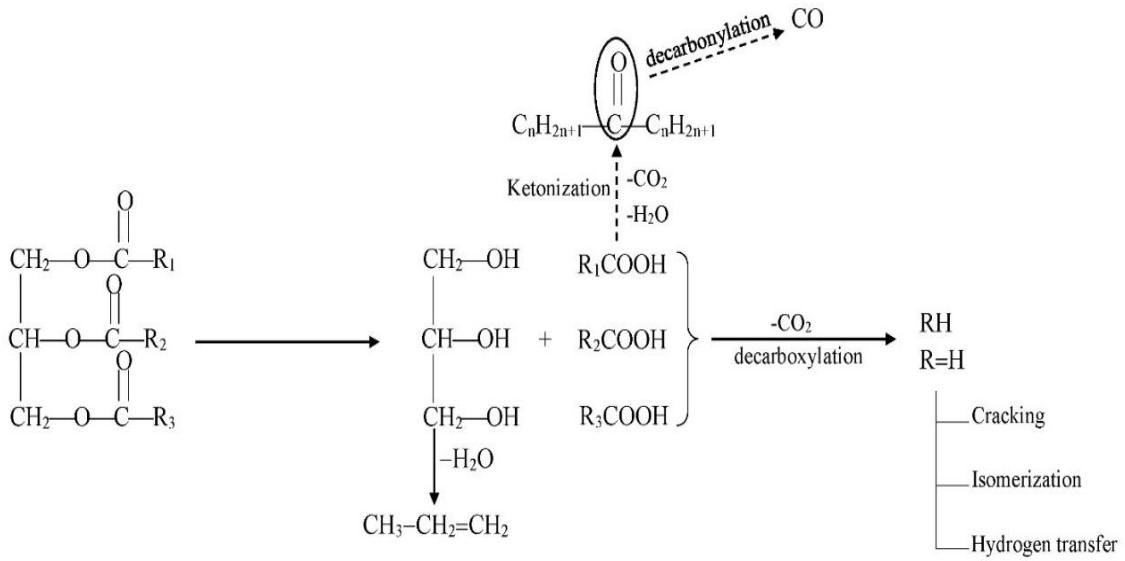

Scheme 2.1 Reaction scheme for catalytic decarboxylation of triglycerides to hydrocarbon

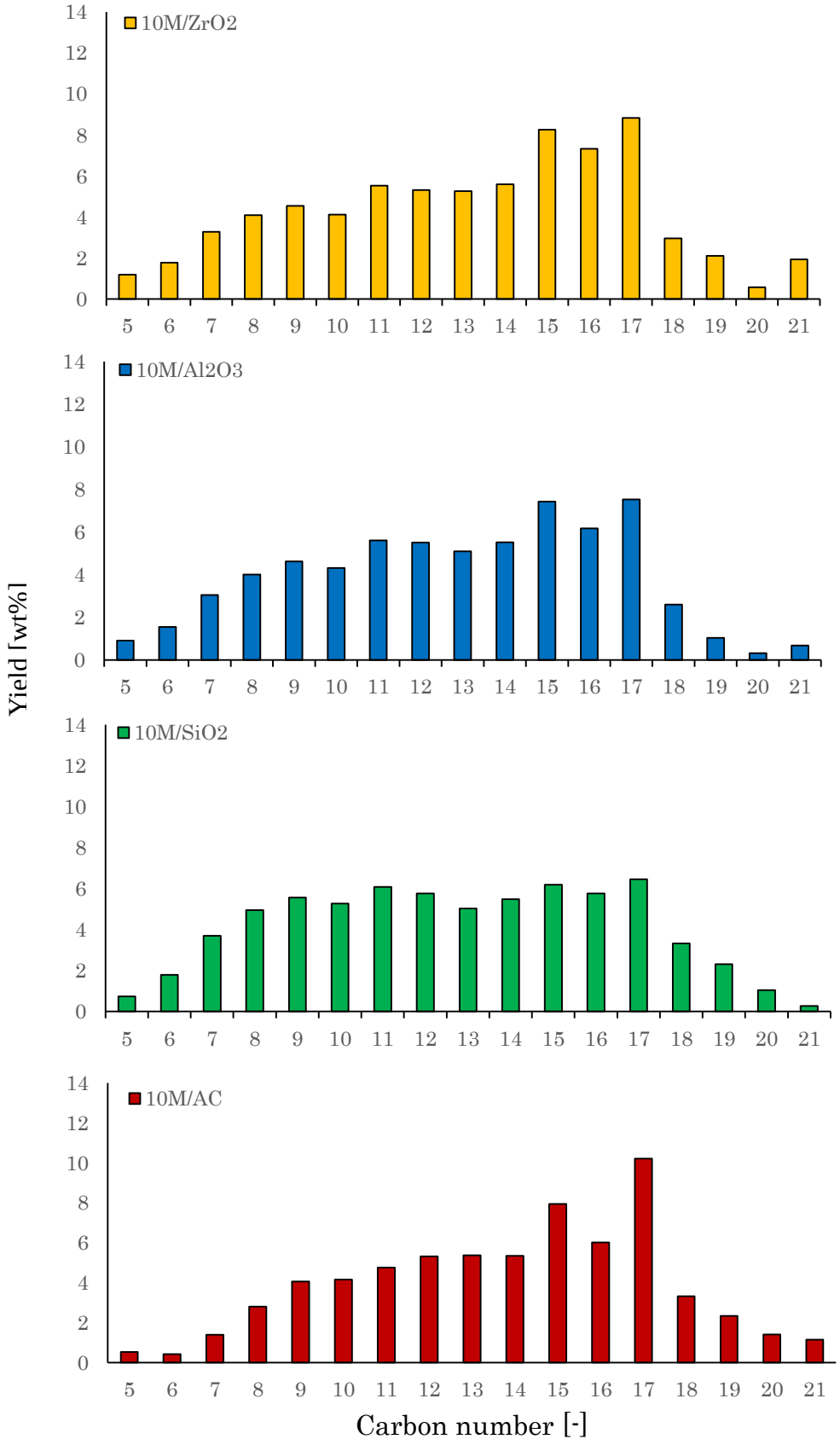

Figure 2.6 Hydrocarbon distribution of the product oils

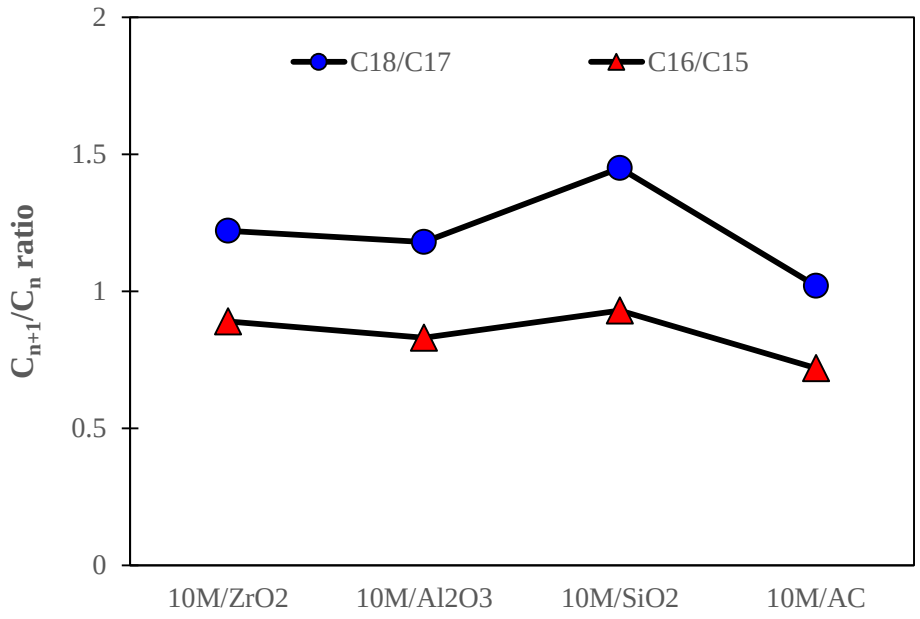

Figure 2.7 The C_{n+1}/C_n ratio of the product oils

Figure 2.6 depicts the hydrocarbon distribution of the product oils. This result demonstrates that all of catalysts can convert triglycerides to long chain hydrocarbons in diesel specification range (C_{10}-C_{20}) and the C_{17} hydrocarbons were the most abundant compounds after catalytic cracking-decarboxylation reaction. Furthermore, the portion of hydrocarbons with shorter chain in diesel fraction C_{10}-C_{14} were also detected, indicating that the C_{16} and C_{18} fatty acids (mainly consist of palmitic acid group of C_{16} and oleic acid group C_{18}) were converted not only to C_{15} and C_{17} hydrocarbons by direct decarboxylation but also to shorter chain by subsequent cracking reaction. The highest C_{15} and C_{17} yield were observed for the 10M/AC catalyst with 8.1 and 10.2 wt%, respectively. This result revealed that decarboxylation was the main reaction pathway. Whereas the lower yield of C_{17} was observed for 10M/SiO_2 and 10M/γ-Al_2O_3 catalysts. This was mainly due to the fact that the cracking reaction is influenced by the highest acidity of the catalysts. Moreover, in **Figure 2.7** when focused on the ratios of C_{16}/C_{15}

and C_{18}/C_{17} of 10M/AC catalyst were lower than other catalysts. This indicated that the 10M/AC prefered to decarbonylation/decarboxylation.

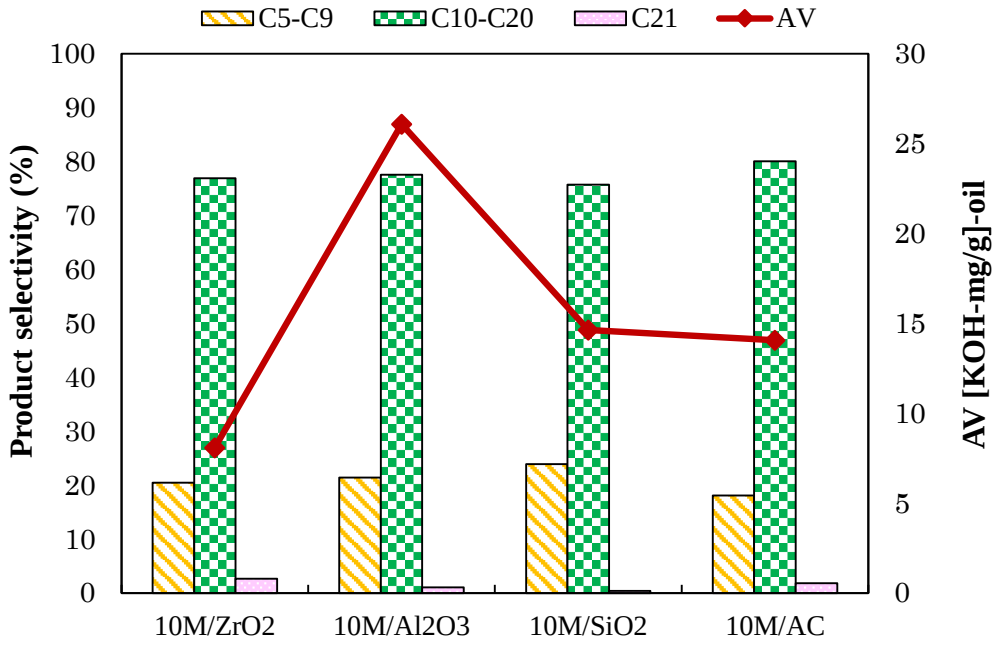

Figure 2.8 Product selectivity and acid value of the cracked oils

Figure 2. 8 shows product selectivity and acid value of the cracked oils. From the results, 10M/ZrO_2 tended to give the lowest acid value followed by 10M/AC, 10M/SiO_2 and 10M/γ-Al_2O_3, respectively, while the selectivity toward the product in diesel range hydrocarbons (C_{10}-C_{20}) was not significantly different for all catalysts. C_{21} compounds were found to be ketones as described above **(Scheme 2.1)** such as methyl ketone and ethyl ketone. By comparison, yield of these compounds on 10M/ZrO_2 catalyst were higher than other catalysts [27].

2.3.2.2 Effect of the addition of ZrO_2 to MgO/AC

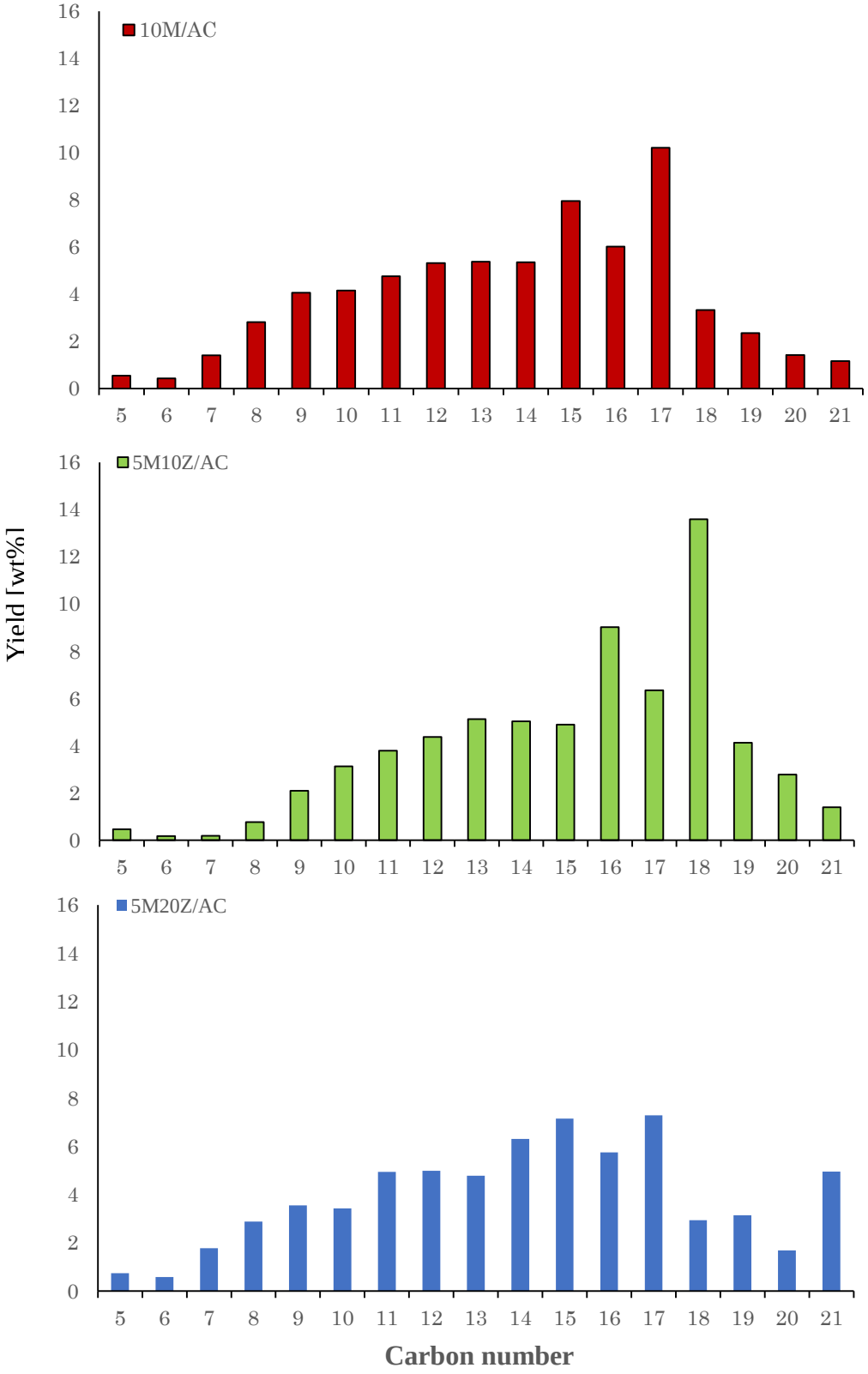

Figure 2. 9 Hydrocarbon distribution of the product oils

The hydrocarbon distribution of the product oils by the addition of ZrO_2 are shown in **Figure 2.9.** The addition of ZrO_2 with 10%wt, it was surprising found that yield of C_{15} and C_{17} increased from 7.9% to 9.0% and 10.2% to 13.6%, respectively. While ratios of C_{16}/C_{15} and C_{18}/C_{17} decreased (**Figure 2.10**), suggesting that the decarboxylation of fatty acid can be greatly promoted with the appropriate amounts of ZrO_2.

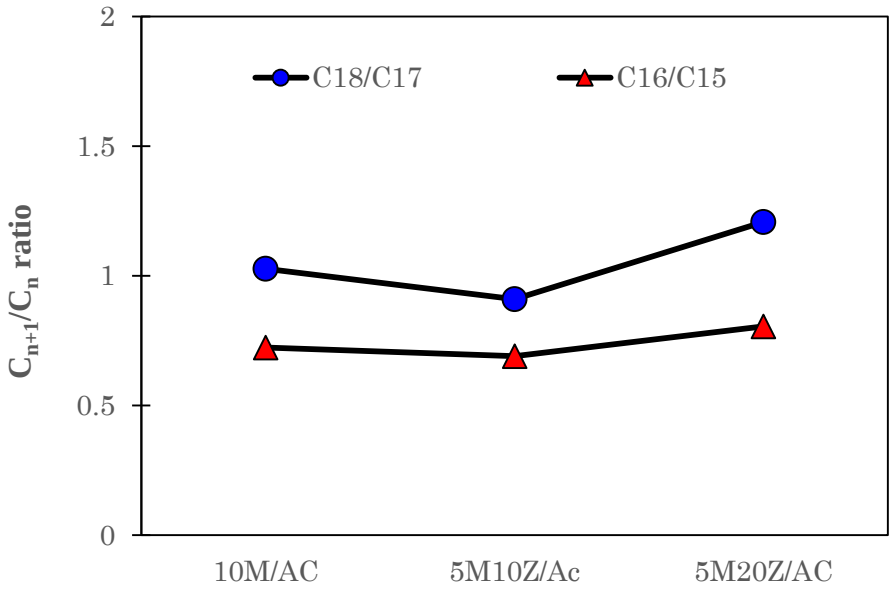

Figure 2.10 The C_{n+1}/C_n ratio of the product oils

Figure 2.11 shows product selectivity and acid value of the cracked oils. From the results, As the ZrO_2 loading of 10wt%, the acid value decreased to 7.779 KOH-mg/g-oil since the oxygen vacancies of ZrO_2 adsorbed carboxylic acid molecules to form carboxylate species. The selectivity to diesel range hydrocarbons was also higher to 87% in accompanied with the decrease of 9% selectivity to gasoline range hydrocarbons. C_{21} compounds were found to be ketones as described above **(Scheme 2.1)** such as methyl ketone and ethyl ketone. It was also found that the selectivity to C_{21} compounds increased with increasing ZrO_2 loading. This was consistent with the literatures that ZrO_2 was the

active component for the ketonization of carboxylic acids [27].

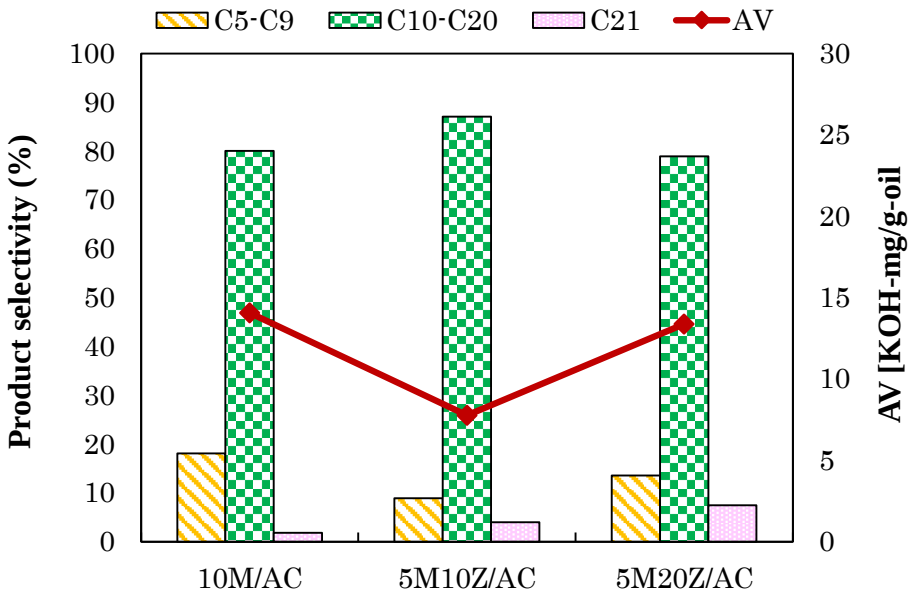

Figure 2.11 Product selectivity and acid value of the cracked oils

2.3.2.3 Effect of reaction temperature

The effect of reaction temperature on decarboxylation was also investigated at various temperatures, from 400 °C-470 °C, shown in **Figure 2.12** and **Figure 2.13**. In the liquid phase reaction, the increasing temperature caused the reduction of product selectivity in the diesel range (C_{10}-C_{20}) due to the formation of the gasoline range (C_5-C_9). In the gas phase reaction, described in **Figure 2.13,** the yield of CO_2 increased with the increasing of reaction temperatures. It is believed that increasing temperature enhanced the activation energy to release CO_2. When the temperature was higher than 430 °C, the yield of dry gas (C_1-C_4) increased because the thermal cracking of long chain hydrocarbons.

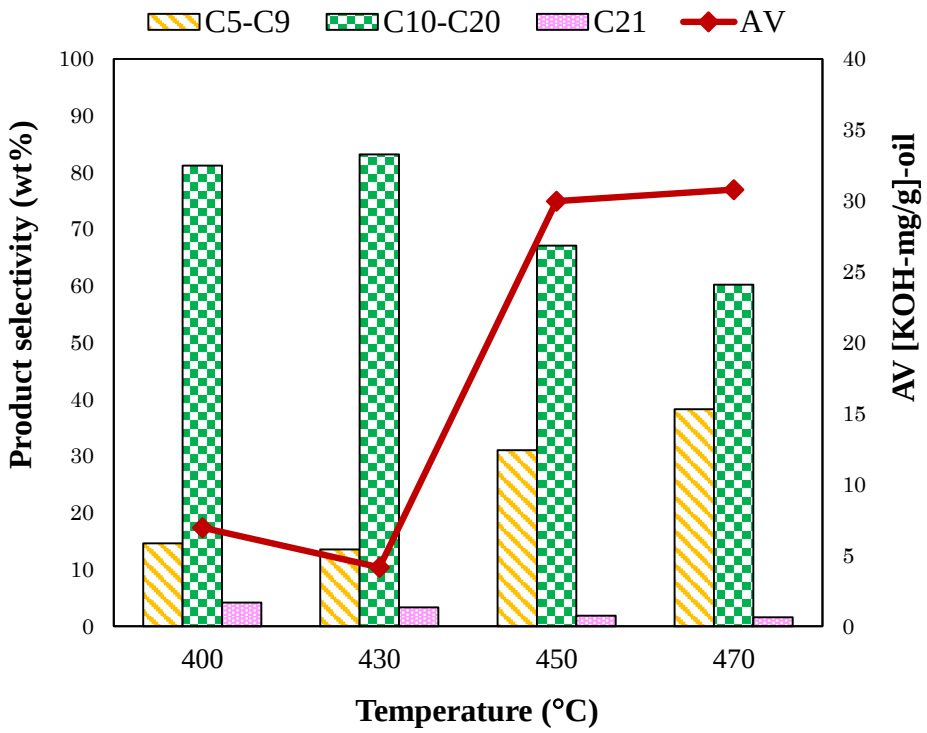

Figure 2.12 Product selectivity and acid value in the liquid phase

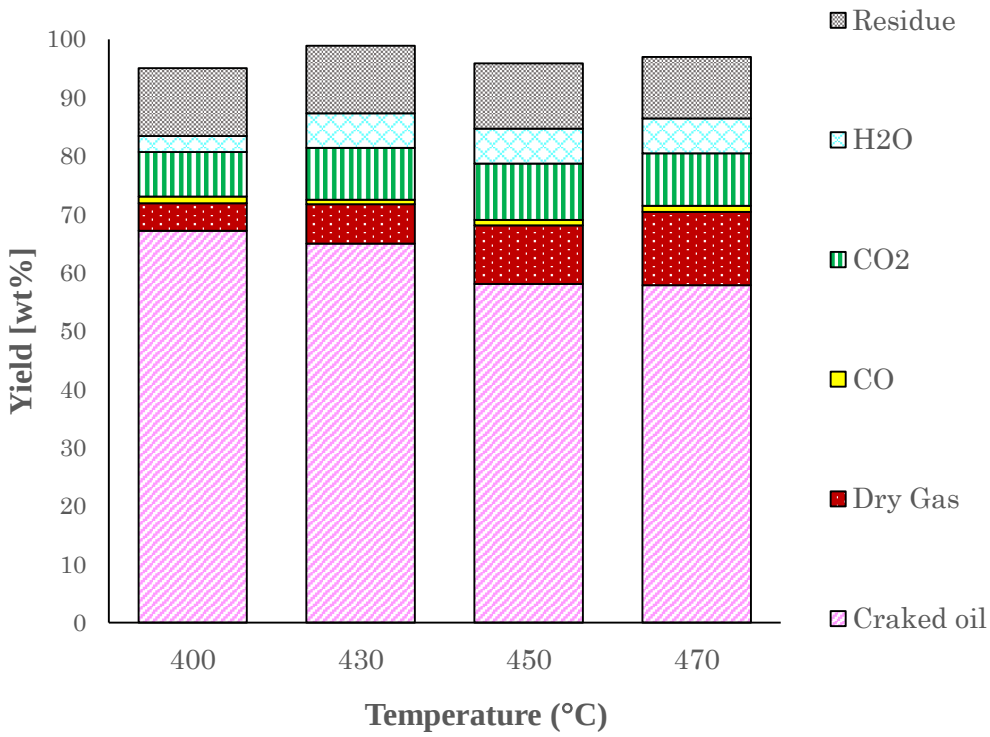

Figure 2.13 Product yield at various temperatures; the reactions were conducted with 0.25 ml/min oil feeding rate and 50 ml/min He flow rate. The catalyst is 5M10Z/AC catalyst

2.4 Conclusion

In this work catalytic decarboxylation of waste cooking oil for the production of new hydrocarbon biodiesel over MgO-based catalysts supported on four types of support material (γ-alumina, silica, active carbon and zirconium oxide) was studied. All catalysts can convert triglycerides into deoxygenated biodiesel (C_{10}-C_{20}). The cracked species hydrocarbons (C_1-C_9) were also observed and were increased with increasing reaction temperature. The main products obtained from all catalysts were C_{15} and C_{17} hydrocarbons, the highest yield was observed for the 10M/AC catalyst. The 10M/AC catalyst became much more active and selective to diesel hydrocarbons production after ZrO_2 loading with 10wt%, and reduced the carbon formation on the catalyst surface. Thus, MgO-ZrO_2 on active carbon may be regarded as the promising decarboxy-cracking catalyst for synthesis HiBD from waste cooking oil.

References

[1] D.Y.C. Leung, X. Wu, and M.K.H Leung, Applied Energy, vol. 87(4), pp. 1083-1095, 2010.

[2] M.P. Sharma, and G. Dwivedi, International Journal of Renewable Energy Research, vol. 3, pp. 827-836, 2013.

[3] G. Dwivedi, and M.P. Sharma, Renewable and Sustainable Energy Review, vol. 15, pp. 4633-4641, 2011.

[4] O.I. Senol, T.R. Viljava, and A.O.I. Krause, Catalysis Today, vol. 106, pp. 186-189, 2005.

[5] O.I. Senol, E.M. Ryymin, T.R. Viljava, and A.O.I. Krause, Journal of Molecular Catalysis A: Chemical, vol. 268, pp. 1-8, 2007.

[6] O.I. Senol, T.R. Viljava, and A.O.I. Krause, Applied Catalysis A: General, vol. 326, pp. 236-244, 2007.

[7] J.G. Na, B.E. Yi, J.N. Kim, K.B. Yi, S.Y. Park, J.H. Park, J.N. Kim, and C.H. Ko, Catalysis Today, vol. 156, pp. 44-48, 2010.

[8] M. Snare, P. Maki-Arvela, I.L. Simakova, J. Myllyoja and D.Y. Murzin, Russian Journal of Physical Chemistry B, vol. 3, pp. 1035-1043, 2009.

[9] I. Simakova, O. Simakova, P. Maki-Arvela, A. Simakov, M. Estrada, and D.Y. Murzin, Applied Catalysis A: General, vol. 355, pp. 100-108, 2009.

[10] S. Lestari, P. Maki-Arvela, I. Simakova, J. Beltramini, G.Q.M. Lu, and D.Y. Murzin, Catalysis Letters, vol. 130, pp. 48-51, 2009.

[11] S. Lestari, P. Maki-Arvela, H. Bernas, O. Simakova, R. Sjoholm, J. Beltramini, G.Q.M. Lu, J. Myllyoja, I. Simakova, and D.Y. Murzin, Energy & Fuels, vol. 23, pp. 3842-3845, 2009.

[12] M. Snare, I. Kubickova, P. Maki-Arvela, D. Chichova, K. Eranen, and D.Y. Murzin, Fuel, vol. 87, pp. 933-945, 2008.

[13] P. Maki-Arvela, M. Snare, K. Eranen, J. Myllyoja, and D.Y. Murzin, Fuel, vol. 87, pp. 3543-3549, 2008.

[14] S. Lestari, I. Simakova, A. Tokarev, P. Maki-Arvela, K. Eranen, and D.Y. Murzin, Catalysis Letters, vol. 122, pp. 247-251, 2008.

[15] M. Snare, I. Kubickova, P. Maki-Arvela, K. Eranen, J. Warna, and D.Y. Murzin, Chemical Engineering Journal, vol. 134, pp. 29-34, 2007.

[16] P. Maki-Arvela, I. Kubickova, M. Snare, K. Eranen, and D.Y. Murzin, Energy & Fuels, vol. 21, pp. 30-41, 2007.

[17] P. Maki-Arvela, I. Kubickova, M. Snare, K. Eranen, and D.Y. Murzin, Industrial & Engineering Chemistry Research, vol. 45, pp. 5708-5715, 2006.

[18] I. Kubickova, M. Snare, K. Eranen, P. Maki-Arvela, and D.Y. Murzin, Catalysis Today, vol. 106, pp. 197-200, 2005.

[19] J.G. Immer, M.J. Kelly and H.H. Lamb, Applied Catalysis A: General, vol. 375, pp. 134-139, 2010.

[20] T.A. Foglia and P.A. Barr, Journal of the American Oil Chemists Society, vol. 53, pp. 737-741, 1976.

[21] W.F. Maier, W. Roth and I. Thies, Chemische Berichte, vol. 115, pp. 808-812, 1982.

[22] H. Tani, M. Hasegawa, K. Asami and K. Fujimoto, Catalysis Today, vol. 164, pp. 410-414, 2012.

[23] H. Tani, M. Shimouchi, M. Hasegawa and K. Fujimoto, Journal of the Japan Institute of Energy, vol. 90, pp. 466-470, 2011.

[24] P. Natewong, Y. Murakami, H. Tani and K. Asami, Journal of the Japan Institute of Energy, vol. 94, pp. 1393-1393, 2015.

[25] A. Zhang, Q. Ma, K. Wang, X. Liu, P. Shuler and Y. Tang, Applied Catalysis A: General, vol. 303, pp. 103-109, 2006.

[26] Y. Sun and C. Yang, Energy Science and Technology, vol. 6, pp. 67-72, 2013.

[27] T.N. Pham, T. Sooknoi, S.P. Crossley and D.E. Resasco, ACS Catalysis, vol. 3, pp. 2456-2473, 2013.

CHAPTER 3

Development of Heterogeneous Basic Catalysts Supported on Silica for the Synthesis of High Quality Bio-Diesel from Waste Cooking Oil

Abstract: Effect of addition of CaO and ZrO_2 to MgO/SiO_2 catalyst, which is effective for synthesis of High Quality Bio-Diesel (HiBD) was investigated using atmospheric agitated reactor at 430 °C and LHSV = 0.3 h^{-1}. Binary $MgO\text{-}CaO/SiO_2$ and $MgO\text{-}ZrO_2/SiO_2$ catalysts and ternary $MgO\text{-}CaO\text{-}ZrO_2/SiO_2$ catalyst were prepared by the incipient wetness impregnation method. Physical properties of these catalysts were characterized by BET, XRD and CO_2-TPD methods. Both the fatty acids and the triglycerides in waste cooking oil were converted into hydrocarbon gases, CO, CO_2, water and hydrocarbon oil. CaO- and/or ZrO_2-added catalysts gave higher CO_2 yields than MgO/SiO_2 alone, and showed lower acid values. These observation indicates that the added oxides promote the decarboxylation reactions. Iodine values also decreased to some extent by the addition of these oxides.

3.1 Introduction

The production of bio-fuels as clean and renewable fuels has recently been paid a keep attention to because of a rapid price rise of petroleum and an increase in the greenhouse gas emission. Fatty acid methyl ester (FAME) and Bio Hydrofined Diesel (BHD) are known as current bio fuels from triglycerides of vegetable oils and animal fats for diesel engine [1-4]. However, sub-raw materials other than oil are required in both FAME and BHD production processes; methanol and high pressure hydrogen gas are necessary for FAME and BHD, respectively. Moreover, the high oxygen content in biodiesel molecules lead to a major problems of using biodiesel as a fuel such as poor cold flow properties and low storage stability [5,6].

Decarboxylation is alternative technique to decrease oxygen content in biodiesel by removing oxygen as CO_2 [7-14]. This reaction has been successfully performed under an inert gas in a semibatch reactor at temperature ranges of 300-360 °C. The catalyst screening studies revealed that Pd and Pt supported on carbon catalysts are the most active and selective catalysts for this reaction. Now we have developed a new biodiesel production process which gives mixed hydrocarbon liquids of diesel fraction with high selectivity without using any sub-materials [15,16], and named this fuel as High Quality Bio-Diesel (HiBD) [17]. HiBD is expected as the next generation biodiesel because its properties are suitable for the latest common rail type engine. The production process of HiBD is quite simple, where triglycerides are converted to liquid hydrocarbons and light hydrocarbon gases though decarboxylation over solid catalysts as shown in **Figure 3.1**. This process can be adapted to a lot of feed materials such as vegetable oil, waste cooking oil, and animal fats.

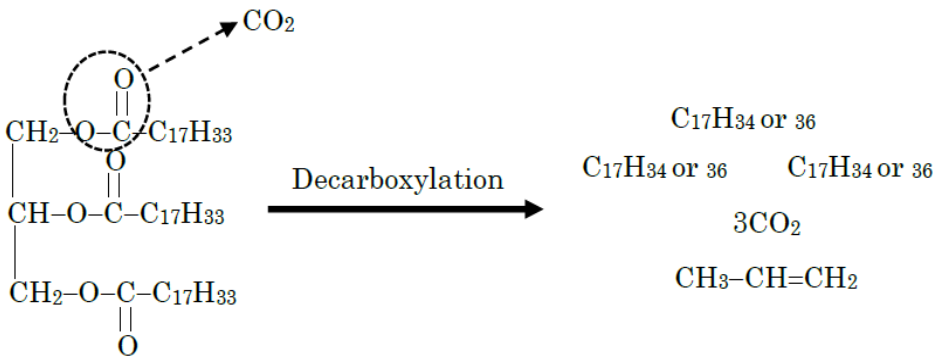

Figure 3.1 The target reaction scheme

One of the most significant factors in the HiBD production is the catalyst which promotes the conversion of triglycerides. A magnesium oxide supported on silica (MgO/SiO_2) catalyst is found to be effective for this reaction, and its basic property promotes the decarboxylation [15,16]. Since porous inorganic metal oxides such as alkali metals or alkali-earth metals providing alkalinity have also been widely used to disperse in porous supports for CO_2 adsorption. The calcium-based adsorbents possessing high adsorption capacity, long-term durability, good mechanical strength and low cost in natural minerals have been widely studied for CO_2 capture [18,19]. Calcium oxide (CaO) can react with CO_2 at high temperatures to form calcium carbonate ($CaCO_3$) which can be regenerated to CaO upon thermal decarbonation. And ZrO_2 is known to have basic and acid character and also ability to enlarge active surface area [20,21], and thus they are expected to enhance the activity. In the present study, therefore, addition of CaO and ZrO_2 to MgO/SiO_2 catalyst was investigated.

3.2 Experimental

3.2.1 Catalyst preparation

Basic oxide supported on silica

The basic oxide catalysts (MgO, CaO and ZrO_2) supported on silica were prepared by the incipient wetness impregnation method with using aqueous solution of magnesium nitrate hexahydrate ($Mg(NO_3)_2.6H_2O$, 99.0% purity, Wako, Japan), calcium nitrate tetrahydrate ($Ca(NO_3)_2.4H_2O$, 98.5% purity, Wako, Japan) and zirconyl nitrate dihydrate ($ZrO(NO_3)_2.2H_2O$, 97.0% purity, Wako, Japan). A commercial silica (S_{BET} = 259 m^2/g and PV = 1.02 cm^3/g) was used as the support. The silica was initially dried at 110 °C overnight to remove adsorbed moisture. Magnesium nitrate hexahydrate or calcium nitrate tetrahydrate or zirconyl nitrate dihydrate was dissolved in the deionized water and then added dropwise into the silica. After the impregnation, the impregnated samples were evaporated at 40 °C and then dried in an oven at 110 °C overnight followed by calcined in air flow at 500 °C for 3 h. The total MgO, CaO and ZrO_2 supported on silica were 10wt%. The catalysts were denoted as $10M/SiO_2$, $10C/SiO_2$ and $10Z/SiO_2$.

The addition of CaO and ZrO_2 to MgO/SiO_2

Silica-supported oxide catalysts were prepared by the incipient wetness impregnation method using aqueous solutions of Mg, Ca, and Zr nitrates. The silica support used was Fuji Silisia Q10 (particle size, 1.18-2.36 mm; SA 300 m^2/g; PV, 0.95 cm^3/g). Magnesium nitrate hexahydrate or calcium nitrate tetrahydrate or zirconyl nitrate dihydrate were mixed in the deionized water and then added dropwise into the silica. After the impregnation, they were dried in an oven at 100 °C for 12 h, and then calcined

in air at 500 °C for 3 h. Components of the catalysts are abbreviated by using loadings (wt%) and the initial letters of the oxides; for example, 5M5C5Z indicates that the catalyst contains 5 wt% of MgO, 5 wt% of CaO, and 5 wt% of ZrO_2, respectively.

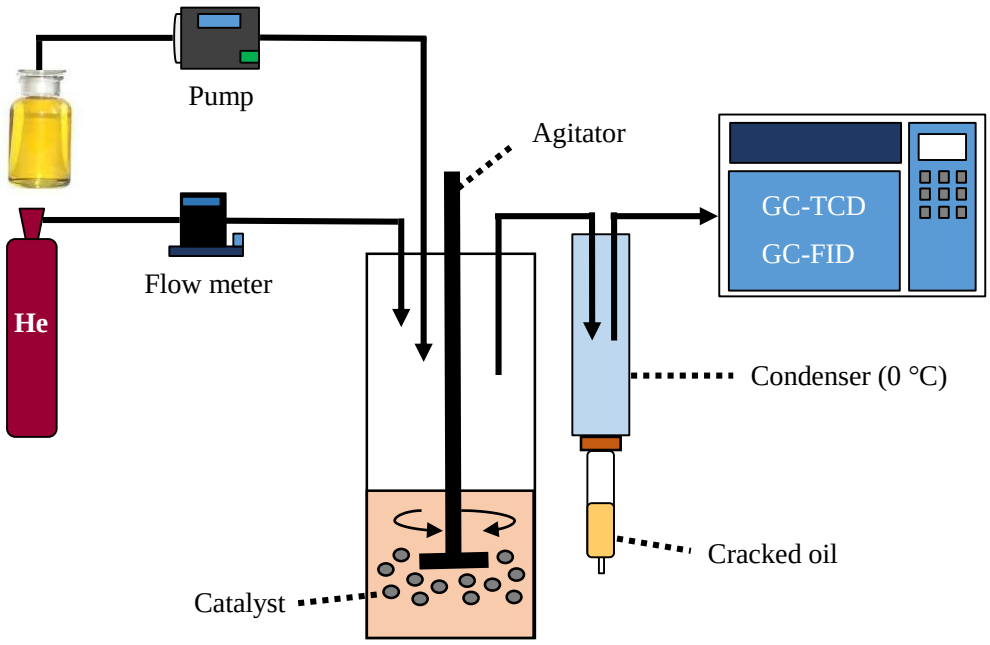

Figure 3.2 Reaction apparatus for catalytic decarboxylation

3.2.2 Catalytic testing

Catalytic reactions were conducted in an agitated reactor system at 430 °C under atmospheric pressure. **Figure 3.2** shows the experimental setup for the HiBD production. 25 g of the granular catalyst was charged into the reactor, and it was heated up to the reaction temperature in an He flow (50 mL/min). Waste cooking oil was supplied from the university restaurant, was introduced into the catalyst bed at 0.25 mL/min with a pump. The gaseous products which came out from the reactor were cooled and condensed at 0 °C, the uncondensed gaseous products were sampled and analyzed every 30 minutes

during the reaction by a gas chromatograph with thermal conductivity detector (GC-TCD) and one with flame ionization detector (GC-FID) on line. Yields of the cracked oil and water were calculated on the basis of weight of the reactant oil fed. Carbon number distribution of the product oil was analyzed off line with another GC-FID. The amount of residue was determined by weight different between catalysts before and after use. Total acid value, index of free acid contents, and iodine value, index of the amount of unsaturated bonding, of the oil were measured by potentiometric titration methods according to JIS 2501-2003 and JIS K0070-1992, respectively. The product selectivity in the upgrade biodiesel was calculated through the following equation:

$$\text{Selectivity (C\%)} = \frac{C\ atoms\ in\ each\ product}{Sum\ of\ C\ atom\ in\ all\ the\ product} \times 100\% \qquad (3.1)$$

3.2.3 Catalyst characterization

The BET measurements in this work were conducted on a BELSORP-mini II apparatus (Japan Bel Inc.) Prior to the BET measurement, all catalyst samples (typically 0.1-0.2 g) were first treated externally at 200 °C under vacuum for 2 h to remove the adsorbed water. BET surface areas and pore volume were calculated from the linear part of the Brunauer-Emmett-Teller method and the N_2 uptake at a P/P_0 value of 0.99.

The crystalline structure of the fresh and spent catalysts were determined by using X-ray diffraction (XRD) with a RIGAKU, XRD-DSC-XII diffractometer using CuKα as the radiation source with λ = 1.54 Å and Ni as the filter in the range of 2θ from 10° to 80°. The X-ray tube was operated at 40 kV and 20 mA at room temperature.

The basicity of the active catalysts were characterized by using temperature-programmed desorption of CO_2 (CO_2-TPD) on a BELCAT (Japan Bel Inc.). The catalyst

(50 mg) was degassed by heating at 10 °C/min under a flow of helium (He) from room temperature to 500 °C and then held at this temperature for 60 min. After it was cooled to 50 °C, CO_2 was saturated with 50 mL/min for 60 min. Subsequently, the catalyst was purged with helium gas at a flow rate of 50 mL/min for 1 h in order to eliminate any physically adsorbed and/or weakly bond species. CO2-TPD was performed at the rate of 10 °C/min from 30 °C up to 900 °C.

3.3 Results and Discussion

3.3.1 Effect of basic metal oxide

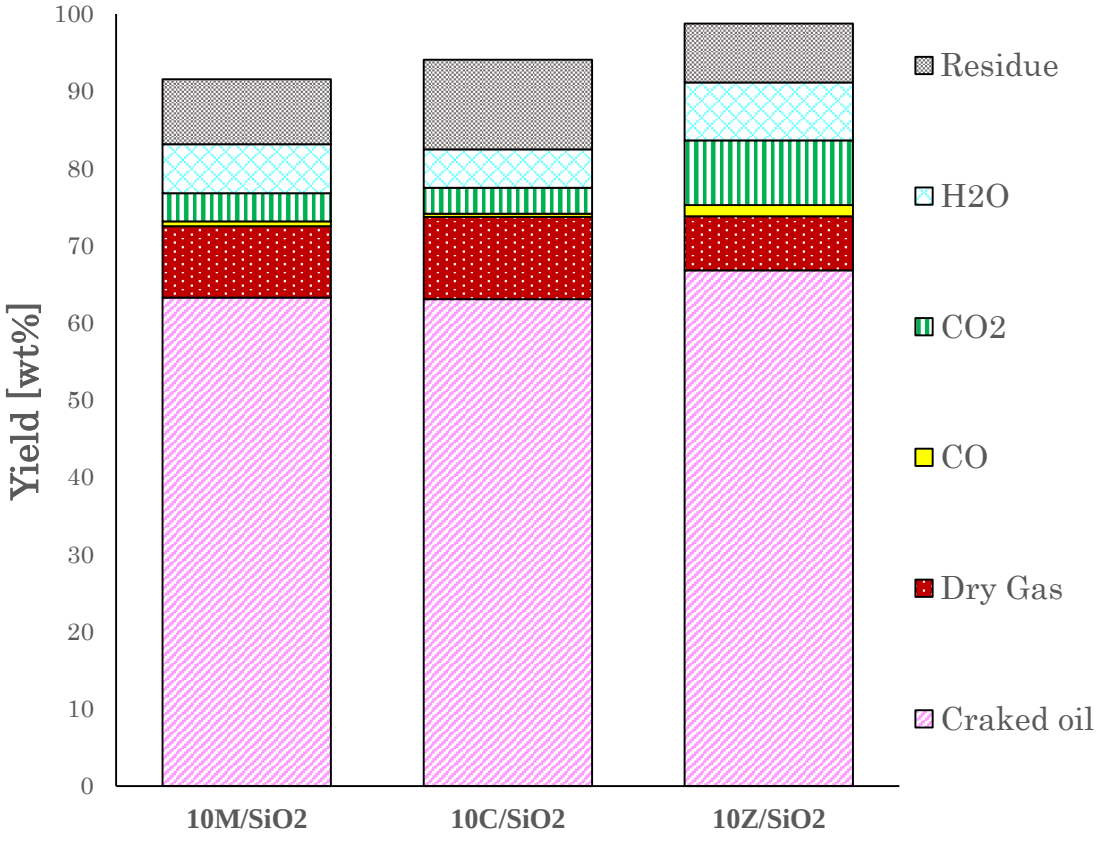

Figure 3.3 Product yield from waste cooking oil over the basic oxide catalysts

Figure 3.3 shows product yield from waste cooking oil over the basic oxide catalysts by decarboxy-cracking. The major products recovered were cracked oil, dry gas (C_1-C_4 hydrocarbons), CO, CO_2, water and residue. The unreacted fatty acids was not detected, as the reacted fatty acids and the unreacted fatty acids may be condensed into liquid products. Therefore, liquid products not only contain the cracked oils but also comprise the unreacted fatty acids. Moreover, unreacted fatty acids would remain as residue. CO_2 yield of MgO, CaO and ZrO_2 supported on silica catalysts were about 3.7%,

3.3% and 8.7%, respectively. In this result, it was found that ZrO_2 has higher CO_2 yield than MgO and CaO, mainly due to the high surface area and pore volume as shown in **Table 3.1**. Moreover, the surface oxygen vacancies of ZrO_2 adsorbed carboxylic acid molecules to form carboxylate species and easily to release by heating for a short while. In contrast, the case of calcium oxide, CaO adsorbed carboxylic acid molecules to form $CaCO_3$, it is more difficult to desorb CO_2 as evidenced by the temperature programmed of CO_2 as shown in **Figure 3.4.** The CO_2 adsorption/desorption behavior of MgO, CaO and ZrO_2 is closely related to the nature of the product formed during the adsorption. Since CO_2 is a weak acid and it is favored by the basic nature of the sorbent. The CO_2 desorption profile for CaO showed one apparent desorption peak with a maximum temperature at 675 °C. Which indicate that $10C/SiO_2$ catalyst requires a high temperature to remove the adsorbed CO_2 [22,23]

Table 3.1 The physical properties of the basic oxide catalyst supported on silica

Catalysts	**SA**	**PV**	**Basicity (mmol/g)**	
	(m^2/g)	**(cm^3/g)**	**Weak**	**Strong**
$10M/SiO_2$	186	0.14	0.031	0.099
$10C/SiO_2$	157	0.79	0.037	0.171
$10Z/SiO_2$	246	0.86	0.028	0.069

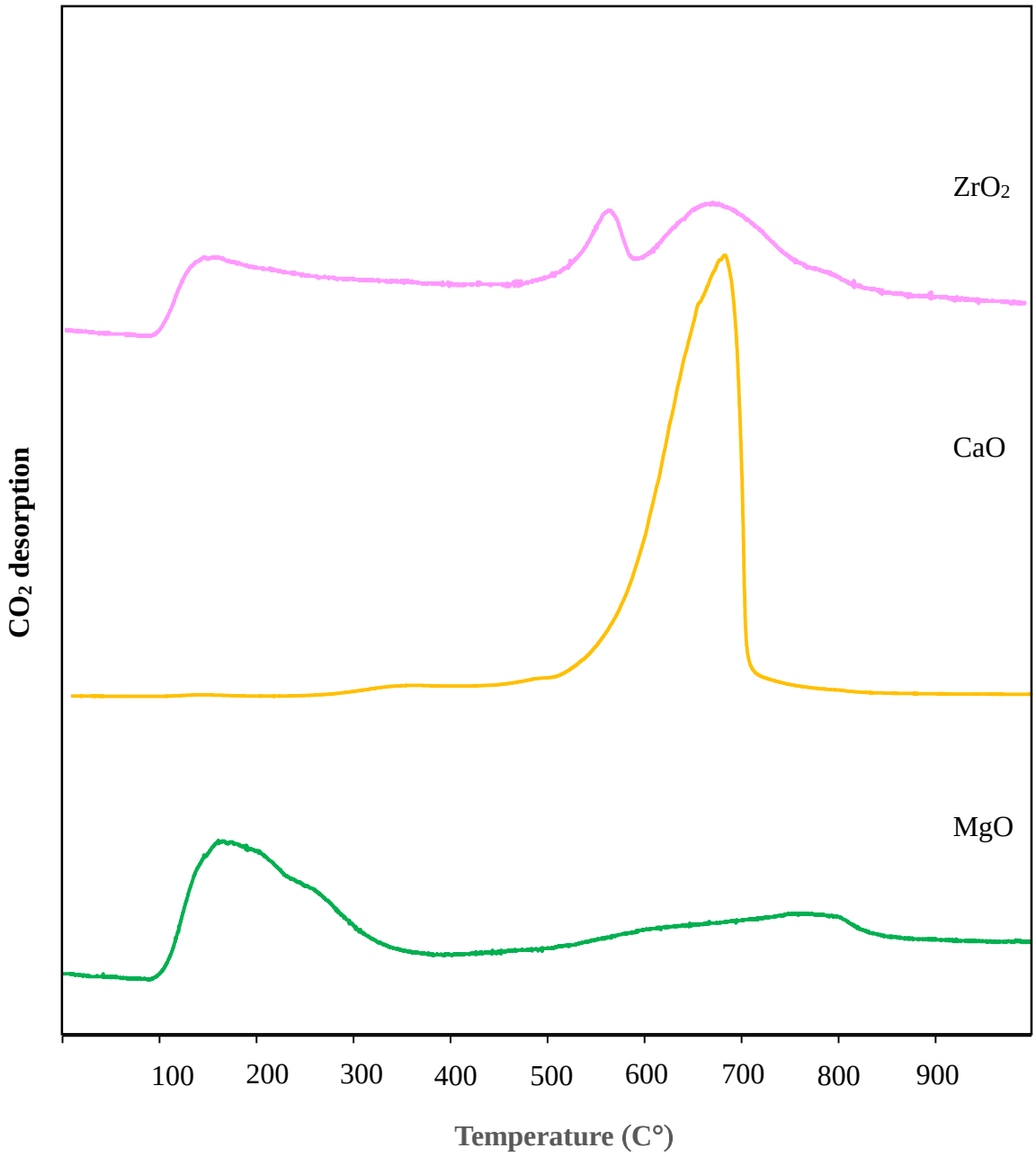

Figure 3.4 Temperature programmed of CO_2 of ZrO_2, CaO and MgO

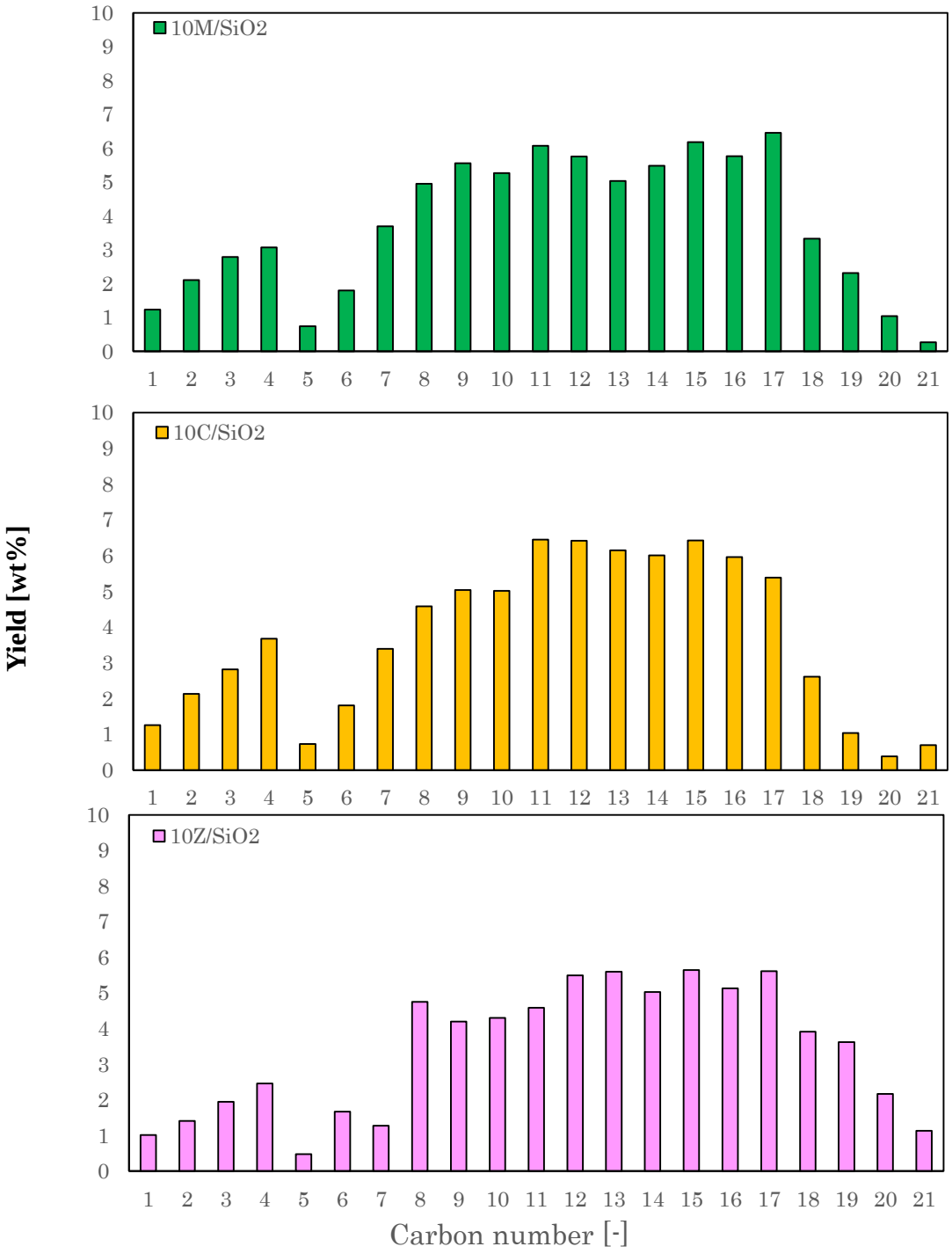

Figure 3.5 Hydrocarbon distribution of the product oil

Figure 3.5 show the hydrocarbon number distribution of the product oils. GC-MS analysis was done by area normalization method, which revealed that more than 99 wt% of the oil were hydrocarbons, and very small amount of free fatty acids and alcohols with different carbon numbers were contained. As a whole, the distribution profiles are similar to each other; a large amount of hydrocarbons with the diesel fraction (C_{10}-C_{20}) are the major products, while the compounds with carbon number higher than 21 were not observed.

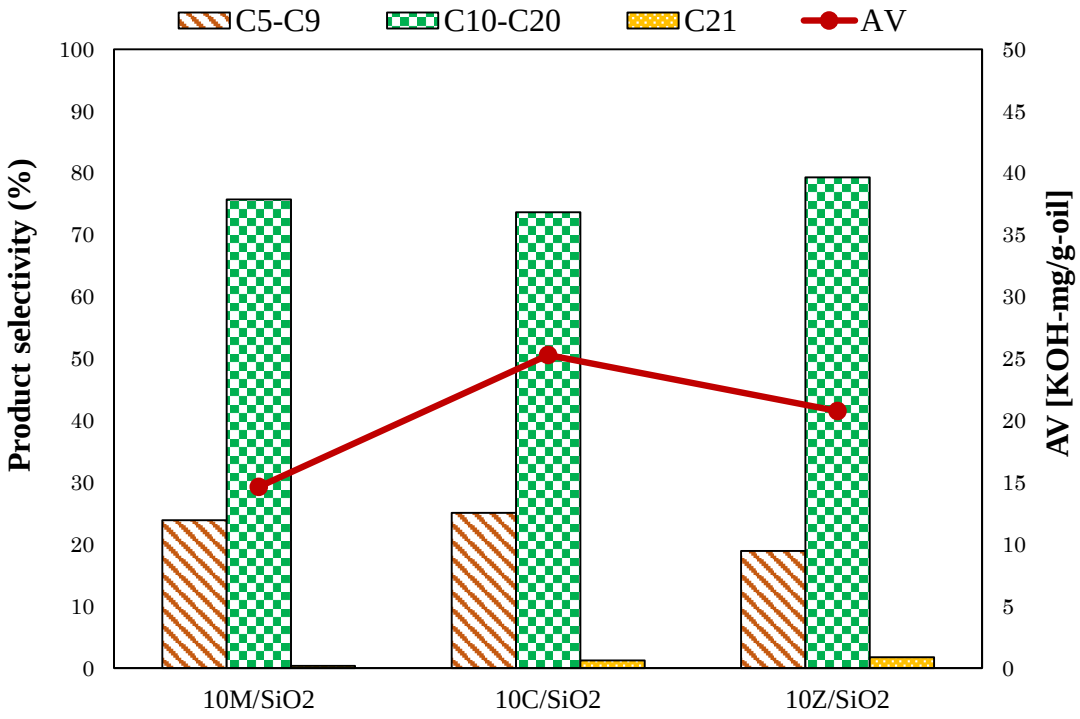

Figure 3.6 Product selectivity and acid value of the cracked oil

Figure 3.6 show the product selectivity and acid value of the cracked oils. From this results, 10M/SiO_2 catalyst gives the lowest acid value was about 14.634 KOH-mg/g-oil followed by 10Z/SiO_2 and 10C/SiO_2 were about 20.759 KOH-mg/g-oil and 25.306 KOH-mg/g-oil, respectively. The product selectivity in diesel range hydrocarbon (C_{10}-

C_{20}) was not significantly different for all basic metal oxide catalysts. C_{21} compounds were found for all catalyst, yield of these compounds on 10M/ZrO_2 catalyst were higher than other catalysts [24].

3.3.2 Effect of the addition of CaO and ZrO_2 to MgO/SiO_2

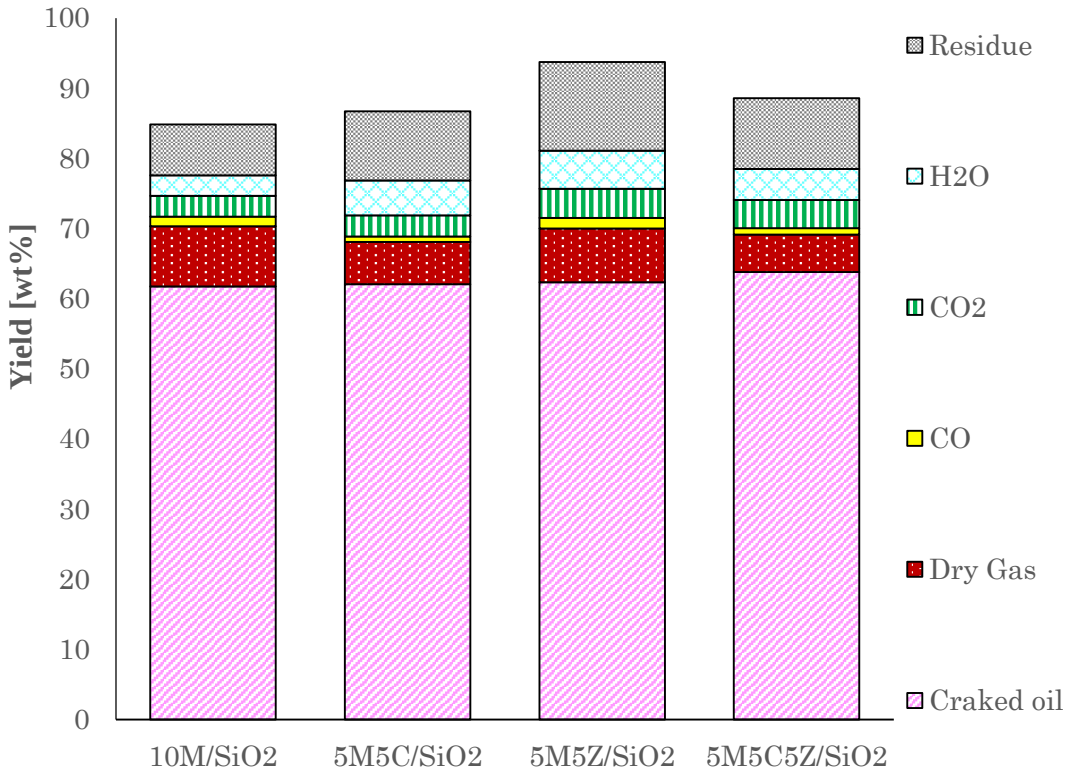

Figure 3.7 Product yield from waste cooking oil over the oxide catalysts

Figure 3.7 shows product yield from waste cooking oil over the oxide catalysts by decarboxy-cracking. The major products recovered were cracked oil, dry gas (C_1-C_4 hydrocarbons), CO, CO_2, water and residue. The unreacted fatty acids was not detected,

as the reacted fatty acids and the unreacted fatty acids may be condensed into liquid products. Therefore, liquid products not only contain the cracked oils but also comprise the unreacted fatty acids. Moreover, unreacted fatty acids would remain as residue. Formation of CO, even the yield was low, was observed over each catalyst. It may be formed by the decomposition of ketones as by-products [25, 26] or through the reverse water-gas shift reaction as the following equations below:

Ketonization

$$R_1{-}COOH + R_2{-}COOH \longrightarrow R_1{-}\overset{\overset{O}{\|}}{C}{-}R_2 \qquad (3.2)$$

Water gas shift

$$CO + H_2O \longleftrightarrow CO_2 + H_2O \qquad (3.3)$$

The CO_2 yields of the binary 5M5Z/SiO_2 and ternary 5M5CZ/SiO_2 catalysts were 1.3～1.4 times higher than that with MgO/SiO_2 and binary 5M5C/SiO_2 catalysts. These facts show that the added oxides would assist MgO and promote the decarboxylation from intermediate free acids as well as triglycerides [25, 26]. The increase in the specific surface area except for 5M5C/SiO_2 would be another effect as shown in **Table 3.2**.

Table 3.2 The physical properties of the catalysts

Catalysts	SA (m^2/g)	PV (cm^3/g)	Basicity (mmol/g)	
			Weak	Strong
10M/SiO_2	186	0.14	0.031	0.099
5M5C/SiO_2	213	0.81	0.033	0.104
5M5Z/SiO_2	253	0.86	0.020	0.084
5M5C5Z/SiO_2	335	1.18	0.035	0.121

The BET surface area (SA) and pore volume (PV) were evaluated from nitrogen physisorption technique. The addition of CaO and/or ZrO_2 to the MgO/SiO_2 have higher surface area and pore volume in comparison to the monometallic 10M/SiO_2 catalyst. This suggests that CaO and ZrO_2 have similar effect on surface area and pore volume. The highest SA and PV were obtained with the ternary 5M5C5Z/SiO_2 catalyst. Moreover, the nitrogen adsorption-desorption isotherm recorded for the fresh catalysts are shown in **Figure 3.8**. As all these catalysts, the shape of the isotherms indicates that they can be classified as type IV isotherm with the presented adsorption-desorption hysteresis loop H2b type according to the IUPAC classification, which is characteristic for mesoporous material. This is suggest that the addition of CaO and ZrO_2 to MgO/SiO_2 had no significant effect on the mesoporous of silica support.

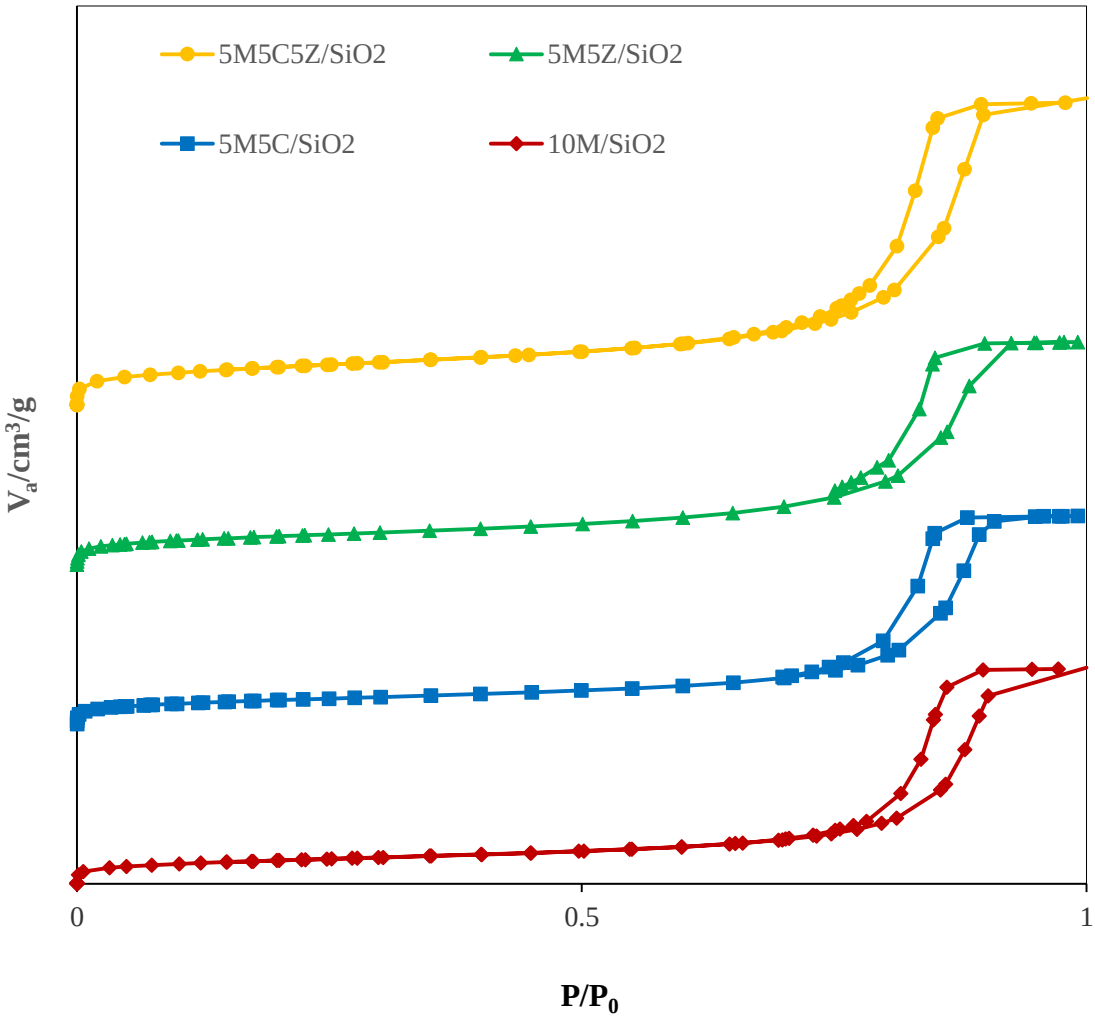

Figure 3.8 Nitrogen adsorption-desorption isotherm of the MgO-based catalysts supported on silica with the addition of CaO and ZrO_2

Figure 3.9 shows the XRD patterns of the fresh and spent MgO-based catalysts supported on silica prepared by incipient wetness impregnation method. There were no significant changes in the XRD patterns between fresh and spent catalysts. In each case, show only a broad diffraction line located at 2θ = 23°-25°, typical of amorphous SiO_2, and no detectable XRD diffraction peaks derived from the supported oxides of MgO, CaO, and ZrO_2 were observed. Thus, these species would exist as highly dispersed ones on the support [27, 28]

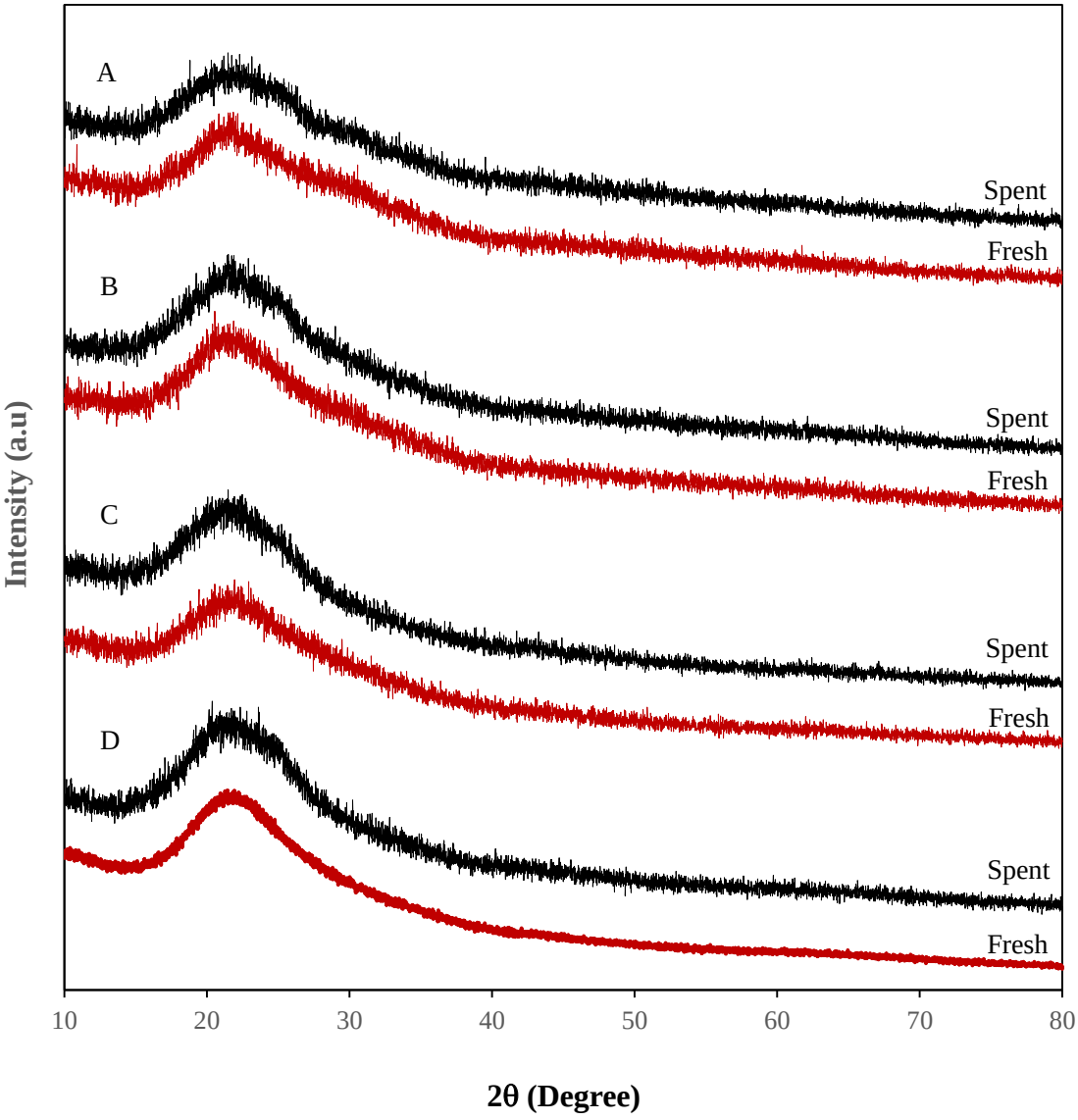

Figure 3.9 XRD patterns of (A) 10M/SiO_2, (B) 5M5C/SiO_2, (C) 5M5Z/SiO_2 and (D) 5M5C5Z/SiO_2 catalysts

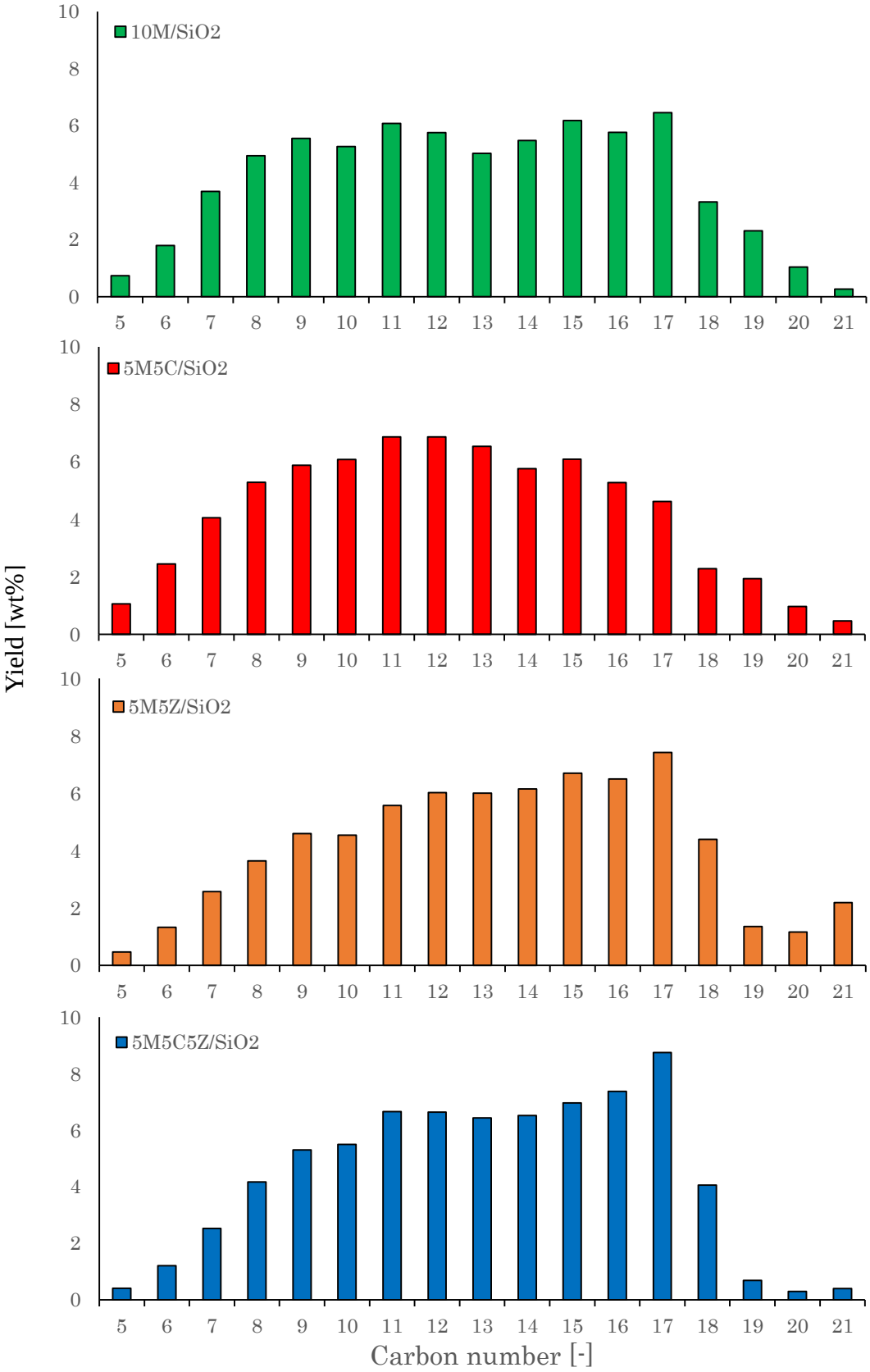

Figure 3.10 Hydrocarbon distribution of the product oil

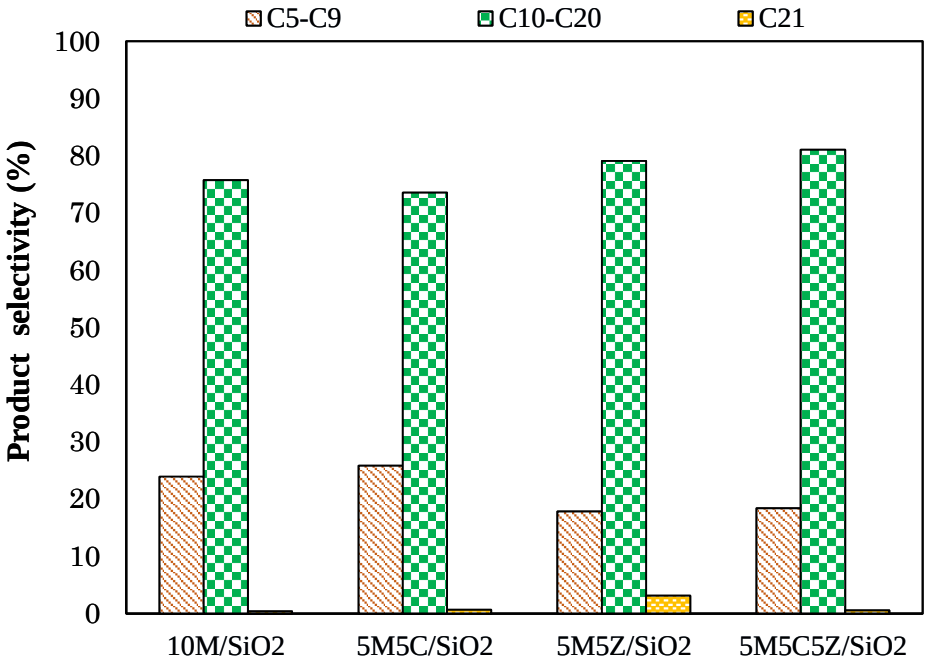

Figure 3.11 Product selectivity of the cracked oil

Figure 3.10 and **Figure 3.11** show the hydrocarbon number distribution and product selectivity of the product oils. As a whole, the distribution profiles are similar to each other; a large amount of hydrocarbons with the diesel fraction (C_{10}-C_{20}) are the major products, while the compounds with carbon number higher than 21 were not observed. The main product obtained with the catalysts except for 5M5C/SiO_2 was C_{17} hydrocarbons, which would be originated from oleic acid group ($C_{17}H_{33}COO$-) and linoleic acid group ($C_{17}H_{31}COO$-) in the waste cooking oil. The C_{17} hydrocarbons could probably be produced from the triglycerides directly and after the decomposition to the corresponding free fatty acids, while the other hydrocarbons with shorter chain than C_{17} would be formed by the cracking of the alkyl groups in the reactants and the products. C_{21} compounds were found to be ketones as described above such as methyl ketone and ethyl ketone. Yield of these compounds increased by adding oxides, especially ZrO_2 [29].

The lower yield of C_{17} with 5M5C/SiO_2 catalyst suggests the higher cracking ability than the other catalysts due to CaO adsorbed carboxylic acid molecules to form $CaCO_3$, it is difficult to desorb CO_2 as evidenced by the temperature programmed of CO_2 as shown in **Figure 3.12.**

The CO_2 desorption of these catalysts were measured by using CO_2-TPD technique. The amounts of CO_2 desorbed for catalysts that calculated from the area below the curve of TPD profiles are also compiled in **Table 3.2**. The characteristic peaks of these profiles can be determined by desorption temperature, which indicating the strength of basic sites. Thus, the CO_2 desorption peaks at low temperature (100-400 °C) and high temperature (500-900 °C) appear in all profiles, suggesting that all catalysts have weak and strong basic sites. The order of base sites of the catalysts are: 5M5C5Z/SiO_2 > 5M5C/SiO_2 > 10M/SiO_2 > 5M5Z/SiO_2. From these results can be observed that the CO_2 uptake increases with the addition of CaO due to CaO as strong base catalyst with the best CO_2 capture capacities, but the adsorption of CO_2 by CaO to form $CaCO_3$ requires a very high energy to decompose into CaO and CO_2 at temperature up to 600 °C.

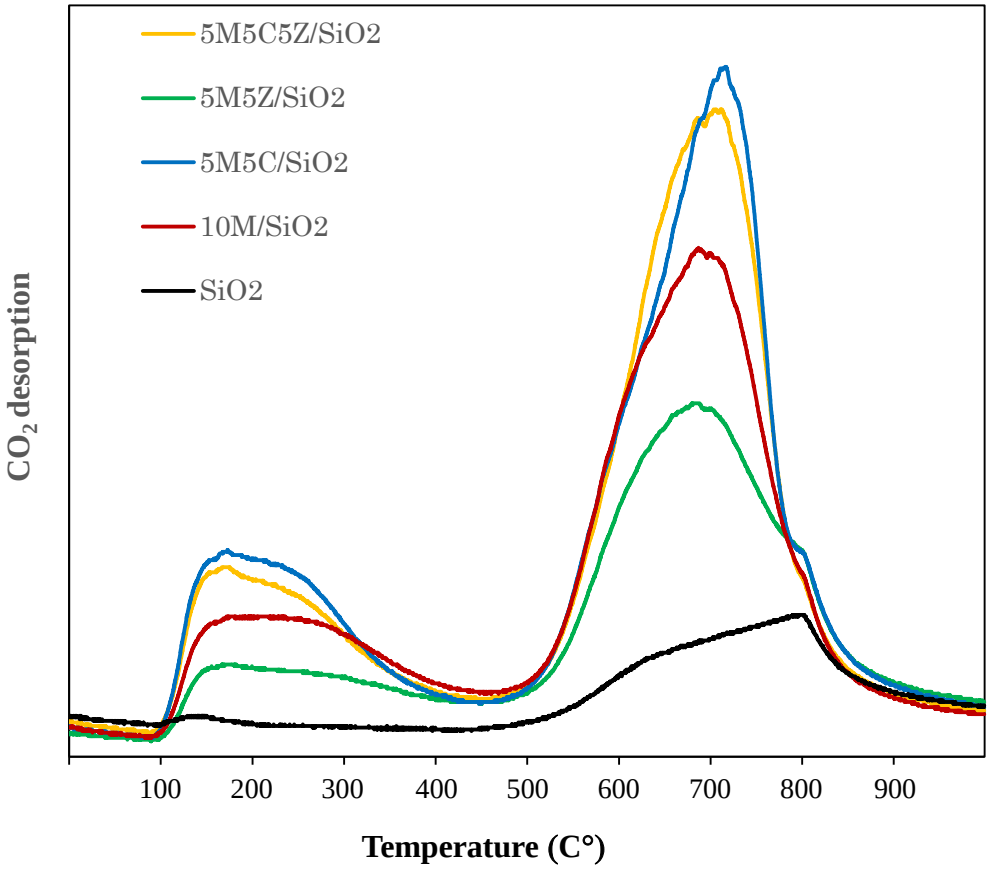

Figure 3.12 Temperature programmed of CO_2 for the MgO-based catalysts supported on silica with the addition of CaO and ZrO_2

Figure 3.13 shows the acid value and iodine value of the cracked oils obtained over the four oxide catalysts. The acid values obtained with the binary MgO-CaO and MgO-ZrO_2 catalysts and the ternary MgO-CaO-ZrO_2 catalyst were about 12.0 mg-KOH/g-oil, and lower than that with MgO alone (14 mg-KOH/g-oil). This would mean the promotion of decarboxylation from the free fatty acid which are the intermediates from triglycerides to hydrocarbons. Although these values were slightly higher than the level of neat regulation (0.5 mg-KOH/g-oil) for the biodiesel fuel, we have already developed an adsorption technique to clear the regulation for the oils with such acid

values [30]. Iodine values of all these oils were about 90 g-I/100 g-oil, which were lower than the neat regulation (120 g-I/100 g-oil). The IV's obtained with the binary and the ternary oxide catalysts were slightly lower than that with MgO alone. The added CaO and ZrO_2 might form new active sites and promote protonation and cracking of C=C double bonds.

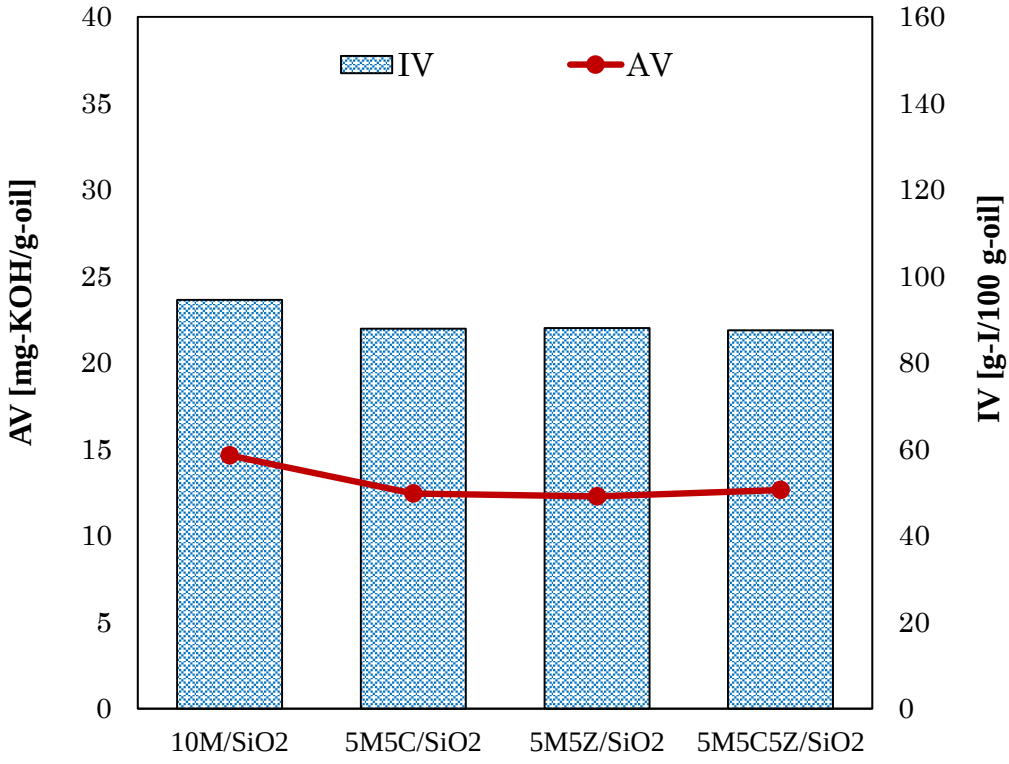

Figure 3.13 The acid value and iodine value of the cracked oils

4. Conclusion

Effects of basic oxide catalysts (MgO, CaO and ZrO_2) and the addition of CaO and ZrO_2 to MgO/SiO_2 catalysts on the HiBD production from waste cooking oil have been investigated and the following conclusions were obtained. The binary MgO-CaO/SiO_2 and MgO-ZrO_2/SiO_2 catalysts and the ternary MgO-CaO-ZrO_2/SiO_2 catalyst were simply synthesized by incipient wetness impregnation method and could be directly used for the HiBD production. The catalyst exhibited good catalytic activities, which gave higher CO_2 yields than MgO/SiO_2 catalyst, and the total acid values of the upgrade biodiesel decreased, indicating that the catalysts promoted decarboxylation reaction by removal of carboxylic acids group as CO_2.

References

[1] Saka S. “All About Biodiesel”, IPC Inc 2006

[2] Maeda S. Sci. Tech. Trends 2007, 11-27

[3] M. Fangrui, and A.H. Milford, Bioresource Technology, vol. 70, pp. 1-5, 1999.

[4] J.B. Hanny, and H. Shizuko. Bioresource Technology, vol. 99, pp. 1716-1721, 2008.

[5] G. Dwivedi, S. Jain, and M.P. Sharma. International Journal of Engineering Science, vol. 3, pp. 292-296, 2013.

[6] G. Dwivedi, S. Jain, and M.P. Sharma. Renew. Sust. Energ. Rev 2011, pp. 4633-4641: vol. 15

[7] O.I. Senol, T.R. Viljava, and A.O.I. Krause, Catalysis Today, vol. 106, pp. 186-189, 2005.

[8] O.I. Senol, E.M. Ryymin, T.R. Viljava, and A.O.I. Krause, Journal of Molecular Catalysis A: Chemical, vol. 268, pp. 1-8, 2007.

[9] O.I. Senol, T.R. Viljava, and A.O.I. Krause, Applied Catalysis A: General, vol. 326, pp. 236-244, 2007.

[10] J.G. Na, B.E. Yi, J.N. Kim, K.B. Yi, S.Y. Park, J.H. Park, J.N. Kim, and C.H. Ko, Catalysis Today, vol. 156, pp. 44-48, 2010.

[11] M. Snare, P. Maki-Arvela, I.L. Simakova, J. Myllyoja and D.Y. Murzin, Russian Journal of Physical Chemistry B, vol. 3, pp. 1035-1043, 2009.

[12] I. Simakova, O. Simakova, P. Maki-Arvela, A. Simakov, M. Estrada, and D.Y. Murzin, Applied Catalysis A: General, vol. 355, pp. 100-108, 2009.

[13] S. Lestari, P. Maki-Arvela, I. Simakova, J. Beltramini, G.Q.M. Lu, and D.Y. Murzin, Catalysis Letters, vol. 130, pp. 48-51, 2009.

[14] S. Lestari, P. Maki-Arvela, H. Bernas, O. Simakova, R. Sjoholm, J. Beltramini,

G.Q.M. Lu, J. Myllyoja, I. Simakova, and D.Y. Murzin, Energy & Fuels, vol. 23, pp. 3842-3845, 2009.

[15] H. Tani, M. Hasegawa, K. Asami and K. Fujimoto, Catalysis Today, vol. 164, pp. 410-414, 2012.

[16] H. Tani, M. Shimouchi, M. Hasegawa and K. Fujimoto, Journal of the Japan Institute of Energy, vol. 90, pp. 466-470, 2011.

[17] Jpn. Reg. Trade Mark, 5468299

[18] C.H. Huang, K.P. Chang, C.T.Yu, P.C. Chiang, and C.F. Wang, Chemical Engineering Journal, vol. 161, pp. 129-135, 2010.

[19] N. Pojananukij, N. Runruksa, S. Neramittagapong, and A. Neramittagapong, International Trasaction Journal of Engineering, Management, &Applied Sciences & Technologies, vol. 5, pp. 77-86, 2014.

[20] X. Jiao, N. Li, F. Xiao, and W. Wei, Energy & Fuels, vol.27, pp. 5407-5415, 2013.

[21] M.J.A. Romero, A. Pizzi, G. Toscano, G. Busca, B. Bosio, and E. Arato, Waste Management, Vol 47, pp. 62–68, 2016.

[22] Y.C. Wong, Y.P. Tan, Y.H. Taufik-Yap, and I. Ramli. Sains Malaysiana, vol. 43(5), pp. 783-790, 2014.

[23] E.P. Reddy and P.G. Smirniotis, The Journal of Physical Chemistry B, vol. 108, pp. 7794-7800, 2004.

[24] T.N. Pham, T. Sooknoi, S.P. Crossley and D.E. Resasco, ACS Catalysis, vol. 3, pp. 2456-2473, 2013.

[25] C.C. Chang, S.W. Wang, Industrial & Engineering Chemistry, vol. 39, pp. 1543-1548, 1947.

[26] M. Watanabe, H. Inomata, R.L. Smith Jr, and K. Arai, Applied Catalysis A: General,

vol. 219, pp. 146-156, 2001.

[27] J. Garcia, T. Lopez, M. Alvarez, D.H. Aguilar, and P. Quintana, J.ournal of Non-Crystalline Solids, vol. 354, pp. 729-732, 2008.

[28] H. Xu, W. Chu, J. Luo, and T. Zhang, Chemical Engineering Journal, vol. 170, pp. 419-423, 2011

[29] R. Pestman, R.M. Koster, A. Van Duijne, J.A.Z. Pieterse, and V. Ponec, Journal of Catalysis, vol. 168, 1997.

[30] K. Fujimoto, Y. Murakami, H. Tani, K. Asami, Japan Patent, 2014-2075: 19

CHAPTER 4

Effect of addition of CaO and ZrO_2 on the performance of MgO/AC catalyst for the synthesis of new biodiesel (HiBD) from waste cooking oil

Abstract: MgO catalysts supported on activated carbon with the addition of CaO and ZrO_2 were successfully prepared by incipient wetness impregnation method used for production of high quality bio-diesel (HiBD) through catalytic-decarboxylation. The prepared catalysts were characterized by BET, XRD and CO_2-TPD. The results of XRD and BET indicated that MgO and added oxides of all of catalysts were highly dispersed on activated carbon and the addition of ZrO_2 lead to a large specific surface area and pore volume. Catalytic conversion of waste cooking oil was carried out with an agitated reactor under conditions of 430 °C in an He flow (50 ml/min). The triglycerides in the oil were converted into a mixture of hydrocarbons, CO, CO_2 and water with a very small amount of oxygenated compounds, mostly free fatty acids. CO_2 yield and acid value (AV) were used to evaluate the decarboxylation performance as indexes. The results indicated that the MgO/AC catalyst with the addition of ZrO_2 exhibited a high activity for the decarboxylation of fatty acids due to it had higher surface area and pore volume.

4.1 Introduction

Biodiesel is one of the promising alternative liquid fuel which can be used as a substitute for petroleum diesel. It has much attention in recent years as an environmentally friendly fuel due to its biodegradability, non-toxic and low emission of green-house gas. Biodiesel can be manufactured from a variety of resources: vegetable oils, animal fats or waste cooking oils [1,2]. Currently, the most common derivative of triglycerides or fatty acids for fuel is fatty acid methyl ester (FAME), which is formed by transesterification of triglyceride with methanol in presence of alkali, acidic or enzymatic catalysts with glycerol as a by-product [3,4]. However, because of high oxygen content of FAME, oxidation stability and performance under cold weather are the major problems [5,6]. Therefore, attention has lately been shifted towards the upgrading of biodiesel by deoxygenation in which oxygen is eliminated either as H_2O or as CO_x.

Catalytic deoxygenation is another alternative technique employed to decrease oxygen content in biodiesel. It is proposed that the major reaction routes of deoxygenation can be via hydrodeoxygenation, decarbonylation and decarboxylation as the following equations below [7].

Hydrodeoxygenation

$$R\text{–}COOH + 3H_2 \longrightarrow R\text{–}CH + 2H_2O \qquad (4.1)$$

Decarbonylation

$$R\text{–}COOH + H_2 \longrightarrow R\text{–}H + CO + H_2O \qquad (4.2)$$

Decarboxylation

$$R\text{–}COOH \longrightarrow R\text{–}H + CO_2 \qquad (4.3)$$

In principle, the decarbonylation (-CO, eq. (4.2)) and decarboxylation (-CO_2, eq.

(4.3)) routes are more applicable than the hydrodeoxygenation pathway (eq. (4.1)), due to less or no hydrogen is required and their higher selectivity to the aliphatic hydrocarbons for diesel applications, respectively, and therefore the production cost is less expensive. Most of the research on decarboxylation of fatty acids as feedstock was carried out over noble metal oxides. Murzin et al. [9-12] have investigated deoxygenation of triglycerides and fatty acids over palladium (Pd) supported on activated carbon catalyst, and the results revealed that Pd/C catalyst displayed as the promising catalyst in the deoxygenation. In addition, Do et al. [13] have reported that alumina-supported Pt (Pt/Al_2O_3) can also be effectively in this reaction. However, considering the high cost of above noble metals, it is more practical in industrial standpoint to develop the catalysts showing similar performance and stability. Zhang et al. [14] investigated the decarboxylation of naphthoic acid over the following series of alkaline-earth metal oxides: CaO, MgO, BaO and SrO. All of these oxides showed high decarboxylation activity for naphthoic acid compound, from which the acid conversion, CO_2 yield and naththalene yield reached 93.9%, 96.9% and 66.2%, respectively. Watanabe et al. [15] have studied the catalytic decarboxylation of stearic acid with alkaline hydroxide (KOH and NaOH) and metal oxides (CeO_2, Y_2O_3 and ZrO_2) in supercritical water. The major products of this reaction were n-heptadecane, n-hexadecane and CO_2. As a consequence, ZrO_2 showed the highest activity with approximately 68% and 9% for conversion of stearic acid and yield of CO_2, respectively.

Recently, we have developed a new biodiesel process which give a mixture of hydrocarbons in the diesel fraction oils of C_{10}-C_{20} aliphatic hydrocarbons as a major products, without using any sub-raw material. We named this fuel as High quality Bio-Diesel (HiBD). HiBD is expected as the second generation diesel fuel which fits the next generation diesel engine due to the physical properties of HiBD is similar to the

conventional diesel fuel and exhibits an excellent low temperature fluidity which enables to use in cold weather as are presented in **Table 4.1**. HiBD can be obtained by catalytic cracking decarboxylation of triglycerides and fatty acids as reaction intermediates over the basic catalyst (MgO/SiO_2) at 400-470 °C and LHSV = 0.3 h^{-1} with releasing oxygen by forming CO_2 [16-20].

In this study, magnesium oxide catalyst supported on active carbon (MgO/AC) is selected as a basic catalyst. However, MgO exhibited a poor CO_2 adsorption properties due to its low surface area and pore volume. This study mainly focuses on improving the performance of MgO/AC catalyst for decarboxylation reaction by the addition of CaO and ZrO_2 to synthesis a new hydrocarbon biodiesel (HiBD) from waste cooking oil, and investigated the CO_2 formation to know the decarboxylation efficiency. Its catalytic activity was evaluated by catalytic cracking and decarboxylation in an agitated reactor.

Table 4.1 Physical properties of high quality bio-diesel (HiBD)

Properties	HiBD (WCO)	JIS Gas oil regulation
Density at 15 °C (g/cm^3)	0.83	0.86 ≥
Kinetic viscosity at 30 °C (mm^2/s)	1.9	≥ 2.5
10% residual carbon	0.1	0.1 ≥
Flash point (°C)	47.5	≥ 50
Cetane number	46.6	≥ 45
Pour point (°C)	-15.0	-7.5 ≥
Blocking point (°C)	-17.0	-5 ≥

4.2 Experimental

4.2.1 Catalyst preparation

MgO/AC catalysts with addition of CaO and ZrO_2 were prepared by the incipient wetness impregnation with a commercially active carbon (SA 862 m^2/g; PV 0.565 cm^3/g) as a support. Precursor materials used for this synthesis were magnesium nitrate hexahydrate ($Mg(NO_3)_2.6H_2O$, 99.0% purity, Wako, Japan), calcium nitrate tetrahydrate ($Ca(NO_3)_2.4H_2O$, 98.5% purity, Wako, Japan) and zirconyl nitrate dihydrate ($ZrO(NO_3)_2.2H_2O$, 97.0% purity, Wako, Japan). After impregnation, they were dried in an oven at 110 °C and then calcined in N_2 at 500 °C for 3 h. Names of the catalyst samples were abbreviated with the loadings; for example, a catalyst containing 5 wt%-MgO, 5 wt%-CaO, and 5 wt%-ZrO_2 on AC was expressed as 5M5C5Z/AC.

4.2.2 Catalyst characterization

The specific surface area of the fresh catalysts was measured by nitrogen adsorption-desorption isotherms at -196 °C. Prior to the BET measurement, the catalysts were preheated at 200 °C for 2 h to remove the adsorbed water. The BET surface areas were determined by a multi-point Brunauer, Emmett and Teller (BET) method at the relative pressures of nitrogen in range of 10^{-6} to 0.99 and pore volume was calculated by applying Barrett, Joyner, and Halenda (BJH) method (BELSORP-mini II, Japan Bel Inc.).

The crystalline structure of the fresh and spent catalysts were determined by X-ray diffraction (XRD) with a RIGAKU, XRD-DSC-XII diffractometer using Cu K_α as the radiation source with $\lambda = 1.54$ Å and Ni as the filter in the range of 2θ from 10° to 80°. The X-ray tube was operated at 40 kV and 20 mA at room temperature.

The basicity of the active catalysts were characterized by using temperature-

programmed desorption of CO_2 (CO_2-TPD) on a BELCAT (Japan Bel Inc.). The catalyst (0.05 g) was heated at 10 °C/min under a flow of helium (He) from room temperature to 500 °C and then held at this temperature for 60 min. After cooling to 50 °C and saturated with 50 ml/min CO_2 for 60 min. Subsequently, the catalyst was purge with He by flowing 50 ml/min for 1 h in order to eliminate any physically adsorbed and/or weakly bond species at 10 °C/min up to 900 °C.

The amount of CO_2, which was adsorbed or reacted with the oxides on the spent catalysts was measured using the thermogravimetric (TG) technique. Around 5 mg of spent catalyst was placed in a platinum crucible that was introduced in a RIGAKU TG 8210. The sample was heated under N_2 flow (100 ml/min) from room temperature up to 900 °C at heating rate of 10 °C/min.

4.2.3 Catalyst testing

The catalytic decarboxylation of waste cooking oil was carried out at 430 °C under atmospheric pressure in an agitated reactor, as shown in **Figure 4.1**. The oil was supplied from the university restaurant with an acid value of 200 mg-KOH/g-oil and iodine value of 101 g-I/100g-oil, respectively. Typically, 25 g of catalyst was charged into the reactor and then it was heated up to the reaction temperature in carrier gas He flow rate = 50 ml/min. It was pumped continuously into the reactor by liquid pump at a rate of 0.25 ml/min. During the reaction, the gaseous products were analyzed every 30 min using an on-line gas chromatograph (Shimadzu GC-14A) with thermal conductivity detector and flame ionization detector. The liquid products were collected by a trap at 0 °C and then analyzed by GC-MS (Agilent GC-7890A). Potentiometric titration methods (JIS 2501-2003 and JIS K0070-1992) were employed to measure total acid value (AV) and iodine

value (IV) of the cracking oil.

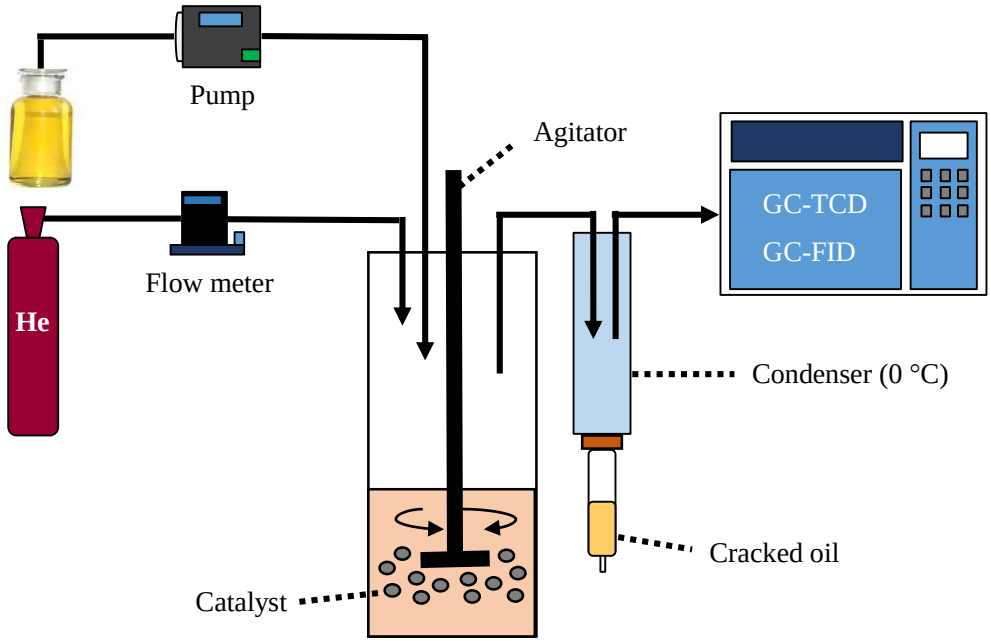

Figure 4.1 Experimental apparatus for catalytic cracking decarboxylation

4.3 Results and discussion

4.3.1 Catalyst Characterization

Table 4.2 Textural properties of the prepared catalysts.

Catalyst	BET surface area (m^2/g)	Pore volume (cm^3/g)	Pore diameter (nm)
AC	813	187	3.14
10M/AC	549	126	3.21
5M5Z/AC	599	138	3.12
5M5C/AC	530	122	2.67
5M5C5Z/AC	466	102	3.21

The catalyst surface area, pore volume and pore diameter are given in **Table 4.2**. It can be seen that the highest surface area was found on the binary 5M5Z/AC catalyst, and the lowest surface area was observed in ternary catalyst, 5M5C5Z/AC. Probably due to the blockage of pore of support by increasing of number of other metals as indicated by the pore volume data.

In order to get information about the strength of basic sites temperature-programmed desorption of CO_2 was carried out**.** The CO_2-TPD profiles over the fresh and spent catalysts are presented in **Figure 4.2.** The spent catalysts was collected after runs of decarboxy-cracking at 430 °C for 7 h. Oil remained in the catalyst was removed by heating in N_2 flow at 250 °C for 4 h. The fresh catalysts showed a similar patterns with two types of CO_2 desorption sites: the first peak centered at lower temperature near 160 °C is assigned to the weak basic sites and the second peak centered at relatively higher temperature (around 500-800 °C) is assigned to the strong basic sites, and contains CO_2 decomposition of activated carbon that the surface contains many oxygen functional

groups: carboxylic, ketone, lactone, phenol. All of these oxygen groups are benefit to adsorb CO_2. The low temperature CO_2 peak at 160 °C of all spent catalysts was very broad or absent, but a sharp CO_2 peak at 675 °C was observed with 5M5C/AC and 5M5C5Z/AC catalysts related to the decomposition of adsorbed CO_2 during the reaction due to $CaCO_3$ requires a high temperature to remove CO_2 [21,22], as evidenced by XRD results (**Figure 4.3**). Moreover a broad peak at 800 °C probably causing CO_2 desorption of activated carbon.

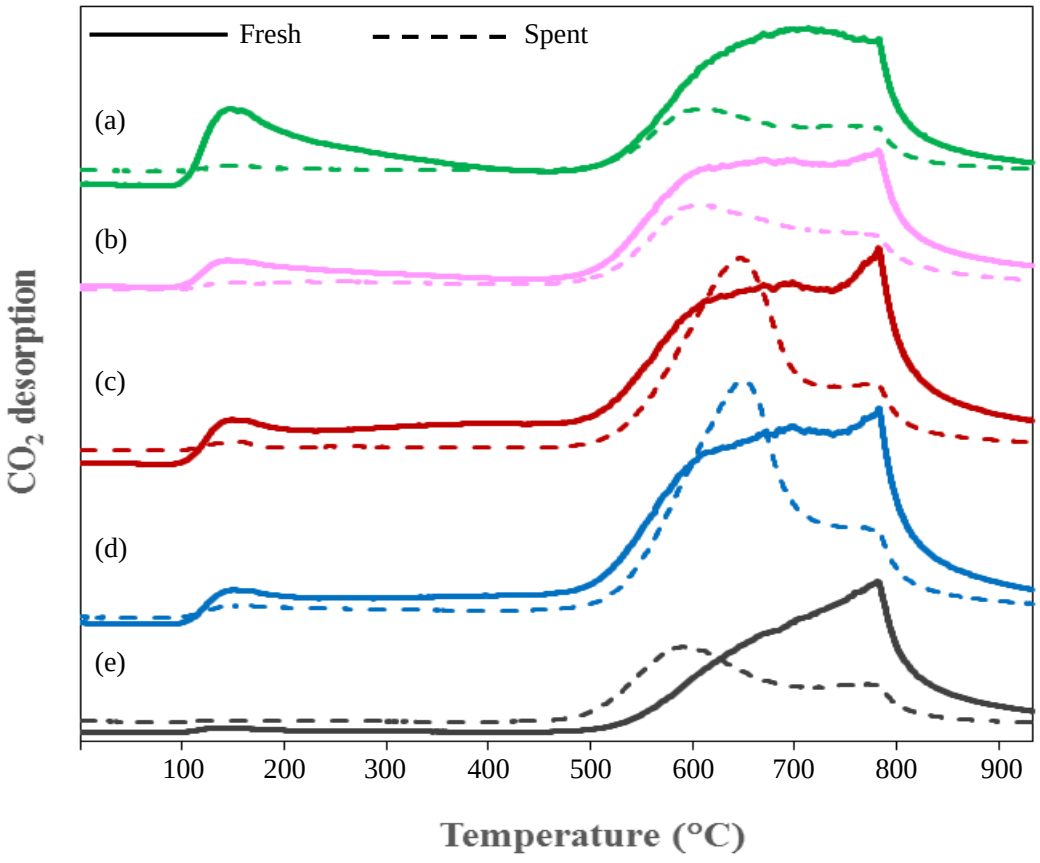

Figure 4.2 CO_2-TPD profiles of the fresh and spent catalysts (a) 10M/AC; (b) 5M5Z/AC; (c) 5M5C/AC; (d) 5M5C5Z/AC; (e) Activated carbon

The total basicity of the fresh and spent catalysts is summarized in **Table 4.3.** On the basis of TPD profiles the basicity of the fresh catalysts can be arranged in the following order: 5M5C5Z > 5M5C > 10M > 5M5Z. Based on these basicity properties of the metal oxide. It has been reported that basic catalysts could improve the adsorption of CO_2 in decarboxylation reaction that supplies more surface oxygen species on the catalyst surface. However, it is quite difficult to estimate the catalyst activity because the catalytic performance also depend on several other important factors including the active surface site, particle size and metal dispersion [23].

Table 4.3 Total basicity of the prepared catalysts.

Catalyst	Total basicity (mmol/g)	
	Fresh	Spent
AC	0.537	0.286
10M/AC	0.857	0.285
5M5Z/AC	0.706	0.350
5M5C/AC	0.818	0.537
5M5C5Z/AC	0.975	0.640

The XRD patterns of the fresh and spent catalysts are shown in **Figure 4.3**. All of catalysts exhibit a broad diffraction peaks around 2θ = 25° and 42°, which suggests an amorphous structure of active carbon. No obvious diffraction peaks of MgO, CaO and ZrO_2, implying that most of MgO, CaO and ZrO_2 species are highly dispersed on the active carbon surface [24]. On the other hand, for the spent catalysts, two typical diffraction lines at around 42° and 62° due to MgO were observable, showing a strong sintering of MgO species. In the cases of catalyst with adding CaO, the XRD peaks assigned to $CaCO_3$ were appeared. This compound was formed by chemical reaction between CaO and CO_2 during the process. In the case of ZrO_2 added catalyst, no clear

diffraction line due to Zr species was observed. It is supposed that the t-ZrO_2 crystal size was extremely small [25]. In these results it can be confirmed the presence of MgO and CaO species in the fresh catalyst.

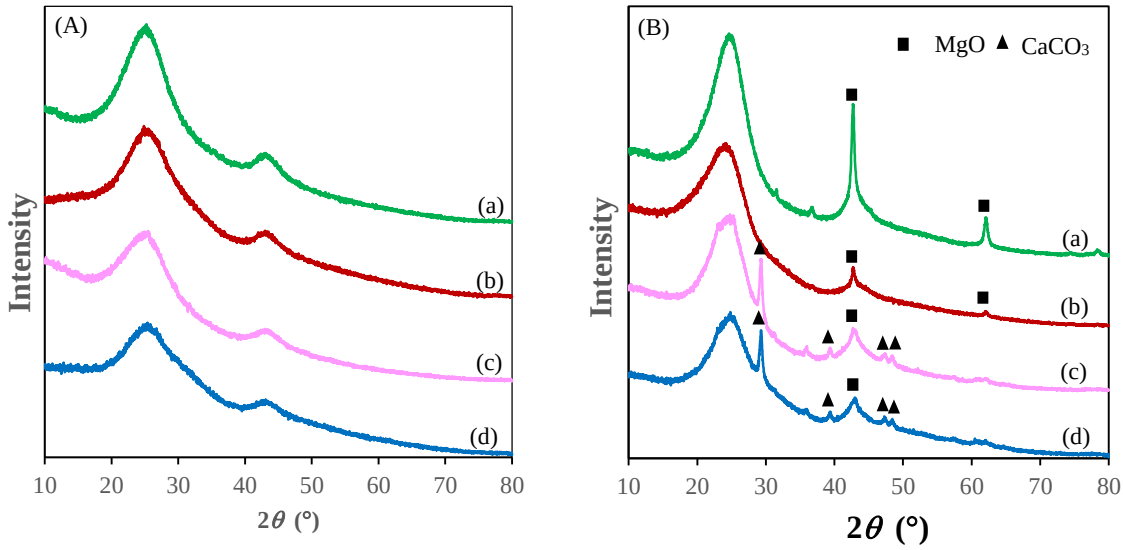

Figure 4.3 XRD patterns of the fresh (A) and (B) spent catalysts. (a) 10M/AC; (b) 5M5Z/AC; (c) 5M5C/AC; (d) 5M5C5Z/AC

4.3.2 Catalytic activity

4.3.2.1 Effect of the addition of CaO and ZrO_2 to MgO/AC

The effect of the addition of metal oxide to MgO/AC catalyst on decarboxylation reaction of waste cooking oil was investigated. For all the catalysts in the study, the major products from this reaction were a mixture of liquid aliphatic hydrocarbons, dry gases (C1-C4 hydrocarbons), CO, CO2, water and residue as presented in **Table 4.4.** The probable reaction pathway of the catalytic decarboxylation of triglycerides is based on three main reactions as shown in **Figure 4.4.** The glycerine formed would then be converted to gaseous hydrocarbons and water by dehydration, while, free fatty acids would be cracked into hydrocarbons and CO2 by decarboxylation. Moreover, two

molecules of the free fatty acids can be dehydrocondensed to produce long chain ketones, which can be further decomposed into hydrocarbons and CO [16,17].

Table 4.4 Material balance of waste cooking oil by decarboxy-cracking

Catalyst	Product yield (%wt)					
	Cracked oil	Dry gas	CO	CO_2	H_2O	Residue
10M/AC	64.8	6.0	0.9	5.9	4.4	11.9
5M5Z/AC	65.2	6.8	1.3	6.9	4.3	10.7
5M5C/AC	62.1	7.3	1.2	5.5	4.6	13.4
5M5C5Z/AC	64.6	6.5	1.2	5.1	3.4	12.1

Reaction conditions: He = 50 ml/min, oil feed flow rate = 0.25 ml/min, reaction temperature 430 °C.

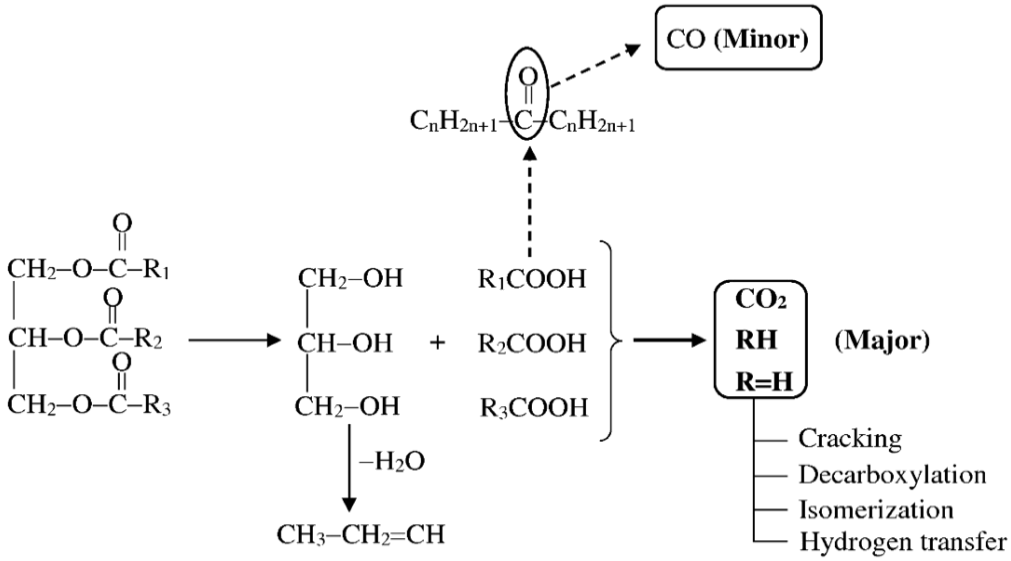

Figure 4.4 Reaction pathway of catalytic decarboxylation of triglycerides

Figure 4.5 shows the effect of the addition of ZrO_2 and CaO on the production of hydrocarbons. All of catalysts gave high yield of hydrocarbons with diesel fraction (C_{10}-C_{20}), while the compounds with carbon number higher than 21 were not observed.

In the cases over the catalysts with CaO, the yield of C_1-C_9 increased, indicating that catalytic cracking of aliphatic groups in the triglycerides into lighter hydrocarbons was promoted by the addition of the compound. C_{21} compounds were found to be ketones as described above such as methyl ketone and ethyl ketone. Yield of these compounds increased by adding oxides, especially ZrO_2 [20, 26,27].

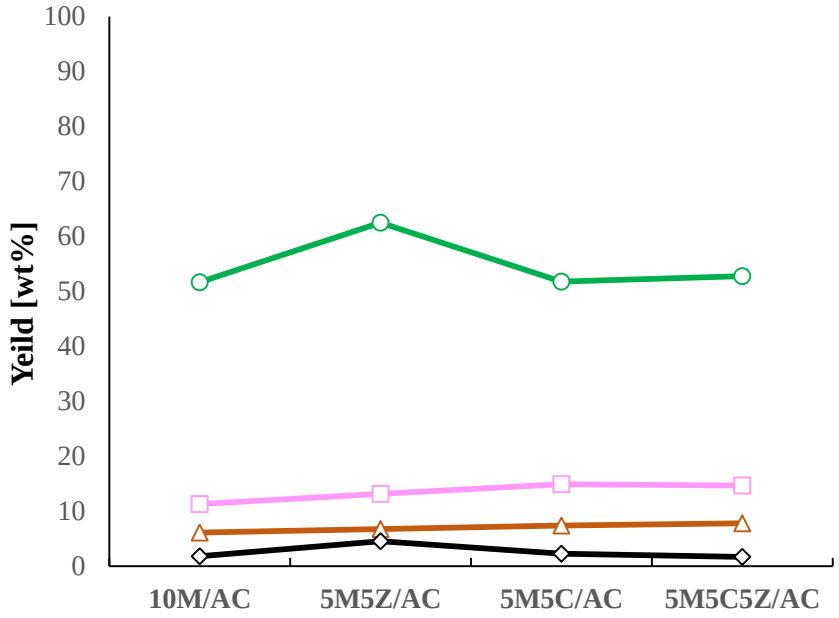

Figure 4.5 Effect of the addition of CaO and ZrO_2 on the production of the main fractions: (△) C_1-C_4; (□) C_5-C_9; (○) C_{10}-C_{20}; (◇) C_{21} compound

According to literature, decarbonylation and decarboxylation are essential reactions in the deoxygenation of carboxylic acids, therefore, removal of CO and H_2O can take place in the deoxygenation step [28]. The decarboxylation activity over four catalysts is presented in **Figure 4.6**. When all the ester groups in the parent oil are converted to CO_2, its yield comes to about 17 wt%, assuming the average formula of the triglycerides as $C_3H_5(OCOC_{17}H_{34})_3$. The results indicated that about half and 10% of molar fraction of the ester groups were converted to CO_2 and CO, respectively. The rest

of them would probably be converted to carbon (coke) and water, and a small amount was transformed to other oxygen containing compounds such as FFA's. Binary 5M5Z/AC catalyst gave highest CO_2 yield due to its high surface area and can reduce carboxylic acids selectively by the interaction between oxygen in the acid groups and oxygen vacancies on ZrO_2 surface and easily removed or desorbed by heating for a short while. In contrast, the low yield of CO_2 over the catalyst with low surface areas (10M/AC, 5M5C/AC and 5M5C5Z/AC catalysts) might be due to diffusion limitation between the reactants and the active sites. Moreover, the addition of CaO could impact on yield of CO_2 since CaO can react with CO_2 to form $CaCO_3$, and its decomposition reaction requires a thermal activation to remove the adsorbed CO_2 [29]. These results are in accordance with TGA analysis of the spent catalysts, though not presented here. Weight loss due to CO_2 release from the catalyst occurred at over 600 °C and the amount of CO_2 formed on the catalysts is also showed in **Figure 4.6.** Clearly, the addition of CaO resulted in a high CO_2 weight loss. It is indicated that CaO significantly improved CO_2 capture capacity of catalyst. Furthermore, the low yield of CO was observed over each catalyst. The presence of CO would probably formed through decomposition of ketones which was formed by dimerization of fatty acids or through a reverse water- gas shift reaction [20,26,27].

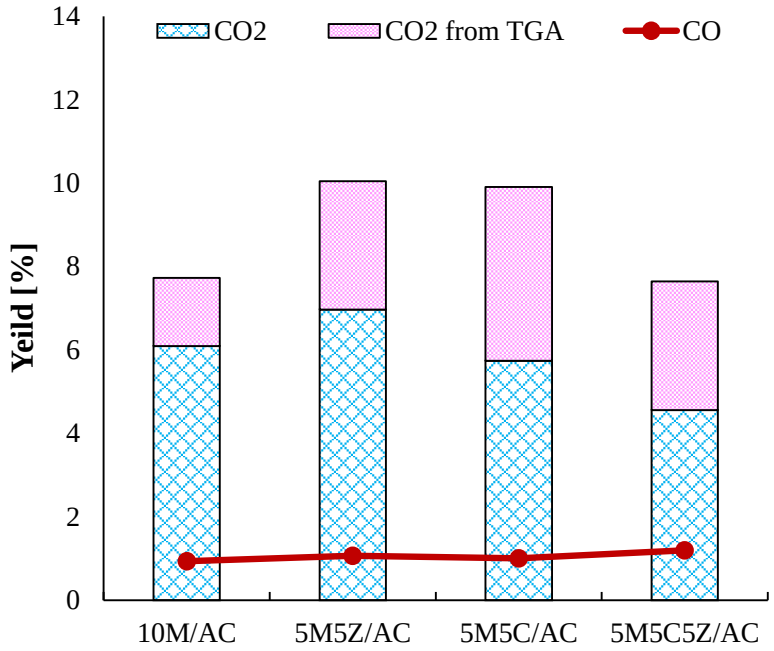

Figure 4.6 Decarboxylation activity of waste cooking oil over the oxide catalysts

Figure 4.7 shows the acid value (AV) and iodine value (IV) of product oils. The acid values with addition of CaO and ZrO_2 were slightly lower than that with MgO alone, about 9.0-11.6 mg-KOH/g-oil. This suggested that the added CaO and ZrO_2 promote the decarboxylation reaction and ketonization of fatty acid to hydrocarbon. Although these values were slightly higher than the level of neat regulation (0.5 mg-KOH/g-oil) for the biodiesel fuel, we have already developed an adsorption technique to clear the regulation for the oils with such acid values. Iodine values of all these oils were less than 80 g-I/100g-oil and slightly lower than that obtained with MgO, indicating that the addition of CaO and ZrO_2 facilitated the cracking of C=C bonds.

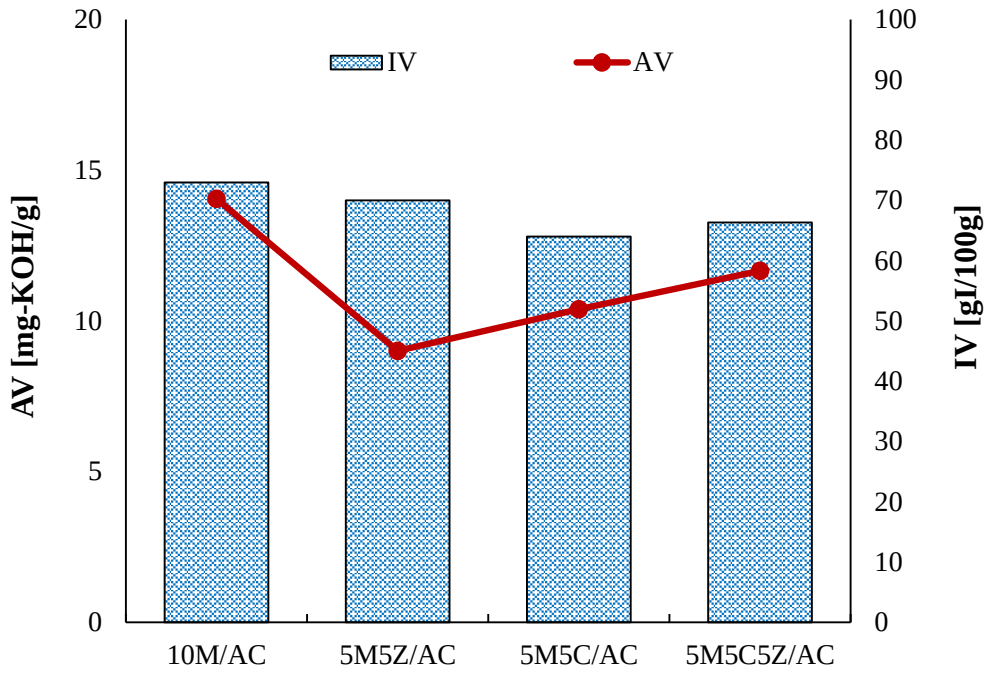

Figure 4.7 Effect of the addition of CaO and ZrO_2 on acid value and iodine value of the cracked oils

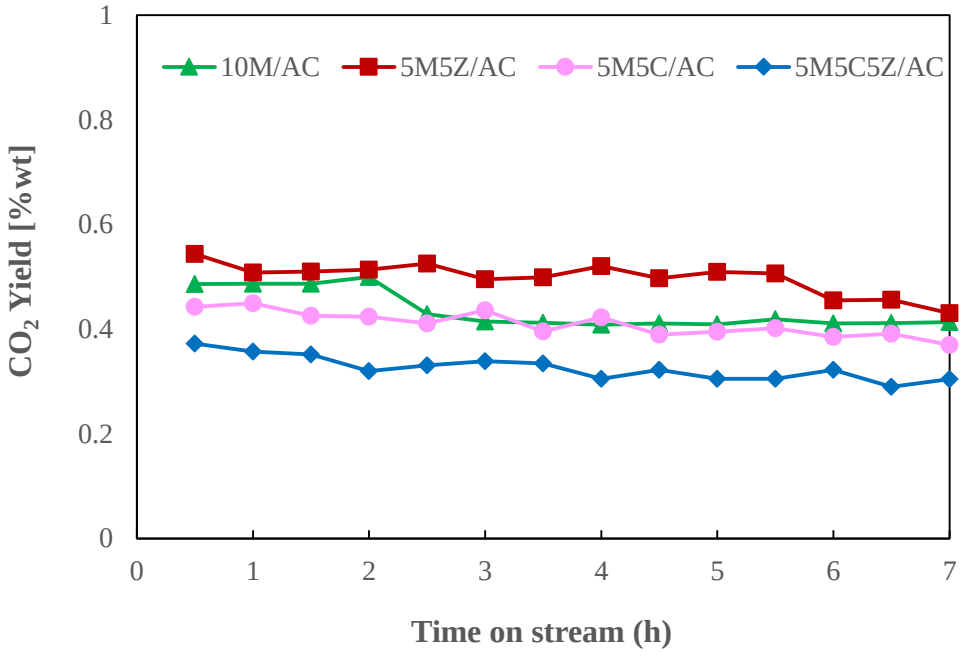

Figure 4.8 The time on stream stability of the oxide catalysts

The stability in term of decarboxylation of waste cooking oil over oxide catalysts, was evaluated at 430 °C for 7 h and their results are shown in **Figure 4.8.** Although rapid deactivation was not so significant for each catalyst, it is observable that the activity of MgO/AC catalyst decreased sharply in the first 2 h on stream and then became stable, while the binary 5M5Z/AC, 5M5C/AC and ternary 5M5C5Z/AC catalysts showed relatively stable behavior under the same conditions. These results suggest that the addition of CaO and ZrO_2 helps to improve the catalytic stability of catalyst.

4.3.2.2 Effect of carrier gas

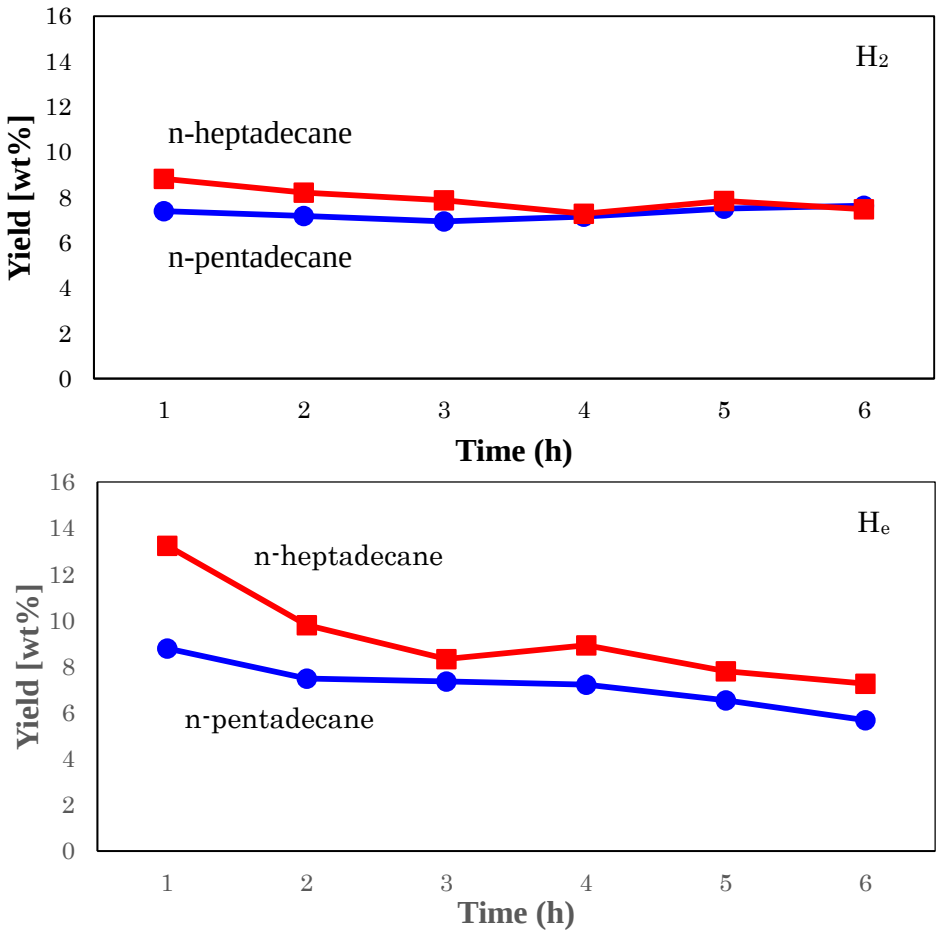

Figure 4.9 Product distribution from catalytic decarboxylation in the flow of H_2 and He at 430 °C

Comparison of the yield of n-pentadecane (C_{15}) and n-heptadecane (C_{17}) in the cracked oil product under flow of two different gases, He and H_2, can be seen in **Figure 4.9.** After 6 h, the yield of C_{15} and C_{17} hydrocarbons at 430 °C under H_2 flow showed relatively stable were approximately 7.6% and 7.5%, respectively. The final yield after 6 h at the same reaction temperature but under He flow were 7.2% and 5.6%, respectively. The decreasing of C_{15} and C_{17} under He is probably due to a faster catalyst deactivation, the presence of H_2 is desirable to maintain stable catalytic activity [30]. In both cases, C_{15} and C_{17} hydrocarbons were the major product.

4.3.2.3 Effect of liquid hourly space velocity (LHSV)

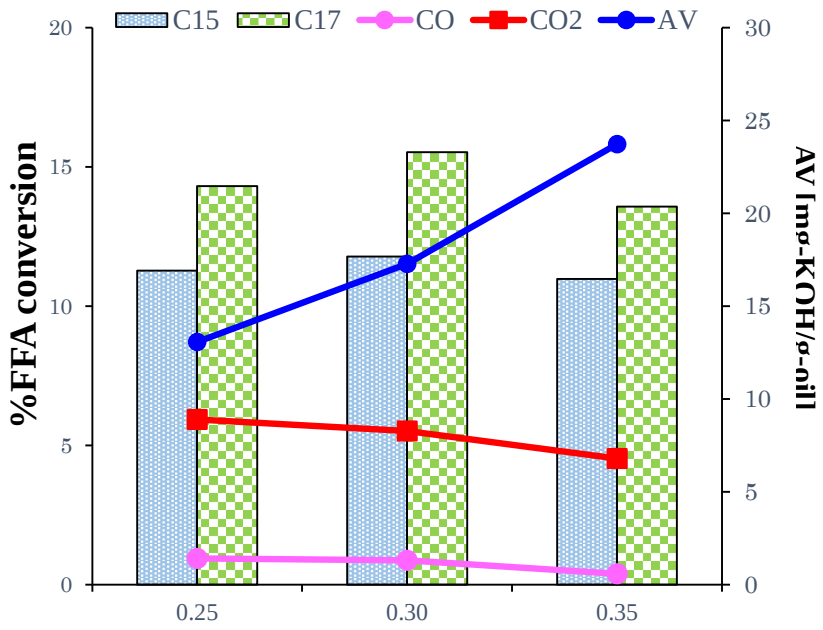

Figure 4.10 Effect of LHSV on catalytic decarboxylation

The effect of LHSV on the catalytic decarboxylation of waste cooking oil was studied in the range of 0.25 h^{-1} to 0.35 h^{-1} by keeping temperature and carrier gas flow rate at 430 °C and 50 mL/min, respectively. The catalyst is 5M5Z/AC. The results are

shown in **Figure 4.10**. The tendency of LHSV decreasing is favorable to the conversions of decarboxylation and decarbonylation of waste cooking oil. The yield of C_{15} and C_{17} increases significantly with LHSV = 0.30 h^{-1}. Obviously, a higher LHSV results in a low yield of C_{15}, C_{17}, CO and CO_2. Moreover, a higher LHSV gave a high acid value of the product oil.

4.4 Conclusion

MgO/AC with the addition of CaO and ZrO_2 were prepared by incipient wetness impregnation method has been successfully applied in a new hydrocarbon biodiesel (HiBD) production which can substitute for petroleum diesel. The catalytic activity for the cracking and decarboxylation of triglycerides greatly depended on surface area of the catalysts. With regard to the finding results, the addition of CaO and ZrO_2 significantly improved the catalyst activity and stability. The addition of ZrO_2 was found to increase the yield in diesel fraction for the catalytic decarboxylation of waste cooking oil whereas the addition of CaO lead to the formation of increased lighter hydrocarbons (C_1-C_9) though the diesel yield was decreased.

References

[1] M. Fangrui, and A.H. Milford, Bioresource Technology, vol. 70, pp. 1-5, 1999.

[2] J.B. Hanny, and H. Shizuko. Bioresource Technology, vol. 99, pp. 1716-1721, 2008.

[3] D. Ayhan. Energy Conversion and Management, vol. 44, pp. 2093-2109, 2003.

[4] D.P. Prafulla, G.G. Veera, K.R. Harvind, M. Tapaswy, and D. Shuguang, Journal of Environmental Protection, vol. 3, pp. 107-113, 2012.

[5] G. Dwivedi, S. Jain, and M.P. Sharma. International Journal of Engineering Science, vol. 3, pp. 292-296, 2013.

[6] G. Dwivedi, S. Jain, and M.P. Sharma. Renew. Sust. Energ. Rev 2011, pp. 4633-4641: vol. 15

[7] J.G. Immer, M.J. Kelly, and H.H. Lamb, Applied Catalysis A: General, vol. 375, pp. 134-139, 2010.

[8] S.J. Eduardo, and M.J. Crocker, Journal of Chemical Technology and Biotechnology vol. 87, pp. 1041-1050, 2012.

[9] M. Snare, Kubickova I, Maki-Arvela P, Eranen K, Warna J, Murzin D Y. Chem. Eng. J 2007, pp. 29-34: vol. 134

[10] M. Snare, I. Kubickova, P. Maki-Arvela, D. Chichova, K. Eranen, and D.Y. Murzin. Fuel, vol. 87, pp. 933-945, 2008.

[11] I. Simakova, O. Simakova, P. Maki-Arvela, A. Simakov, M. Estrada, and D.Y. Murzin, Applied Catalysis A: General, vol. 355, pp. 100-108, 2009.

[12] P. Maki-Arvela, M. Snare, K. Eranen, J. Myllyoja, and D.Y. Murzin, Fuel, vol. 87, pp. 3543-3549, 2008.

[13] P.T. Do, M. Chiappero, L.L. Lobban, and D.E. Resasco, Catalysis Letters, vol. 130, pp. 9-18, 2009.

[14] A. Zhang, Q. Ma, K. Wang, X. Lui, P. Shuler, and Y. Tang. Applied Catalysis A: General, vol. 303(1), pp. 103-109, 2006.

[15] M. Watanabe, T. Iida, and H. Inomata. Energy Conversion and Management, vol. 47, pp. 3344-3350, 2006.

[16] H. Tani, M. Shimouchi, M. Hasegawa and K. Fujimoto, Journal of the Japan Institute of Energy, vol. 90, pp. 466-470, 2011.

[17] H. Tani, M. Hasegawa, K. Asami and K. Fujimoto, Catalysis Today, vol. 164, pp. 410-414, 2012.

[18] Y. Murakami, H. Tani K. Asami, and Fujimoto K, Journal of the Japan Institute of Energy, vol. 94, pp. 1074-1078, 2015.

[19] K. Asami, Y. Komatsu, K. Ono, and K. Fujimoto, Journal of the Japan Petroleum Institute, vol. 58 (5), pp. 293-301, 2015.

[20] P. Natewong, Y. Murakami, H. Tani and K. Asami, Journal of the Japan Institute of Energy, vol. 94, pp. 1393-1393, 2015.

[21] M.C.G. Albuquerque, I. Jimenez-Urbistondo, J. Santamaria-Gonzalez, J.M. Merida Robles, R. Moreno-Tost, E. Rodriguez-Castellon, A. Jimenez-Lopez, D.C.S Azevedo, C.L. Cavalcante Jr, and P. Maireles-Torres. Applied Catalysis A: General, vol. 334 (1), pp. 35-43, 2008.

[22] H.V. Lee, J.C. Juan, N.F.B Abdullah, and Y.H. Taufiq-Yap, Chemistry Central Journal, vol. 8, pp. 30-33, 2014.

[23] K.Y. Koo, H.S. Roh, U.H. Jung, D.J. Seo, Y.S. Seo, and W.L. Yoon. Catalysis Today, vol. 146, pp. 166-171, 2009.

[24] H. Chen, X. Zhou, H. Shang, C. Liu, J. Qiu, and F. Wei, Journal of Natural Gas Chemistry, vol. 13, pp. 209-217, 2004.

[25] S.G. Liu, S.Y. Huang, L.X. Guan, J.P. Li, N. Zhao, W. Wei, and Y.H. Sun. Microporous and Mesoporous Materials, vol. 102 (1-3), pp. 304-309, 2007.

[26] B. Peng, C. Zhao, S. Kasakov, S. Foraita, and J.A. Lercher, Chemistry-A European Journal, vol. 19(15), pp. 4732-4741, 2013.

[27] M. Watanabe, H. Inomata, R.L. Smith Jr, and K. Arai, Applied Catalysis A: General, vol. 219, pp. 146–156, 2001.

[28] P. Maeki-Arvela, I. Kubickova, M. Snare, K. Eranen, and D.Y. Murzin, Energ. Fuel, vol.21, pp. 30-41, 2007.

[29] Y.C. Wong, Y.P. Tan, Y.H. Taufik-Yap, and I. Ramli. Sains Malaysiana, vol. 43(5), pp. 783-790, 2014.

[30] P.T. Do, M. Chiappero, L.L. Lobban, and D.E. Resasco, Catalyst Letter, vol. 130, pp. 9-18, 2009.

CHAPTER 5

CONCLUSIONS

Biodiesel is a one promising alternative fuels, which can be used as a diesel engines fuel. It has much attention because it is clean renewable fuel, non-toxic and producing lower greenhouse gas emissions than conventional diesel. However, the high oxygen content in the biodiesel molecules which lead to a major problems of using biodiesel as a fuel. Lowering oxygen content of the fuel would improve the fuels properties, such as pour point, stability, energy density, etc. This research presents an important hydrocarbon biodiesel production technology which can lower oxygen content by catalytic decarboxylation to synthesis a new hydrocarbon in diesel specification range (C_{10}-C_{20}) from waste cooking oil on the MgO-based catalyst.

Catalysts play an important role in hydrocarbon biodiesel synthesis. Therefore, MgO-based catalysts supported on different supports for waste cooking oil decarboxylation was first conducted. Using an agitated reactor under inert gas helium at a flow rate 50 mL/min and oil feed flow rate 0.25 mL/min. The MgO-based catalysts supported on different supports: γ-Al_2O_3, SiO_2, ZrO_2 and active carbon, were successfully prepared by incipient wetness impregnation method and then tested for their effectiveness on catalytic decarboxylation. The experiment results are follows:

1. All catalysts could convert triglycerides and their derivatives into hydrocarbons in diesel range (C_{10}-C_{20}). Particularly, the major liquid products are n-pentadecane (C_{15}) and n-heptadecane (C_{17}), which contain one carbon atom shorter than the total length of corresponding fatty acid $C_{(n-1)}$ i.e.

palmitic acid and oleic acid.

2. Such n-pentadecane (C_{15}) and n-heptadecane (C_{17}) can be produced from two parallel pathway: decarboxylation or subsequent cracking reaction. The highest C_{15} and C_{17} yield were observed for the 10M/AC catalyst with 8.1 and 10.2 wt%, respectively. The high external surface area of active carbon may result in a high dispersion of MgO active sites. While 10M/ZrO_2 catalyst has the smallest surface area among all catalysts, but shows a higher C_{15} and C_{17} yield than 10M/SiO_2 and 10M/Al_2O_3 catalysts due to that ZrO_2 is a good catalyst support and has high oxygen vacancies, which can improve the adsorption of carboxylic group in the waste cooking oil. However, the surface areas of the spent 10M/SiO_2 was preserved and easily regenerated by calcination in air.
3. The effect of reaction temperature on decarboxylation was also investigated at various temperatures from 400 - 470 °C. The yield of CO_2 increased with the increasing of reaction temperatures. It is believed that increasing temperature enhanced the activation energy to release CO_2, whereas the yield of dry gas (C_1-C_4) increased because the thermal cracking of long chain hydrocarbons.

Therefore, further studies were carried out on the catalytic performance of the 10M/SiO_2 and 10M/AC catalysts. The activity, durability and decarboxylation selectivity of the 10M/SiO_2 and 10M/AC catalysts with the addition of CaO and ZrO_2 were investigated. Points are follows:

1. The binary MgO-CaO and MgO-ZrO_2 catalysts and the ternary MgO-CaO-

ZrO_2 catalyst supported on SiO_2 or active carbon significantly improved the catalyst activity and stability due to they had higher surface area and pore volume in comparison to the monometallic 10M/SiO_2 or 10M/AC catalysts.

2. The addition of CaO lead to the formation of increased lighter hydrocarbons (C_1-C_9) though the diesel yield was decreased, whereas the addition of ZrO_2 was found to increase the yield in diesel fraction for the catalytic decarboxylation of waste cooking oil and also improved resistance to coke formation on the surface catalyst.
3. Moreover, the addition of CaO and ZrO_2 to MgO/AC catalyst improved the stability of the catalysts. This support became much more active and selective to diesel hydrocarbons production with 10wt % ZrO_2 loading.

Future works

1. In this study, MgO, CaO and ZrO_2 were employed on the high support material to study the catalytic decarboxylation of waste cooking oil. But the addition of CaO lead to the formation of increased lighter hydrocarbons (C_1-C_9), while ZrO_2 can be the promoter for MgO catalysts. Thus, MgO-ZrO_2 based catalysts will be synthesized in the future by using different preparation techniques (Co-precipitation, sol-gel method and hydrothermal synthesis) to study the effects on the activity and selectivity of catalysts.
2. This particular idea for future research. The problem of durability of active carbon due to coke formation deposit on catalyst surface. I recommend future studies to include hydrogen for extends the catalyst lifetime, the presence of H_2 is highly desirable to maintain stable catalytic activity.
3. As a result of MgO supported on silica, the surface area was preserved after reaction. Although, the decarboxylation was accompanied by cracking reaction. For future research, the silica support will continue to study. Acid phosphotungstic heteropoly (HPW) or acidic cesium hetetropoly salt (CsPW) supported on silica were active for decarbonylation and decarboxylation of carboxylic because of there are metal-oxygen octahedral as a basic structure.

Acknowledgments

I would like to thank to all the people who have contributed to this thesis in innumerable ways during the past three years.

First and foremost, I would like to express my sincere gratitude to my advisor Prof. Dr. Asami Kenji for his kind support during my Ph.D study and research. I would like to thank him for his patience, enthusiasm and guidance at all times during the research. He always gave me sound advice that helped me to achieve my aims. By benefiting from his experience, I learned many fundamental skills and acquired much invaluable knowledge of catalysis. Without him, this thesis would not have been written or completed.

I am very grateful to Prof. Fujimoto Kaoru for your support. I learned many things from the valuable discussions with you.

Then I would like to thank to Dr. Tani, Ms. Murakami, Mr. Takada for them kind assistance in conducting experiments throughout my laboratory work. I appreciate the value of them work in our group to solve the technical issues.

I would also like to thank all members of the technical support team in the analysis center, especially Mr. Tarada. Whenever I need help to solve technical problems.

To my close friend and sister by choice, Natthawan Prasongthum, a deep gratitude for enriching my life and be my pillar of strength.

Last but not least, I appreciate the encouragement, support and understanding from each member of my family. Thank you very much.

Many thanks to all of you, Paweesuda

LIST OF PUBLICATIONS

1. **Natewong P**, Murakami Y, Tani H, Asami K, Effect of Support Material on MgO-Based Catalyst for Production of New Hydrocarbon Bio-Diesel, American Scientific Research Journal for Engineering, Technology, and Sciences, 22 (2016) 153-165.
2. **Natewong P**, Murakami Y, Tani H, Asami K, Development of Heterogeneous Basic Catalysts Supported on Silica for the Synthesis of High Quality Bio-Diesel from Waste Cooking Oil, Journal of the Japan Institute of Energy, 94 (2015) 1393-1396.
3. **Natewong, P**, Murakami, Y, Tani, H, Asami, Kenji. Effect of the Addition of CaO and ZrO_2 on the Performance of MgO/AC Catalysts for the Synthesis of New Biodiesel (HiBD) from Waste Cooking Oil. American Scientific Research Journal for Engineering, Technology, and Sciences, 24 (2016): 76-89.
4. Prasongthum, N, **Natewong, P,** Reubroycharoen, P. Highly active and stable Ni supported on CNTs-SiO_2. Fuel Processing Technology, Submitted (2016)

LIST OF CONFERENCE

International conference

1. **Natewong P,** Murakami Y, Tani H, Asami K, Development of Heterogeneous Basic Catalysts Supported on Silica for the Synthesis of High Quality Bio-Diesel from Waste Cooking Oil, The 2nd Asian Conference on Biomass Science (ACBS2015), Tsukuba, Japan, January 2015,
2. **Natewong P,** Murakami Y, Tani H, Asami K, Effect of the addition of CaO and ZrO_2 on the performance of MgO/AC catalyst for the synthesis of new biodiesel (HiBD) from waste cooking oil, The 13th China-Japan Symposium on Coal and C1 Chemistry, Dunhuang, China, September 2015.
3. **Natewong P,** Murakami Y, Tani H, Asami K, Effect of ZrO_2 addition to active carbon-supported MgO catalyst for production of new hydrocarbon biodiesel, The 45th Petro.-Petrochem. Symposium of JPI, Nagoya, Japan, November 2015.
4. **Natewong P,** Murakami Y, Tani H, Asami K, Effect of ZrO_2 addition to active carbon-supported MgO catalyst for production of new hydrocarbon biodiesel, SATREPS Special International Conference on Biomass Energy, Osaka, Japan, March 2016.

Appendix

Calculation for preparation of 10wt% MgO/SiO_2 catalyst (10M/SiO_2)

Precursors

$Mg(NO_3)_2.6H_2O$ (256 g/mol)

Silica (pore volume = 1.06 mL/g)

Deionized water

Assume silica = 100 g

10% MgO/SiO_2 catalyst $\Rightarrow$ SiO_2 90 g + MgO 10 g

Therefore, SiO_2 90 g = MgO 10 g

Silica 100 g = MgO (10 x 100)/90 g

= MgO 11.11 g

	MgO 1 mol	= $Mg(NO_3)_2.6H_2O$	1 mol
Therefore,	MgO 40.00 g	= $Mg(NO_3)_2.6H_2O$	256 g
From above	MgO 11.11 g	= $Mg(NO_3)_2.6H_2O$	(256 x 11.11)/40 g
		= $Mg(NO_3)_2.6H_2O$	71.1 g

Pore volume of silica = 1.06 mL/g

Therefore, silica 1 g in volume of solution 1.06 mL

From above Assume silica = 100 g

Thus, silica 100 g in volume of solution (1.06 x 100)/1 mL

volume of solution = 106 mL

Therefore,	$Mg(NO_3)_2.6H_2O$ 256 g	= H_2O 108 g
	$Mg(NO_3)_2.6H_2O$ 71.1 g	= H_2O (71.1 x 108)/256 g

= H_2O 29.99 g

So, $Mg(NO_3)_2.6H_2O$ 71.1 g

SiO_2 100 g

DI water 76.01 g

Calculation for preparation of 10wt% CaO/SiO_2 catalyst (10C/SiO_2)

Precursors

$Ca(NO_3)_2.4H_2O$ (236.15 g/mol)

Silica (pore volume = 1.06 mL/g)

Deionized water

Assume silica = 100 g

10% CaO/SiO_2 catalyst $\Rightarrow$ SiO_2 90 g + CaO 10 g

Therefore, SiO_2 90 g = CaO 10 g

Silica 100 g = CaO (10 x 100)/90 g

= CaO 11.11 g

	CaO 1 mol	= $Ca(NO_3)_2.4H_2O$	1 mol
Therefore,	CaO 56.07 g	= $Ca(NO_3)_2.4H_2O$	236.15 g
From above	CaO 11.11 g	= $Ca(NO_3)_2.4H_2O$	(236.15 x 11.11)/56.07 g
		= $Ca(NO_3)_2.4H_2O$	46.8 g

Pore volume of silica = 1.06 mL/g

Therefore, silica 1 g in volume of solution 1.06 mL

From above Assume silica = 100 g

Thus, silica 100 g in volume of solution (1.06 x 100)/1 mL

volume of solution = 106 mL

Therefore, $Ca(NO_3)_2.4H_2O$ 236.15 g = H_2O 72 g

$Ca(NO_3)_2.4H_2O$ 46.8 g = H_2O (46.8 x 72)/236.15 g

= H_2O 14.27 g

So, $Ca(NO_3)_2.4H_2O$ 46.8 g

SiO_2 100 g

DI water 91.7 g

Calculation for preparation of 10wt% ZrO_2/SiO_2 catalyst (10Z/SiO_2)

Precursors

$ZrO(NO_3)_2.2H_2O$ (267.26 g/mol)

Silica (pore volume = 1.06 mL/g)

Deionized water

Assume silica = 100 g

10% ZrO_2/SiO_2 catalyst $\Rightarrow$ SiO_2 90 g + ZrO_2 10 g

Therefore, SiO_2 90 g = ZrO_2 10 g

Silica 100 g = ZrO_2 (10 x 100)/90 g

= ZrO_2 11.11 g

ZrO_2 1 mol = $ZrO(NO_3)_2.2H_2O$ 1 mol

Therefore, ZrO_2 123.22 g = $ZrO(NO_3)_2.2H_2O$ 267.26 g

From above ZrO_2 11.11 g = $ZrO(NO_3)_2.2H_2O$ (267.26 x 11.11)/ 123.22 g

= $ZrO(NO_3)_2.2H_2O$ 24.10 g

Pore volume of silica = 1.06 mL/g

Therefore, silica 1 g in volume of solution 1.06 mL

From above Assume silica = 100 g

Thus, silica 100 g in volume of solution (1.06 x 100)/1 mL

volume of solution = 106 mL

Therefore, $ZrO(NO_3)_2.2H_2O$ 267.26 g = H_2O 36 g

$ZrO(NO_3)_2.2H_2O$ 24.10 g = H_2O (24.10 x 36)/267.26 g

= H_2O 3.25 g

So, $ZrO(NO_3)_2.2H_2O$ 24.10 g

SiO_2 100 g

DI water 102.75 g

Calculation for preparation of 5wt%MgO 5wt% ZrO_2/SiO_2 catalyst (5M5Z/SiO_2)

Precursors

$Mg(NO_3)_2.6H_2O$ (256 g/mol)

$ZrO(NO_3)_2.2H_2O$ (267.26 g/mol)

Silica (pore volume = 1.06 mL/g)

Deionized water

Assume silica = 100 g

5wt%MgO 5wt% ZrO_2/SiO_2 catalyst $\Rightarrow$ SiO_2 90 g + MgO 5 g + ZrO_2 5 g

Therefore, SiO_2 90 g = MgO 5 g = ZrO_2 5 g

Silica 100 g = MgO (5 x 100)/90 g

= MgO 5.55 g

Silica 100 g = ZrO_2 (5 x 100)/90 g

= ZrO_2 5.55 g

	MgO 1 mol	= $Mg(NO_3)_2.6H_2O$	1 mol
Therefore,	MgO 40.00 g	= $Mg(NO_3)_2.6H_2O$	256 g
From above	MgO 5.55 g	= $Mg(NO_3)_2.6H_2O$	(256 x 5.55)/40 g
		= $Mg(NO_3)_2.6H_2O$	35.52 g
	ZrO_2 1 mol	= $ZrO(NO_3)_2.2H_2O$	1 mol
Therefore,	ZrO_2 123.22 g	= $ZrO(NO_3)_2.2H_2O$	267.26 g
From above	ZrO_2 5.55 g	= $ZrO(NO_3)_2.2H_2O$	(267.26 x 5.55)/ 123.22 g
		= $ZrO(NO_3)_2.2H_2O$	12.04 g

Pore volume of silica = 1.06 mL/g

Therefore, silica 1 g in volume of solution 1.06 mL

From above Assume silica = 100 g

Thus, silica 100 g in volume of solution (1.06 x 100)/1 mL

volume of solution = 106 mL

Therefore,	$Mg(NO_3)_2.6H_2O$ 256 g	= H_2O 108 g
	$Mg(NO_3)_2.6H_2O$ 35.52 g	= H_2O (35.52 x 108)/256 g
		= H_2O 14.99 g
	$ZrO(NO_3)_2.2H_2O$ 267.26 g	= H_2O 36 g
	$ZrO(NO_3)_2.2H_2O$ 12.04 g	= H_2O (12.04 x 36)/267.26 g
		= H_2O 1.62 g

So,	$Mg(NO_3)_2.6H_2O$	35.52 g
	$ZrO(NO_3)_2.2H_2O$	12.04 g
	SiO_2	100 g

DI water 89.39 g

Calculation for preparation of 5wt%MgO 5wt% CaO/SiO_2 catalyst (5M5C/SiO_2)

Precursors

$Mg(NO_3)_2.6H_2O$ (256 g/mol)

$Ca(NO_3)_2.4H_2O$ (236.15 g/mol)

Silica (pore volume = 1.06 mL/g)

Deionized water

Assume silica = 100 g

5wt%MgO 5wt% CaO/SiO_2 catalyst $\Rightarrow$ SiO_2 90 g + MgO 5 g + CaO 5 g

Therefore, SiO_2 90 g = MgO 5 g = CaO 5 g

Silica 100 g = MgO (5 x 100)/90 g

= MgO 5.55 g

Silica 100 g = CaO (5 x 100)/90 g

= CaO 5.55 g

	MgO 1 mol	= $Mg(NO_3)_2.6H_2O$	1 mol
Therefore,	MgO 40.00 g	= $Mg(NO_3)_2.6H_2O$	256 g
From above	MgO 5.55 g	= $Mg(NO_3)_2.6H_2O$	(256 x 5.55)/40 g
		= $Mg(NO_3)_2.6H_2O$	35.52 g
	CaO 1 mol	= $Ca(NO_3)_2.4H_2O$	1 mol
Therefore,	CaO 56.07 g	= $Ca(NO_3)_2.4H_2O$	236.15 g
From above	CaO 5.55 g	= $Ca(NO_3)_2.4H_2O$	(236.15 x 5.55)/56.07 g
		= $Ca(NO_3)_2.4H_2O$	23.37 g

Pore volume of silica = 1.06 mL/g

Therefore, silica 1 g in volume of solution 1.06 mL

From above Assume silica = 100 g

Thus, silica 100 g in volume of solution (1.06 x 100)/1 mL

volume of solution = 106 mL

Therefore, $Mg(NO_3)_2.6H_2O$ 256 g = H_2O 108 g

$Mg(NO_3)_2.6H_2O$ 35.52 g = H_2O (35.52 x 108)/256 g

= H_2O 14.99 g

$Ca(NO_3)_2.4H_2O$ 236.15 g = H_2O 72 g

$Ca(NO_3)_2.4H_2O$ 23.37 g = H_2O (23.37 x 72)/236.15 g

= H_2O 7.13 g

So, $Mg(NO_3)_2.6H_2O$ 35.52 g

$Ca(NO_3)_2.4H_2O$ 23.37 g

SiO_2 100 g

DI water 83.88 g

Calculation for preparation of 5wt%MgO5wt%CaO5wt%ZrO_2/SiO_2 catalyst (5M5C5Z/SiO_2)

Precursors

$Mg(NO_3)_2.6H_2O$ (256 g/mol)

$Ca(NO_3)_2.4H_2O$ (236.15 g/mol)

$ZrO(NO_3)_2.2H_2O$ (267.26 g/mol)

Silica (pore volume = 1.06 mL/g)

Deionized water

Assume silica = 100 g

5wt%MgO 5wt% CaO5wt%ZrO_2/SiO_2 catalyst

$\Rightarrow$ SiO_2 90 g + MgO 5 g + CaO 5 g + ZrO_2 5 g

Therefore, SiO_2 85 g = MgO 5 g = CaO 5 g = ZrO_2 5 g

Silica 100 g = MgO (5 x 100)/85 g

= MgO 5.88 g

Silica 100 g = CaO (5 x 100)/85 g

= CaO 5.88 g

Silica 100 g = ZrO_2 (5 x 100)/85 g

= ZrO_2 5.88 g

	MgO 1 mol	= $Mg(NO_3)_2.6H_2O$	1 mol
Therefore,	MgO 40.00 g	= $Mg(NO_3)_2.6H_2O$	256 g
From above	MgO 5.88 g	= $Mg(NO_3)_2.6H_2O$	(256 x 5.88)/40 g
		= $Mg(NO_3)_2.6H_2O$	37.63 g
	CaO 1 mol	= $Ca(NO_3)_2.4H_2O$	1 mol
Therefore,	CaO 56.07 g	= $Ca(NO_3)_2.4H_2O$	236.15 g
From above	CaO 5.88 g	= $Ca(NO_3)_2.4H_2O$	(236.15 x 5.88)/56.07 g
		= $Ca(NO_3)_2.4H_2O$	24.76 g
	ZrO_2 1 mol	= $ZrO(NO_3)_2.2H_2O$	1 mol
Therefore,	ZrO_2 123.22 g	= $ZrO(NO_3)_2.2H_2O$	267.26 g
From above	ZrO_2 5.88 g	= $ZrO(NO_3)_2.2H_2O$	(267.26 x 5.88)/ 123.22 g
		= $ZrO(NO_3)_2.2H_2O$	12.75 g

Pore volume of silica = 1.06 mL/g

Therefore, silica 1 g in volume of solution 1.06 mL

From above Assume silica = 100 g

Thus, silica 100 g in volume of solution (1.06 x 100)/1 mL

volume of solution = 106 mL

Therefore, $Mg(NO_3)_2.6H_2O$ 256 g = H_2O 108 g

$Mg(NO_3)_2.6H_2O$ 37.63 g = H_2O (37.63 x 108)/256 g

= H_2O 15.88 g

$Ca(NO_3)_2.4H_2O$ 236.15 g = H_2O 72 g

$Ca(NO_3)_2.4H_2O$ 24.76 g = H_2O (24.76 x 72)/236.15 g

= H_2O 7.55 g

$ZrO(NO_3)_2.2H_2O$ 267.26 g = H_2O 36 g

$ZrO(NO_3)_2.2H_2O$ 12.75 g = H_2O (12.75 x 36)/267.26 g

= H_2O 1.72 g

So,

$Mg(NO_3)_2.6H_2O$	37.63 g
$Ca(NO_3)_2.4H_2O$	24.76 g
$ZrO(NO_3)_2.2H_2O$	12.75 g
SiO_2	100 g
DI water	80.85 g

Calculation for preparation of 10wt% MgO/AC catalyst (10M/AC)

Precursors

$Mg(NO_3)_2.6H_2O$ (256 g/mol)

Active carbon (pore volume = 0.565 mL/g)

Deionized water

Assume active carbon = 100 g

10% MgO/AC catalyst $\Rightarrow$ AC 90 g + MgO 10 g

Therefore, AC 90 g = MgO 10 g

Active carbon 100 g = MgO (10 x 100)/90 g

= MgO 11.11 g

	MgO 1 mol	= $Mg(NO_3)_2.6H_2O$	1 mol
Therefore,	MgO 40.00 g	= $Mg(NO_3)_2.6H_2O$	256 g
From above	MgO 11.11 g	= $Mg(NO_3)_2.6H_2O$	(256 x 11.11)/40 g
		= $Mg(NO_3)_2.6H_2O$	<u>71.1 g</u>

Pore volume of active carbon = 0.565 mL/g

Therefore, active carbon 1 g in volume of solution 0.565 mL

From above Assume active carbon = 100 g

Thus, active carbon 100 g in volume of solution (0.565 x 100)/1 mL

volume of solution = <u>56.5 mL</u>

Therefore,	$Mg(NO_3)_2.6H_2O$ 256 g	= H_2O 108 g
	$Mg(NO_3)_2.6H_2O$ 71.1 g	= H_2O (71.1 x 108)/256 g
		= H_2O 29.99 g

So,	$Mg(NO_3)_2.6H_2O$	<u>71.1 g</u>
	Active carbon	<u>100 g</u>
	DI water	<u>26.51 g</u>

Calculation for preparation of 5wt%MgO 5wt% ZrO_2/ AC catalyst (5M5Z/AC)

Precursors

$Mg(NO_3)_2.6H_2O$ (256 g/mol)

$ZrO(NO_3)_2.2H_2O$ (267.26 g/mol)

Active carbon (pore volume = 0.565 mL/g)

Deionized water

Assume active carbon = 100 g

5wt%MgO 5wt% ZrO_2/AC catalyst $\Rightarrow$ AC 90 g + MgO 5 g + ZrO_2 5 g

Therefore, AC 90 g = MgO 5 g = ZrO_2 5 g

Active carbon 100 g = MgO (5 x 100)/90 g

= MgO 5.55 g

Active carbon 100 g = ZrO_2 (5 x 100)/90 g

= ZrO_2 5.55 g

	MgO 1 mol	= $Mg(NO_3)_2.6H_2O$	1 mol
Therefore,	MgO 40.00 g	= $Mg(NO_3)_2.6H_2O$	256 g
From above	MgO 5.55 g	= $Mg(NO_3)_2.6H_2O$	(256 x 5.55)/40 g
		= $Mg(NO_3)_2.6H_2O$	35.52 g
	ZrO_2 1 mol	= $ZrO(NO_3)_2.2H_2O$	1 mol
Therefore,	ZrO_2 123.22 g	= $ZrO(NO_3)_2.2H_2O$	267.26 g
From above	ZrO_2 5.55 g	= $ZrO(NO_3)_2.2H_2O$	(267.26 x 5.55)/ 123.22 g
		= $ZrO(NO_3)_2.2H_2O$	12.04 g

Pore volume of active carbon = 0.565 mL/g

Therefore, active carbon 1 g in volume of solution 0.565 mL

From above Assume active carbon = 100 g

Thus, active carbon 100 g in volume of solution (0.565 x 100)/1 mL

volume of solution = 56.5 mL

Therefore, $Mg(NO_3)_2.6H_2O$ 256 g = H_2O 108 g

$Mg(NO_3)_2.6H_2O$ 35.52 g = H_2O (35.52 x 108)/256 g

= H_2O 14.99 g

$ZrO(NO_3)_2.2H_2O$ 267.26 g = H_2O 36 g

$ZrO(NO_3)_2.2H_2O$ 12.04 g = H_2O (12.04 x 36)/267.26 g

= H_2O 1.62 g

So,

$Mg(NO_3)_2.6H_2O$	35.52 g
$ZrO(NO_3)_2.2H_2O$	12.04 g
Active carbon	100 g
DI water	39.89 g

Calculation for preparation of 5wt%MgO 5wt% CaO/AC catalyst (5M5C/AC)

Precursors

$Mg(NO_3)_2.6H_2O$ (256 g/mol)

$Ca(NO_3)_2.4H_2O$ (236.15 g/mol)

Active carbon (pore volume = 0.565 mL/g)

Deionized water

Assume active carbon = 100 g

5wt%MgO 5wt% CaO/AC catalyst $\Rightarrow$ AC 90 g + MgO 5 g + CaO 5 g

Therefore, AC 90 g = MgO 5 g = CaO 5 g

Active carbon 100 g = MgO (5 x 100)/90 g

= MgO 5.55 g

Active carbon 100 g = CaO (5 x 100)/90 g

= CaO 5.55 g

	MgO 1 mol	= $Mg(NO_3)_2.6H_2O$	1 mol
Therefore,	MgO 40.00 g	= $Mg(NO_3)_2.6H_2O$	256 g
From above	MgO 5.55 g	= $Mg(NO_3)_2.6H_2O$	(256 x 5.55)/40 g
		= $Mg(NO_3)_2.6H_2O$	<u>35.52 g</u>
	CaO 1 mol	= $Ca(NO_3)_2.4H_2O$	1 mol
Therefore,	CaO 56.07 g	= $Ca(NO_3)_2.4H_2O$	236.15 g
From above	CaO 5.55 g	= $Ca(NO_3)_2.4H_2O$	(236.15 x 5.55)/56.07 g
		= $Ca(NO_3)_2.4H_2O$	<u>23.37 g</u>

Pore volume of active carbon = 0.565 mL/g

Therefore, active carbon 1 g in volume of solution 0.565 mL

From above Assume active carbon = 100 g

Thus, active carbon 100 g in volume of solution (0.565 x 100)/1 mL

volume of solution = <u>56.5 mL</u>

Therefore,	$Mg(NO_3)_2.6H_2O$ 256 g	= H_2O 108 g
	$Mg(NO_3)_2.6H_2O$ 35.52 g	= H_2O (35.52 x 108)/256 g
		= H_2O 14.99 g

	$Ca(NO_3)_2.4H_2O$	236.15 g	= H_2O 72 g
	$Ca(NO_3)_2.4H_2O$	23.37 g	= H_2O (23.37 x 72)/236.15 g
			= H_2O 7.13 g

So,	$Mg(NO_3)_2.6H_2O$	35.52 g
	$Ca(NO_3)_2.4H_2O$	23.37 g
	Active carbon	100 g
	DI water	34.38 g

Calculation for preparation of 5wt%MgO5wt%CaO5wt%ZrO_2/AC catalyst (5M5C5Z/AC)

Precursors

$Mg(NO_3)_2.6H_2O$ (256 g/mol)

$Ca(NO_3)_2.4H_2O$ (236.15 g/mol)

$ZrO(NO_3)_2.2H_2O$ (267.26 g/mol)

Active carbon (pore volume = 0.565 mL/g)

Deionized water

Assume active carbon = 100 g

5wt%MgO 5wt% CaO5wt%ZrO_2/AC catalyst

$\Rightarrow$ AC 90 g + MgO 5 g + CaO 5 g + ZrO_2 5 g

Therefore, AC 85 g = MgO 5 g = CaO 5 g = ZrO_2 5 g

Active carbon 100 g	= MgO (5 x 100)/85 g
	= MgO 5.88 g
Active carbon 100 g	= CaO (5 x 100)/85 g

= CaO 5.88 g

Active carbon 100 g = ZrO_2 (5 x 100)/85 g

= ZrO_2 5.88 g

	MgO 1 mol	= $Mg(NO_3)_2.6H_2O$	1 mol
Therefore,	MgO 40.00 g	= $Mg(NO_3)_2.6H_2O$	256 g
From above	MgO 5.88 g	= $Mg(NO_3)_2.6H_2O$	(256 x 5.88)/40 g
		= $Mg(NO_3)_2.6H_2O$	37.63 g
	CaO 1 mol	= $Ca(NO_3)_2.4H_2O$	1 mol
Therefore,	CaO 56.07 g	= $Ca(NO_3)_2.4H_2O$	236.15 g
From above	CaO 5.88 g	= $Ca(NO_3)_2.4H_2O$	(236.15 x 5.88)/56.07 g
		= $Ca(NO_3)_2.4H_2O$	24.76 g
	ZrO_2 1 mol	= $ZrO(NO_3)_2.2H_2O$	1 mol
Therefore,	ZrO_2 123.22 g	= $ZrO(NO_3)_2.2H_2O$	267.26 g
From above	ZrO_2 5.88 g	= $ZrO(NO_3)_2.2H_2O$	(267.26 x 5.88)/ 123.22 g
		= $ZrO(NO_3)_2.2H_2O$	12.75 g

Pore volume of active carbon = 0.565 mL/g

Therefore, active carbon 1 g in volume of solution 0.565 mL

From above Assume active carbon = 100 g

Thus, active carbon 100 g in volume of solution (0.565 x 100)/1 mL

volume of solution = 56.5 mL

Therefore,	$Mg(NO_3)_2.6H_2O$ 256 g	= H_2O 108 g
	$Mg(NO_3)_2.6H_2O$ 37.63 g	= H_2O (37.63 x 108)/256 g

		= H_2O 15.88 g
$Ca(NO_3)_2.4H_2O$	236.15 g	= H_2O 72 g
$Ca(NO_3)_2.4H_2O$	24.76 g	= H_2O (24.76 x 72)/236.15 g
		= H_2O 7.55 g
$ZrO(NO_3)_2.2H_2O$	267.26 g	= H_2O 36 g
$ZrO(NO_3)_2.2H_2O$	12.75 g	= H_2O (12.75 x 36)/267.26 g
		= H_2O 1.72 g

So,	$Mg(NO_3)_2.6H_2O$	37.63 g
	$Ca(NO_3)_2.4H_2O$	24.76 g
	$ZrO(NO_3)_2.2H_2O$	12.75 g
	Active carbon	100 g
	DI water	31.35 g

Calculation the acid value of the cracked oil

Reagent

Reagent : 0.1N potassium hydroxide

Additives : Mix solution (toluene + DI water + 2-propanol)

Measurement procedure

1) Deliver 20 g oil to a 300 mL beaker. Add 120.0 mL mix solution and shake for 30 second.

2) Titrate with 0.1N potassium hydroxide to obtain acid value. Likewise, perform blank test to obtain blank level.

The acid value, mg KOH/g of cracked oil = (A-B) * N * 56.1/W

Where; A = mL of standard alkali (0.1N or 0.01N KOH) used in the titration

B = mL of standard alkali (0.1N or 0.01N KOH) used in the titrating the blank

N = normality of the standard alkali (0.1 or 0.01N KOH)

W = grams of cracked oil

Calculation the iodine value of the cracked oil

Reagent

Reagent : 0.1mol/L sodium thiosulfate（f＝1.006）

Additives : DI water, Cyclohexane, wijis reagent, 10% Potassium iodide

Measurement procedure

1) Deliver 0.5 g oil to a 300 mL beaker. Add 10.0 mL Cyclohexane and 25.0 mL wijis reagent and then seal. Shake for 30 second.

2) Keep it sealed and leave in a dark at room temperature for 30 minutes.

3) Add 20.0mL of 10% potassium iodide and 100 mL DI water, and seal. Shake for 30 seconds.

4) Titrate with 0.1mol/L sodium thiosulfate to obtain iodine value. Likewise, perform blank test to obtain blank level.

The iodine value (cg / g) = (BL1 － EP1) × TF × C1 ×K1 / Size

EP1 = Titration volume (mL)

BL1 = Blank level (mL)

TF = Factor of titrant (1.006)

C1 = Concentration conversion coefficient (1.269)

(Atomic mass of iodine: 126.9/100)

K1 = Unit conversion coefficient (1)

Size = Sample size (g)

TCD-Gas chromatographs of CO and CO_2 gas standards

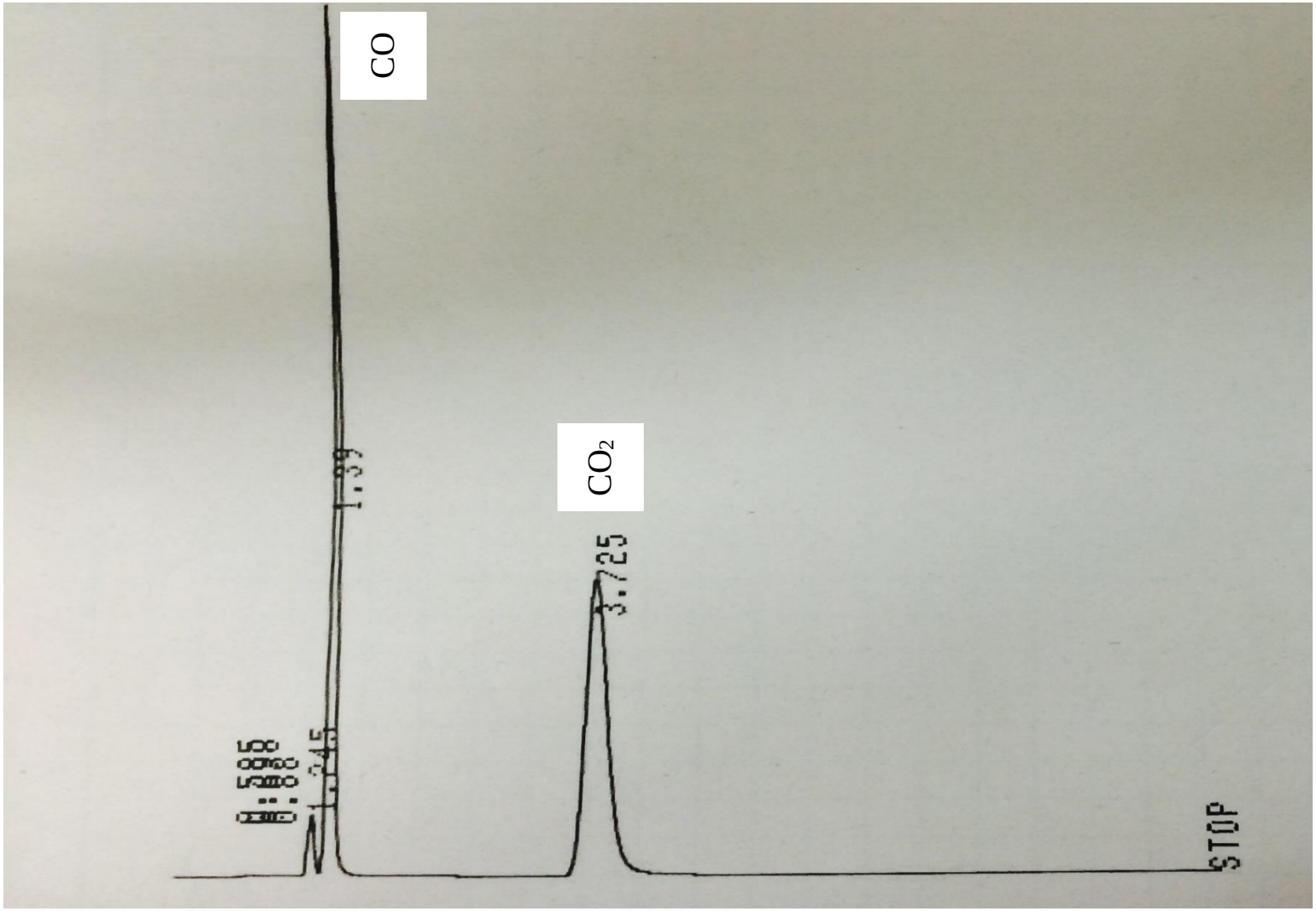

FID-Gas chromatographs of hydrocarbon gas standards